

AJ, in press

The Molonglo Southern 4 Jy Sample (MS4). II. ATCA Imaging and Optical Identification

A. M. Burgess¹

annb@psych.usyd.edu.au

and

R. W. Hunstead

School of Physics, University of Sydney, NSW 2006, Australia

rwh@physics.usyd.edu.au

ABSTRACT

Of the 228 sources in the Molonglo Southern 4 Jy Sample (MS4), the 133 with angular sizes $< 35''$ have been imaged at 5 GHz at $2 - 4''$ resolution with the Australia Telescope Compact Array. More than 90% of the sample has been reliably optically identified, either on the plates of the UK Schmidt Southern Sky Survey or on *R*-band CCD images made with the Anglo-Australian Telescope. A subsample of 137 sources, the SMS4, defined to be a close southern equivalent of the northern 3CRR sample, was found to have global properties mostly consistent with the northern sample. Linear sizes of MS4 galaxies and quasars were found to be consistent with galaxy-quasar unification models of orientation and evolution.

Subject headings: radio continuum: galaxies — galaxies: active — surveys

¹present address: School of Psychology, University of Sydney, NSW 2006, Australia.

1. INTRODUCTION

In the preceding paper (Burgess & Hunstead 2006, hereafter Paper I), the Molonglo Southern 4 Jy sample (MS4) was defined according to the following selection criteria: declination $-85^\circ < \delta < -30^\circ$; flux density $S_{408\text{MHz}} > 4.0\text{ Jy}$; Galactic latitude $|b| > 10^\circ$; not in the Magellanic Cloud regions; and not a known Galactic source. The sample thus defined contained 228 radio sources. These sources were all imaged at 843 MHz with the Molonglo Observatory Synthesis Telescope (MOST) at a resolution of $43'' \times 43'' \text{ cosec } |\delta|$, giving radio positions accurate to around $1\text{--}2''$, and estimates of angular size.

A subsample of 137 sources, the SMS4, was defined to have $S_{178\text{MHz}} > 10.9\text{ Jy}$, making it a southern equivalent of the northern 3CRR sample (Laing et al. 1983). This sample was found to have properties mostly consistent with those of 3CRR, though with slight, possibly significant differences in angular-size distributions and source densities, in the sense that SMS4 has slightly higher source density and larger angular sizes than 3CRR.

In this paper we present higher-resolution radio images of those MS4 sources of smaller angular size (Section 2), as well as optical identifications based on the Schmidt plates and on *R*-band CCD images (Section 3). Section 4 contains notes on individual sources. In Section 5 we use the radio and optical data to compare derived properties of MS4, SMS4, and 3CRR, such as their radio luminosity distributions, quasar fractions, and radio linear sizes.

2. RADIO IMAGING AT 5 GHZ

We used our 843 MHz MOST data from Paper I to select the 133 sources with largest angular size ($\text{LAS} \leq 35''$) for high-resolution imaging with the Australia Telescope Compact Array (ATCA). The ATCA is an east-west array consisting of six 22 m-diameter paraboloidal antennas (Frater et al. 1992). We used an observing frequency of 5 GHz, with a bandwidth of 128 MHz. The observing was done in twelve different runs between 1990 and 1993, at an early stage of ATCA operations. The first eight observing runs used five antennas with a longest spacing of 3 km, with nominal resolution $\sim 4'' \times 4'' \text{ cosec } |\delta|$. The last five observing runs were made after the 6 km antenna was commissioned, giving a resolution of $\sim 2'' \times 2'' \text{ cosec } |\delta|$.

The observations were done in ‘cuts’ or ‘snapshot’ mode, a method of time-sharing in which sources are observed at several hour angles (Burgess & Hunstead 1995). We usually observed about ten sources in a twelve-hour run. About eight cuts of 8-minutes’ duration, spread in hour angles, were observed per source, bringing the total integration time per source to about one hour. We included at least two secondary phase calibrators in each

cycle, with ‘cuts’ of length four minutes, and observed the primary flux-density calibrator, PKS B1934–63, once in each twelve-hour run. Table 1 contains a summary of the ATCA imaging runs.

A few sources were excluded either because they were unresolved ATCA calibrators (MRC B1740–517 and MRC B2259–375), or because they had been imaged by others: MRC B0521–365 (Keel 1986), MRC B0743–673 (Duncan & Sproats 1992; Rayner et al. 2000), MRC B1814–519 (M. Wieringa, private communication), and MRC B2153–699 (Norris et al. 1990). MRC B1933–587 had already been observed in a different project. We also observed a few sources which were more extended than our $35''$ limit. A summary of the observations for each source is given in Table 2. The columns of this table are as follows:

1. Source name.
2. Run number (see column 1 of Table 1).
3. Number of cuts.
4. Total integration time in minutes.
5. Dynamic range of the final image, expressed as the ratio of the peak flux density to the RMS noise.
6. FWHM major and minor axes of the CLEAN beam in arcseconds, and position angle of the major axis in degrees east of north (modulo 90).

For most of our target sources, the ATCA snapshot observations enabled us to obtain images with dynamic ranges of around 100:1. These images provided morphological information with a resolution of a few arcseconds, allowing us to classify the radio structures and direct our searches for optical identifications.

The data were reduced in the AIPS (Astronomical Image Processing System) software package. Because most of our observing was done before polarisation calibration was feasible, we imaged only the total intensity. Images were constructed using uniform weighting of the antenna baselines. The procedures for deconvolution and self-calibration of ATCA snapshot data are described in more detail in Burgess & Hunstead (1995).

2.1. Calibration and Imaging

In continuum ATCA observing the 128 MHz bandwidth is divided into 32 channels. We usually averaged the central 20 channels, giving an effective bandwidth of ~ 80 MHz.

Because the ratio of bandwidth to observing frequency was low, and the sources had angular extent $< 2'$ and were close to the field centre, any resultant bandwidth smearing would not have been significant.

The flux-density scale was based on the radio spectrum of PKS B1934–63 measured by Reynolds (1994). Secondary phase calibrators were observed at regular intervals to monitor the relative antenna gains. A few secondary calibrators were found to be slightly resolved: MRC B0438–436, MRC B1424–418, MRC B1814–637, and MRC B1827–360. In these cases we either used the other secondary calibrator, or excluded the baselines on which the calibrator was resolved.

The raw images were deconvolved with the Cotton-Schwab CLEAN algorithm (Schwab 1984), using the AIPS task `mx`. The CLEANed images typically contained artefacts caused by antenna phase gain variations too rapid to be corrected by the secondary phase calibrator, limiting the dynamic range to about 20:1. Because most of the target sources were strong (peak $S_{5\text{GHz}} > 100\text{mJy/beam}$) and compact ($\text{LAS} < 35''$), it was usually feasible to use self-calibration (Cornwell & Fomalont 1989) to improve the dynamic range to about 100:1. Self-calibrating the phases was sufficient: the strongest 200–300 CLEAN components were used as the starting model, which was updated after each cycle. We stopped self-calibrating when the dynamic range of the image ceased to improve, usually after four to ten cycles. The final self-calibrated data set was then imaged and CLEANed, usually with a loop gain of 0.1 and about 500 iterations. Contour maps of these final images are shown in Figure 1, with crosses denoting the positions of the likely optical counterpart. Maps of sources without resolved structure have been omitted.

We tested the reliability of our ATCA images by comparing them with Very Large Array (VLA) images for 12 sources. Structures for each source showed good agreement above the 1–2% contour levels. A potential hazard of self-calibration is the loss of absolute positional information (e.g. Bridle 1989). These effects have been reduced by applying successive models for self-calibration to the original uv data set. Comparison with VLBI and optical data (§ 2.3) shows that our positions are reliable at the levels stated.

2.2. Measurements from the ATCA Images

Quantities measured from the radio images are summarised in Table 3. The columns of the table are as follows:

1. Source name.

2. Code for Fanaroff-Riley (Fanaroff & Riley 1974) or other structural classification.
3. Right ascension, in J2000 co-ordinates.
4. Declination, in J2000 co-ordinates.
5. Code for the type of position measurement (§ 2.3).
6. Integrated flux density in mJy (§ 2.4). The integrated flux densities are uncertain and sometimes underestimated, due to the limited *uv* coverage. They have been measured mainly to provide an estimate of the fraction of emission present in compact components.
7. Core flux density in mJy. In the absence of spectral-index information, a compact component is called the ‘core’ if it coincides with an optical counterpart. However, for close doubles identified with galaxies, a component coincident with the optical counterpart has not been classified as the core, because D2 structures (Macdonald & Miley 1971) are rare in galaxies. For most sources the core flux density is an upper limit. If extended emission lies near the core, the flux density has been flagged with a colon (:). For doubles with widely separated lobes, we adopted an upper limit of three times the r.m.s. noise in a box of size 6×6 pixels centred at the optical counterpart. For close doubles we set an arbitrary upper limit of 1/3 of the integrated flux density of the brighter lobe. For compact-steep-spectrum (CSS) sources no attempt was made to estimate the core flux density.
8. Ratio R of core to extended flux density at 5 GHz (observed). These ratios are uncertain, because of the uncertainty in the core flux densities. R was calculated from the core flux density in column 7 and the Parkes single-dish flux density (see Table 5 of Paper I), which was interpolated to the ATCA observing frequency using the radio spectrum. In a few cases the ATCA core flux density was greater than the single-dish total flux density, presumably because of variability. For these sources the ATCA integrated flux density was used instead of the Parkes value. Because of their uncertainty, the values of R have not been used elsewhere in the paper.
9. Largest angular extent in arcseconds (§ 2.5).
10. Position angle of the extension in degrees east of north (modulo 90).

2.3. Positions

Positions of compact sources (angular size $\lesssim 3''$) were measured in AIPS with IMFIT, which performs a least-squares fit to an elliptical Gaussian. Centroid positions of more extended sources were measured above a contour level which depended on the dynamic range, but was usually about 2% of the peak. For double sources with edge-brightened (Fanaroff-Riley class II or FR 2) structure, we also measured the peak positions of the radio lobes so as to calculate the largest angular extent.

To test the accuracy of the ATCA positions, the core positions of eight quasars were compared with VLBI positions from Ma et al. (1998). Because of the comparatively low resolution of the ATCA images, the ATCA ‘core’ position may be affected by blending. This will increase the scatter in the ATCA-VLBI offsets, so that the errors quoted below may be slightly overestimated. The mean offset in RA was $0''.07$, with $\sigma = 0''.32$. The mean offset in declination was $0''.08 \text{ cosec } |\delta|$, with $\sigma = 0''.40 \text{ cosec } |\delta|$. The ATCA position errors are therefore around $0''.3$ in right ascension and $0''.4 \text{ cosec } |\delta|$ in declination. The errors will be larger for extended sources, and for a few sources with calibration problems.

Positions for sources in Run 9 (see Table 1) were affected by a telescope error and were therefore corrected with a mean radio-optical offset in right ascension of $0''.9$ ($\sigma = 1''.5$), and in declination of $1''.1 \text{ cosec } |\delta|$ ($\sigma = 0''.9 \text{ cosec } |\delta|$), calculated from 6 sources with small angular extent or a detected core. The positions for Run 9 are flagged in Table 3.

2.4. Flux Densities

Flux densities were measured mainly to estimate the fraction of emission coming from compact components. For compact sources we used the integrated flux density of the Gaussian fitted with IMFIT. For extended sources of irregular shape we used the AIPS verb TVSTAT, which sums the flux density of each pixel in a polygonal region specified by the user. We also used TVSTAT to correct for a nonzero base level by finding the average flux density per pixel in an annulus surrounding the source.

For slightly extended sources we measured integrated flux densities with the method of Jones & McAdam (1992), i.e. by calculating a set of volumes in the radio image with upper bound given by the surface defined by the radio contours, and lower bounds given by a set of lower flux-density limits, and then extrapolating the results to the local zero level.

2.5. Measurement of Angular Sizes and Position Angles

For sources with a single compact component, the quoted angular size is the deconvolved FWHM of the Gaussian fitted with IMFIT. Sources with deconvolved angular sizes below a limit of 0.46 times the major axis of the dirty beam (a value chosen after examination of the interferometer fringe visibilities for compact sources) were given this value as an upper limit.

For edge-brightened (FR 2) doubles, angular sizes and position angles were defined using the separation between the outer peaks of the lobes, usually the hot-spots. For edge-darkened (FR 1) doubles, and sources of irregular structure, we measured the largest separation between 3σ contours on the contour maps. The position angle was taken to be that of the line joining the two points which had the largest separation.

Angular sizes were compared with those in Paper I obtained with MOST. For FR 2 sources the ATCA angular size tends to be similar to the MOST value, but slightly larger. This is expected, both because the hot-spots at the edge of the structure are resolved better with ATCA, and because the steep-spectrum extended emission between the lobes contributes a larger fraction of the flux density at 843 MHz, reducing the width of the fitted Gaussian. For two FR 1 sources, MRC B1416–493 and MRC B2354–350, the ATCA detected only the inner structure, leading to an underestimate of angular size. The remaining FR 1 sources had larger angular sizes with ATCA than with MOST, owing to a difference in definition: with MOST we measured the FWHM of an elliptical Gaussian, whereas with the ATCA we measured the separation between outer contour levels in a higher-resolution image.

3. OPTICAL IDENTIFICATION OF THE SAMPLE

Optical identification of MS4 sources was conducted using first the UK Schmidt sky survey, followed by *R*-band CCD imaging of the fainter objects and blank fields at the prime focus of the Anglo-Australian Telescope (AAT). We used the identifications of Jones & McAdam (1992) for objects which we had not imaged with MOST, as their optical positions were measured in the same way as for the other MS4 sources.

Using Schmidt plates and AAT CCD images we found optical candidates for 222 of the 228 sources in the sample. There are spectroscopic redshifts in the literature or from our unpublished observations for 111 of the sources, mostly quasars and low-redshift galaxies. Most of the remaining optical counterparts are sufficiently faint that measurement of spectroscopic redshifts will require a major observing program on 4-m or 8-m telescopes.

3.1. Measurement from the UK Schmidt Plates

Optical positions on film copies of the IIIaJ plates were measured by B. Piestrzynska using a purpose-built measuring machine (Hunstead 1991, 1994). These positions, hereafter referred to as BP positions, are accurate to about $0''.5$ in each co-ordinate (§ 3.3). Candidates were classified as galaxies or stellar by visual inspection of the Schmidt plates. We used the MOST and ATCA positions to choose between candidates, using the following search criteria:

1. For the 64 sources with $LAS \leq 8''$, the ATCA peak or the MOST centroid from Paper I was used as the search position. In a few cases of asymmetric structure in the ATCA image, the MOST centroid was preferred.
2. 75 sources had $LAS > 8''$ and a radio core position from the ATCA image (§ 2.2) or the literature. For these the radio core position was used as the search position.
3. 73 sources had $LAS > 8''$ and FR 2 structure with no detected radio core. The search position was defined to be the “midway point”: the point midway between the MOST centroid and the midpoint of the outermost hot spots in the ATCA image. The justification for this choice is described below.
4. 6 sources had $LAS > 8''$ and FR 1 structure with no measured radio core position. If there were two well defined inner peaks, their midpoint was used as the search position, otherwise the MOST centroid was used.
5. The MOST centroid was used for 10 sources with $LAS > 8''$ with no radio core position, and for which structure had not been classified as FR 1 or 2.

For extended sources we used a circular search area of radius 0.2 times the largest angular extent, centred at the search position. For point sources and radio cores we checked if the displacement vector for the radio-optical offset fell within an elliptical search area with semiminor axis proportional to the radio and optical right ascension errors summed in quadrature, and semimajor axis proportional to the radio and optical declination errors summed in quadrature. For sources with $LAS < 8''$ the constant of proportionality used was 2, and for radio cores it was 2.5. The search area had to be slightly larger for the radio cores, because core positions were often affected by extended emission in the image.

The search position for FR 2 sources was chosen empirically to be the point midway between the radio centroid and the midpoint of the radio hot-spots. In various studies, the radio midpoint (e.g. Laing et al. 1983; Röttgering et al. 1995) and the radio centroid (e.g. Bridle & Fomalont 1978; Perryman 1979) have been found to be good approximations

of the core position of double radio sources. We tested their reliability, as well as the reliability for the point midway between them, for 43 FR 2 sources in the MS4 sample with spectroscopically confirmed optical counterparts.

For each radio source we calculated the offsets between the optical position and the following three positions: the MOST centroid, the midpoint on the ATCA image, and the point midway between the MOST centroid and the ATCA midpoint. The MOST rather than ATCA centroid was used because the ATCA images were often missing extended emission. Median and mean distances from the candidate position to the search position are listed in Table 4 for the three different types of search position. The mean and median distances to the “midway point” are the smallest, and it was therefore used as the search position where possible.

In total 156 sources could be identified using the Schmidt plates. Two fields were obscured by stars; another two sources were unidentified cluster sources (PKS B1400–33 and MRC B2006–566). There were 54 blank fields. The remaining 14 sources had candidates selected from the Schmidt plates which were later rejected on the basis of the CCD images.

3.2. Magnitudes from the COSMOS Database

Optical b_J magnitudes were obtained from Version 2 of the UKST/COSMOS database of the southern sky (Yentis et al. 1992; Drinkwater et al. 1995). The bandpass b_J for the UK Schmidt southern sky survey lies roughly between B and V (e.g. Evans 1989). Errors in COSMOS magnitudes are typically around 0.3 to 0.5 mag (Unewisse et al. 1993). We did not use COSMOS magnitudes for 18 sources which were affected by blending.

The COSMOS classification of objects as stars or galaxies is often inaccurate (Unewisse et al. 1993), sometimes leading to large photometric errors. The nonlinearity of plate opacity with source brightness, and the differing light profiles of stars and galaxies, require COSMOS to use different photometric algorithms for each (Heydon-Dumbleton et al. 1988). We therefore applied the relevant algorithm to each candidate, depending on our classification from visual inspection of the plates. Photometric errors may still be large for objects with uncertain morphology.

3.3. Accuracy of Schmidt-plate Positions

For some objects, we used optical positions from digitised Schmidt-plate data from COSMOS or the Digitized Sky Survey (DSS-I: Morrison 1995; Lasker et al. 1990). We

measured positions from the DSS-I images in AIPS with a 9-pixel least-squares quadratic fit to the peak.

To estimate optical position accuracy, we compared DSS-I and BP positions with VLBI radio positions (Ma et al. 1998) of $\lesssim 10$ milliarcsecond accuracy. For DSS-I we used 14 MS4 quasars, 5 of which were on two or more DSS-I images. The average offsets in right ascension and declination were $\overline{\Delta\alpha} = 0''.01$ ($\sigma = 0''.65$), and $\overline{\Delta\delta} = 0''.08$ ($\sigma = 0''.64$) respectively. For the hand-measured BP positions we used 20 quasars from MS4 or the Molonglo calibrator list (Campbell-Wilson & Hunstead 1994). The average offsets in right ascension and declination were $\overline{\Delta\alpha} = 0''.08$ ($\sigma = 0''.57$), and $\overline{\Delta\delta} = 0''.32$ ($\sigma = 0''.58$) respectively.

COSMOS positions are affected by errors in the plate solutions (Drinkwater et al. 1995), but nevertheless have good internal consistency over small areas of sky, and being extracted from images with relatively small pixel size, are more reliable than DSS for faint objects. We therefore used COSMOS positions to define the reference frame in many of our CCD images (§ 3.5). Because of the systematic errors, COSMOS positions of reference stars were corrected wherever possible with DSS or BP positions.

To establish the systematic reliability of the optical positions in the south, we compared BP and VLBI positions for 31 sources from the MS4 sample or the Molonglo calibrator list. A cross-plot is shown in Figure 2. There was no observed systematic effect or increased scatter in the errors of right ascension and declination as a function of declination.

3.4. Imaging at *R* Band with the Anglo-Australian Telescope

Objects fainter than $b_J \sim 21$ were selected for imaging with the 3.9 m Anglo-Australian Telescope (AAT), to identify blank-field sources, to classify faint candidates, and to obtain more information about optical morphologies. Observing was done at *R*-band to maximise sensitivity to galaxies. We used the 1024×1024 Tektronix CCD detector at the f/3.3 prime focus to acquire images with a field size of 6.7×6.7 arcmin 2 and a pixel size of $0''.39$. As the seeing was typically $1 - 2''$, the pixel images were well sampled. The observing runs are summarised in Table 5.

Most of the observing was done in photometric conditions, except for runs 3 and 4, which were affected by cloud or poor seeing for much of the night. Most objects from these runs were therefore re-observed in run 6. Two sources, MRC B1358–493 and MRC B1445–468, were observed in a service run on 1994 February 14. As well as the target sources, dome and sky flat fields were observed. Standard stars in the E-regions (Graham 1982) were observed at the beginning and end of each night.

Exposures of 300 seconds were used; for a few faint objects we used two or three exposures, and offset successive frames by $40''$. Guide stars were not used, but this generally did not lead to noticeable tracking errors.

Bias subtraction and flat fielding were done using the STARLINK Figaro software package. After flat-fielding, multiple images of faint sources were shifted and co-added using median offsets from about 10 stars in the field.

Grey-scale plots of subsets of the CCD images are shown in Figure 3. The images are centred at the optical candidates, and have north to the top and east to the left. Images of some very faint candidates in the following fields have been smoothed to improve the visibility of faint regions of emission: MRC B0008–421, MRC B0315–685, MRC B0615–365, MRC B0647–475, MRC B1143–316, MRC B1247–401, MRC B1633–681, MRC B1721–836, MRC B1756–663, and MRC B1923–328. We used ISMOOTH in Figaro to perform a 9-point smooth, approximating the effect of convolution with a Gaussian of FWHM $0''.5$.

3.5. Position Measurement

Centroid positions of candidates were measured in FIGARO with CPOS and CENTERS. We typically used a circular aperture with radius of 3 to 5 pixels, depending on the seeing. For a few extended candidates we used a radius of up to 8 pixels. We used COSMOS, BP, or DSS-I positions of stars in the field to solve for equatorial positions as a function of pixel position. Because of systematic offsets in COSMOS, we then used the BP or DSS-I positions of one or two brighter stars in the field to correct the COSMOS-referenced positions. The r.m.s value of the DSS-COSMOS offsets was around $0''.9$ in α and $1''.1$ in δ .

To check the accuracy of the CCD positions we compared optical with VLBI positions for 6 sources: MRC B0252–712, MRC B0407–658, MRC B0615–365, MRC B0647–475, MRC B1740–517, and MRC B2259–375. The VLBI-optical offsets are $\overline{\Delta\alpha} = 0''.14$ ($\sigma = 0''.54$), $\overline{\Delta\delta} = 0''.09$ ($\sigma = 0''.58$). The r.m.s offset is similar to the VLBI-BP and VLBI-DSS offsets found in Section 3.3, indicating that the position error is dominated by errors in the reference-star positions.

3.6. Measurement of R Magnitudes

R magnitudes were measured from the CCD images for the fainter galaxy candidates. It was not possible to do accurate photometry, because standard stars had been observed only at the beginning and end of each night, but the magnitudes obtained are still useful for

providing rough redshift estimates, as well as indicating the likely observing time needed for spectroscopy.

No magnitudes were calculated for runs 3 and 4 which were affected by cloud, nor for run 5, which had only two objects. Photometric solutions were kindly provided by Gary Da Costa for runs 1 and 2 and by Tanya Hill for run 6. The solutions are listed in Table 6.

Magnitudes were measured by summing pixels within a circular aperture of radius 5 pixels ($\sim 2''$) using IMEXAMINE in IRAF. The fixed aperture size may have led to an underestimation of the flux in cases of poor seeing or very extended objects. From repeat observations of two fields, we estimate the error in our R magnitudes to be about 0.5 mag, about the same as the errors in the COSMOS magnitudes. Most of this is expected to be systematic error, with internal errors a factor of 10 smaller. For those candidates affected by blending with a neighbouring star or galaxy, we made a rough magnitude estimate by deblending the objects by eye. These estimates have been flagged with “:”. The R magnitudes are listed in column 6 of Table 7.

3.7. Likelihood of Chance Identifications

We have estimated the number of spurious identifications among the 65 sources identified from the AAT images for which R magnitudes have been measured. These are the objects for which such an estimate is most useful, because of the substantial observing time required for follow-up spectroscopy. The estimated number of spurious identifications, derived using the method of Downes et al. (1986), came to about 13.

To make the estimate, source densities of galaxies in the field were estimated from the R -band counts of Jones et al. (1991). Those of foreground stars were estimated from the star-count model of Bahcall & Soneira (1980), using the Fortran program `model.f` (J. Bahcall, 1997, *priv. comm.*), and assuming the following colour transformation for giant and main-sequence stars:

$$R - V = -1.576(B - V) + 0.304, \quad (1)$$

based on a least-squares fit to the colours measured by Gunn & Stryker (1983). Because of clustering, the errors in both star and galaxy counts for any particular field are expected to be large. Also, the model of Bahcall & Soneira (1980) applies to fields with $|b| > 20^\circ$, whereas many MS4 sources have $10^\circ < |b| < 20^\circ$. The estimate of 13 chance IDs is therefore uncertain.

3.8. Estimation of Redshifts from Magnitudes

Because few of the MS4 galaxies with $b_J > 19$ have measured spectroscopic redshifts, it was necessary to use an alternative distance estimate. The most common method for radio galaxies is to use the fact that their absolute magnitudes show a small scatter about a mean M_V of -23 (Sandage 1972). The scatter in the relation between K and $\log z$ is smaller than in the optical (Eales 1985), but as K magnitudes were unavailable, R and b_J were used instead. There will be large uncertainties in the magnitude-based redshifts, but they are still useful for calculating parameters such as linear size and the V/V_m ratio, which do not depend strongly on redshift.

We fitted a straight line to $\log z$ versus R for 11 reliable identifications, using an orthogonal least-squares fit (Isobe et al. 1990). This gave a relation of

$$\log_{10} z = (-3.0 \pm 0.9) + (0.14 \pm 0.05) R \quad (2)$$

A plot of the fit is shown in Figure 4a. As there are few data points and large scatter, redshifts estimated from this relation should be used with extreme caution.

As not all the galaxies had measured R magnitudes, we fitted a line to $\log_{10} z$ versus b_J for the galaxies which were visible on the Schmidt plates. The fit was done using the ordinary-least-squares bisector method (Isobe et al. 1990), and gave the result

$$\log_{10} z = (-3.95 \pm 0.18) + (0.17 \pm 0.01) b_J \quad (3)$$

A plot of the fit is shown in Figure 4b.

Galaxy redshift estimates, based on equations 2 or 3, are given in parentheses in Table 7. Their errors are indeterminate, because of various factors which are hard to quantify, such as dust extinction at high redshift. The estimates are provided purely as a guide, until full spectroscopic data can be obtained. For quasar candidates we assumed $z = 1$ when calculating linear sizes or other physical quantities which do not strongly depend on redshift.

3.9. Summary of Optical Data

Optical candidates have now been found for 97% of the MS4 sample, on the basis of the Schmidt plates or R -band CCD images. Optical data for each source are given in Table 7.

Candidates which appear compact on the Schmidt plates but have no measured spectra

have been flagged with “Q?” in Table 7. Several candidates appear unresolved on the CCD but are faint or invisible on the Schmidt plates. If not foreground stars, these could either be compact radio galaxies or reddened quasars. These have been given the flag “Q?” or “g?” in Table 7, depending on the faintness of the optical candidate, and whether a radio core is present. Spectroscopy will be necessary to classify these objects with more certainty.

Deeper CCD images are necessary for the two blank-field sources. For around 20 sources with $R \gtrsim 22.5$, deeper CCD images would be useful for giving more accurate optical positions. IDs of 5 compact radio sources are in doubt because of a significant radio-optical offset. 29 sources have extended radio structure and more than one optical candidate; spectroscopy or higher-resolution radio images will be necessary to confirm these identifications.

Apart from the two fields totally obscured by foreground stars, a further 27 identifications are partially blended with stars. Their photometry and in a few cases their positional accuracy may be affected. Badly affected sources are discussed in more detail in the comments in Section 4.

The columns for Table 7 are as follows:

1. IAU source name. Other names are listed in the Comments on Individual Sources.
2. Classification of the optical counterpart.
3. Right ascension of the optical counterpart, in J2000 co-ordinates.
4. Declination of the optical counterpart, in J2000 co-ordinates.
5. b_J magnitude, usually from the COSMOS database.
6. R magnitude, from the AAT CCD image.
7. Seeing of the AAT CCD image.
8. Redshift. Values in parentheses are estimated from R or b_J , and are therefore uncertain.
9. References: for the first ID in the literature, finding chart, the optical position, the b_J magnitude, and the redshift respectively.

4. COMMENTS ON INDIVIDUAL SOURCES

In the comments below, radio-optical offsets use ATCA radio positions from Table 3 in this paper and MOST radio positions from Table 5 of Paper I. The abbreviation “ACO89” stands for the cluster catalogue of Abell, Corwin, & Olowin (1989).

MRC B0003–567: Unusual S-shaped radio structure, suggestive of a precessing jet. The ATCA image contains strong sidelobes caused by poor *uv*-coverage. The tentative IDs of Westerlund & Smith (1966) and Bajaja (1970) are rejected on positional grounds.

MRC B0008–421: Gigahertz-Peaked-Spectrum (GPS) source. A deeper CCD image will be needed for this very faint ID. The images of di Serego Alighieri et al. (1994) and de Vries et al. (1995) were blank to limiting magnitudes of $V \sim 23$ and $i \sim 23$ respectively. de Vries (2003) found $R = 24.3$, much fainter than our value of $R = 22.6$. One or both values may be affected by error due to the faintness of the source, or the source may be optically variable.

MRC B0013–634: The optical field is partially obscured by the $b_J = 8.7$ star HD 1208.

MRC B0023–333: Wide-angle-tailed source; the VLA image (Ekers et al. 1989) shows a radio core coincident with the optical counterpart, the galaxy ESO 350–G–15, brightest member of the cluster AS 41 (ACO89).

MRC B0036–392: Quasar, blended with a foreground M star at $1''.5$ E, $3''.3$ S (Thomson et al. 1990), and surrounded by several faint objects, possibly an associated cluster.

MRC B0042–357: Large ATCA-optical offset in right ascension ($1''.3$); a higher-resolution radio image is necessary to confirm the ID.

MRC B0043–424: The redshift of 0.116 (Tadhunter et al. 1993) supersedes that reported by Whiteoak (1972). The optical spectrum (Tadhunter et al. 1993) shows weak [O II] and [O III] emission lines. The object is therefore a member of the class of radio galaxies with FR 2 structure and low-excitation optical spectra (Laing et al. 1994).

MRC B0048–447: The ID of Bolton & Shimmins (1973) is rejected on positional grounds.

MRC B0049–433: The fuzzy emission to the east and west of the galaxy is roughly aligned with the radio axis.

MRC B0103–453: Because the radio structure is extended and does not show a core (Jones & McAdam 1992), a higher-resolution radio image will be necessary for a secure ID. Our candidate galaxy lies $17''$ from the MOST centroid.

MRC B0110–692: Blank field on the Schmidt plates. The ID of Jones & McAdam (1992), a $b_J = 21.7$ object, and the two other candidates mentioned by them, all lie too far from the radio axis in a 5 GHz ATCA image (P. Jones, 1992, *priv. comm.*). There is a possible faint counterpart at $01^{\text{h}}11^{\text{m}}43\overset{\text{s}}{.}08 -68^{\circ}59'46\overset{\text{s}}{.}21$ (J2000) on a poor-seeing R -band CCD image.

PKS B0131–36: S0 galaxy NGC 612, studied in detail by Ekers et al. (1978). It contains

a prominent dust lane, and is a rare example of a radio galaxy with a disk.

MRC B0214–480: ESO 198–G–1, in the cluster AS 239 (ACO89).

MRC B0216–366: Stellar object, candidate (b) of Schilizzi (1975), lies 5'' from the MOST centroid. A higher-resolution radio image is necessary to confirm the ID.

MRC B0223–712: The tentative ID of Lasker & Smith (1974) is rejected.

MRC B0240–422: Asymmetric image; possible blend. A $b_J = 20.5$ galaxy, the candidate of Savage et al. (1977), lying 24''.3 E, 22''.0 N of our ID, is closer to the radio centroid but further from the midpoint.

MRC B0251–675: The Savage & Wright (1981) redshift ($z = 2.11$) was based on incorrect line identifications. The ID of Price & Milne (1965) with a cluster of galaxies is rejected on positional grounds.

MRC B0252–712: The ID is blended with a foreground star at 2''.2 E, 1''.1 S (see Tadhunter et al. 1993).

MRC B0315–685: The large ATCA-optical offset of 1''.4 may be due to the extreme faintness of the optical counterpart; a deeper optical image is needed.

PKS B0319–45: The host galaxy ESO 248–G–10 has a dust lane, and coincides with a weak core in the ATCA image of Saripalli et al. (1994). A detailed study of the host galaxy is given by Bryant & Hunstead (2000). The ID of Tritton & Whitworth (1973) is rejected on positional grounds.

MRC B0320–373: Well studied radio galaxy Fornax A, identified with the nearby elliptical galaxy NGC 1316 (Mills 1954). The optical position in Table 7 is that of the nucleus (Schweizer 1981).

PKS B0332–39: ID first suggested by Bolton et al. (1965), and verified by the radio images of Smith (1983) and Ekers et al. (1989). In the cluster A 3135 (ACO89).

MRC B0336–355: Blended at low resolution with the weaker radio source MRC B0336–356, and at first wrongly identified with that source's optical counterpart, the galaxy NGC 1399 (Mills et al. 1960).

MRC B0344–345: In a sparse cluster behind the Fornax cluster. Several other galaxies lie within the bounds of the radio structure, including a $b_J = 17.0$ elliptical galaxy coincident with the peak in the eastern lobe (Smith 1983; Ekers et al. 1989).

MRC B0357–371: A $b_J = 19.5$ galaxy at 1''.7 W, 17''.6 S was suggested as the ID by

Bolton & Shimmins (1973), Wall & Cannon (1973), and Jones & McAdam (1992), but lies outside the radio structure in an ATCA image (R. Subrahmanyan, 1992, *priv. comm.*), and is therefore rejected.

MRC B0407–658: The tentative IDs of Hunstead (1971) and Prestage & Peacock (1983) are rejected on positional grounds.

MRC B0409–752: Our ATCA image has poor hour-angle coverage; the 8.6 GHz image of Reynolds et al. (1993) has higher resolution and dynamic range. The tentative ID of Westerlund & Smith (1966) is rejected on positional grounds, and the IRAS source B04099–7514 is associated not with the radio source but with a galaxy in a foreground cluster.

MRC B0411–647: ‘Fat double’ with extended lobes; a faint possible core lies close to the galaxy ID. Probably associated with the cluster A 3231 (ACO89).

MRC B0420–625: The ID of Lasker & Smith (1974) and Savage et al. (1976a) is rejected on positional grounds.

MRC B0427–366: The central peak of the radio triple is likely to be a hot spot rather than the core, as no object coincides with it on the CCD image. The probable ID, a stellar object, lies further to the south. Spinrad et al. (1979) note this candidate but mark the wrong object on their finding chart.

PKS B0427–53: Dumb-bell galaxy IC 2082, the brightest member of the small cluster AS 463 (ACO89). Identified by Shapley (Basinski et al. 1959). McAdam et al. (1988) find that the radio source is associated with the fainter optical nucleus.

MRC B0429–616: The ID of Jones & McAdam (1992) is rejected on the basis of an ATCA image (Reid 1999), showing a WAT structure with a radio core coinciding with the ID of Unewisse (1993). In the cluster A 3266 (ACO89).

MRC B0436–650: The radio image has low dynamic range. The candidate ID is a faint diffuse galaxy which lies on the radio axis and close to the radio centroid. The stellar ID of Savage et al. (1976a) is rejected.

MRC B0456–301: A VLA image (A. Unewisse, 1993, *priv. comm.*) reveals an amorphous structure with no core or hot spots; possibly a fat double viewed end-on. In the cluster A 3297 (ACO89).

MRC B0509–573: Stellar object, confirmed as a quasar in an unpublished AAT spectrum obtained by R.W.H.

PKS B0511–30: Galaxy, AM 0511–303, coincident with the core in the image of Ekers

et al. (1989). The optical morphology is very disturbed and peculiar (Subrahmanyan et al. 1996). Candidates *b* and *c* of Schilizzi (1975) are rejected.

MRC B0511–484: The long wisps described by Robertson & Smith (1981), and interpreted as tidal debris, appear clearly in the CCD image (Figure 3).

MRC B0513–488: Stellar object, confirmed as a quasar in an unpublished AAT spectrum obtained by R.W.H.

MRC B0521–365: Well studied radio source (Ekers et al. 1989; Keel 1986), identified with ESO 362–G–21. The ID has been classified at different times as an N galaxy (Bolton et al. 1965) and as a BL Lac object (Stein et al. 1976), as both the continuum (Eggen 1970; Shen et al. 1972) and spectral lines (Ulrich 1981) are highly variable. The redshift of 0.061 found by Westerlund & Stokes (1966) is incorrect, possibly because the emission lines were diluted at the time of measurement (Searle & Bolton 1968).

MRC B0602–647: Dumb-bell galaxy; the radio centroid is slightly closer to the south-eastern member of the pair.

MRC B0618–371: Dumb-bell galaxy, ESO 365–IG–6. In the VLA image of Ekers et al. (1989) the radio core is between the two galaxies, but in that of Parma et al. (1991) it coincides with the eastern galaxy.

MRC B0620–526: The optical field is partially obscured by Canopus.

MRC B0625–354: Dumb-bell galaxy, in the cluster A 3392 (ACO89). Partially confused on the Schmidt plates by two foreground stars (Prestage & Peacock 1983).

MRC B0625–536: Dumb-bell galaxy ESO 161–IG–7, the brightest member of the cluster A 3391 (ACO89). An ATCA image (Gregorini et al. 1994) shows that the radio core coincides with the eastern galaxy of the pair.

MRC B0625–545: In the cluster A 3395 (ACO89).

MRC B0658–656: The optical field is obscured by a $b_J = 14.5$ stellar object, suggested as the ID by White et al. (1987), but found to be a foreground star by Thomson et al. (1990).

MRC B0704–427: Stellar object, confirmed as a quasar in an unpublished AAT spectrum obtained by R.W.H.

PKS B0707–35: Galaxy, with an extended asymmetric halo, coincides with the radio core. The ID of Schilizzi (1975) is rejected on positional grounds.

MRC B0743–673: The redshift of 0.395 (Tritton 1971) is incorrect (Jauncey et al. 1989).

MRC B0842–754: Unusual source with radio lobes roughly perpendicular to one another. The radio peak in the ATCA image lies near the optical counterpart, which shows an apparent extension to the north-east on the CCD image (Figure 3). Tadhunter et al. (1993) comment that the emission lines may be extended.

MRC B0846–811: The ID consists of two faint emission regions, aligned with the radio axis: they could be unrelated galaxies, or part of the same galaxy. The position given in Table 7 is that of their centroid.

MRC B0906–682: The optical field is partially obscured by the star HD 78913.

MRC B0943–761: The galaxy ID appears to be the cD of a cluster. This is supported by its detection as a ROSAT source (Brinkmann et al. 1994).

MRC B1030–340: Partially blended with another galaxy 1''.4 E which shows wispy trails, suggesting a tidal interaction. The galaxy pair appears on the Schmidt plate as a single $b_J = 20.7$ galaxy, the ID of De Breuck et al. (2000).

MRC B1036–697: The candidate described by Hunstead et al. (1971) as ‘possibly an unusual galaxy’ appears as two stellar objects on the Schmidt plate; the correct ID is to the south of these.

MRC B1056–360: The elliptical galaxy ID coincides with a weak radio core in the image of Ekers et al. (1989).

MRC B1123–351: Elliptical galaxy ESO 377–G–46, in the cluster AS 665 (ACO89).

MRC B1136–320: Our proposed ID lies on the radio axis and coincides with a possible core in the image of Duncan & Sproats (1992). The ID of Jones & McAdam (1992) is rejected.

MRC B1151–348: Quasar, $z = 0.258$, appears slightly non-stellar on the Schmidt plates.

MRC B1221–423: Unusual galaxy, with a bright nucleus, diffuse envelope, and a blue ‘knot’ of more compact emission to the south (Safouris et al. 2003; Johnston et al. 2005).

MRC B1232–416: The large ATCA-optical offset of 1''.8 may mean this ID is incorrect. The IDs suggested by Savage (1976) and Lasker & Smith (1974) are rejected on positional grounds.

MRC B1234–504: The ID is uncertain: the large radio-optical offset of 2''.5, together with the crowded field at low Galactic latitude, could indicate that the candidate is a foreground star. Deeper observations in good seeing are needed.

MRC B1243–412: Stellar object, confirmed as a quasar in an AAT spectrum obtained by the authors.

MRC B1246–410: Compact steep-spectrum source with unusual Z-shaped radio structure, possibly a short wide-angle-tail source (Burns 1986). The largest angular extent of $32''$ corresponds to 6 kpc, well within the host galaxy, the well studied elliptical galaxy NGC 4696, and brightest member of the Centaurus cluster A 3526 (ACO89).

MRC B1259–769: The ID is unusually faint. The fuzzy object at $4''.3$ W, $0''.9$ N showed no strong emission lines in an AAT spectrum, and is much redder. The two objects are aligned with the radio structure; the redder object may be a companion galaxy, or possibly a foreground object.

MRC B1259–445: Several stellar objects and faint galaxies lie near the radio position. The most likely candidate is the brightest galaxy in a small group. The ID of Jones & McAdam (1992) is probably a foreground star.

MRC B1302–491: Edge-on spiral NGC 4945. The optical properties have been studied in detail by de Vaucouleurs (1964), Peterson (1980), and others.

MRC B1303–827: Stellar object, confirmed as a quasar in an unpublished AAT spectrum.

PKS B1318–434: Elliptical galaxy NGC 5090, interacting with the spiral galaxy NGC 5091; studied in detail by Smith & Bicknell (1986).

MRC B1322–427: Well studied low-luminosity radio source Centaurus A, the nearest radio galaxy, reviewed by Ebneter & Balick (1983) and Israel (1998). The optical counterpart is the dust-lane elliptical galaxy NGC 5128.

MRC B1330–328: The radio structure appears similar to a head-tail source, but the confirmed optical counterpart, a galaxy, lies between the mid-point and the centroid, rather than at one end of the structure. The source is probably a highly asymmetric FR 2 double. The ID of Gearhart et al. (1972) is too far south of the radio position, and that of Peterson & Bolton (1973) was found to be a foreground star by Jauncey et al. (1978). The correct ID is just to the east of this star, not to the west as stated by Simpson et al. (1993).

PKS B1333–33: Galaxy IC 4296, brightest member of the cluster A 3565 (ACO89).

MRC B1346–391: Very faint diffuse ID is partly blended with a stellar object at $2''.2$ W, $1''.4$ S, and a brighter stellar object at $3''.7$ W, $0''.2$ S.

PKS B1400–33: Probable relic radio source associated with the poor cluster around NGC 5419. Refer to Subrahmanyan et al. (2003) for the most up-to-date interpretation of

this enigmatic source.

MRC B1407–425: Unusual amorphous radio source, consisting of extended emission confined within $50''$ (about 50 kpc). Identified with elliptical galaxy ESO 271–G–20. The ATCA image contains a deep negative bowl, because of the sparse coverage at short baselines.

MRC B1445–468: ID is partially obscured by a $b_J = 16.6$ stellar object at $0''.5$ W, $2''.4$ N. The galaxy position could not be measured accurately, but appears to coincide with a probable core in the ATCA image.

MRC B1451–364: The ID of Jones & McAdam (1992) at $18''.3$ E, $13''.8$ S appears stellar on the CCD, and is too far from the radio axis. Our ID is one of their other candidates.

MRC B1526–423: Galaxy, partially blended with a star $2''.1$ W.

MRC B1540–337: Galaxy, partially obscured by a $b_J = 16.5$ stellar object at $3''.4$ E, $1''.2$ N, suggested as the ID by Jauncey et al. (1982), but found later to be a foreground star (Jauncey et al. 1984; Thomson et al. 1990).

MRC B1540–730: Compact object, $6''.7$ from the MOST centroid.

MRC B1549–790: Galaxy, candidate (b) of Prestage & Peacock (1983), is extended north-south on the CCD image, and may be interacting with a close companion. Detected in the IRAS Point Source Catalog (Joint IRAS Science Working Group 1988).

MRC B1610–771: Quasar with a flat radio spectrum and steep optical spectrum (Hunstead & Murdoch 1980; Courbin et al. 1997), blended by COSMOS with a foreground star (Courbin et al. 1997) at $3''.0$ W, $3''.5$ N. b_J was estimated from SuperCOSMOS magnitudes of stars of similar brightness in the same field (Hambly et al. 2001).

MRC B1622–310: The large ATCA-optical offset of $3''.7$ is probably due to poor phase calibration of the ATCA image, as there is good agreement between the MOST and optical positions.

MRC B1633–681: Extended radio source in a crowded optical field – a higher-resolution radio image will be necessary for an unambiguous ID. Tentative ID with faint galaxy, $9''.7$ from the radio centroid.

MRC B1637–771: The redshift of 0.024 reported by Danziger & Goss (1983) may be a typographical error, because the redshifts of Burbidge & Burbidge (1972), Tadhunter et al. (1993) and Simpson et al. (1993) agree with the value of 0.0423 found by Whiteoak (1972).

MRC B1655–776: The redshift of 0.0663 (Whiteoak 1972) is inconsistent with the later value of $z = 0.0944$ (Simpson et al. 1993), which we assume to be correct.

MRC B1716–800: The ID of Price & Milne (1965) with the spiral galaxy IC 4640 is rejected on positional grounds.

MRC B1721–836: The optical candidate is extremely faint: a deeper optical and a higher-resolution radio image are necessary for a secure ID.

MRC B1740–517: The two candidates of Prestage & Peacock (1983) are rejected on positional grounds. The images on the CCD are slightly elongated east-west, owing to tracking errors, and are affected by scattered light from a bright star to the south-west.

MRC B1754–597: The optical object has a faint wisp of emission extending about 4'' to the south-west along a position angle of -108° . The candidates of Bajaja (1970) and Hunstead et al. (1971) are rejected on positional grounds.

MRC B1756–663: Faint galaxy. The ID of Savage (1976) is rejected on positional grounds.

MRC B1814–519: The candidate of Hunstead et al. (1971), a $b_J = 15.8$ stellar object, was found to be a foreground star by Thomson et al. (1990).

MRC B1814–637: Galaxy, partially obscured by a foreground star; ID wrongly rejected by Tritton (1972).

MRC B1817–391: Very crowded optical field: ID is uncertain.

MRC B1818–557: Marked galaxy is the most plausible ID for this extended radio source.

MRC B1840–404: As there is no visible radio core (Duncan & Sproats 1992), and several candidates lie within the radio structure, the ID remains tentative.

MRC B1853–303: Proposed ID is compact and lies 1''.7 from the radio centroid.

MRC B1917–546: The ATCA snapshot image has low dynamic range because of the weakness of the source. There is very faint diffuse emission at around $19^{\text{h}}21^{\text{m}}52\overset{\text{s}}{.}88$, $-54^\circ31'54\overset{\text{s}}{.}0$ (J2000), near the radio core in an unpublished 1.4 GHz ATCA image. A deep image in good seeing is required.

MRC B1922–627: The ID of Jones & McAdam (1992) was found to be a foreground star in an AAT spectrum obtained by the authors.

MRC B1923–328: A deeper optical image is necessary for a secure ID.

MRC B1929–397: Dumb-bell galaxy ESO 338–IG–11, brightest member of the poor cluster AS 820 (ACO89). The radio core in the image of Ekers et al. (1989) coincides with the brighter, south-east member of the pair.

MRC B1932–464: Prestage & Peacock (1983) wrongly rejected this ID.

MRC B1933–587: An AAT spectrum taken on 1989 August 03 shows narrow lines of Ly α and C IV, characteristic of other CSS quasars observed by Baker & Hunstead (1995).

MRC B1940–406: In the cluster A 3646 (ACO89). The two candidates of Schilizzi (1975) are rejected on positional grounds.

MRC B1953–425: The nearby $b_J = 16.8$ stellar object suggested as the ID by Hunstead (1972) was found to be a foreground star by Jauncey et al. (1978).

MRC B1954–552: Bright elliptical galaxy, partially obscured by a bright foreground G0 star (Westerlund & Smith 1966).

MRC B2006–566: Very extended, diffuse ultra-steep-spectrum radio source, associated with the cluster A 3667 (ACO89). This source belongs to the rare class of diffuse relic sources associated with clusters but not with any particular galaxy. The ID of Jones & McAdam (1992) is rejected on the basis of the ATCA image of Röttgering et al. (1997).

MRC B2009–524: The ATCA image has very low dynamic range.

MRC B2020–575: Compact galaxy, possibly blended with a fainter object to the south.

MRC B2028–732: The ID of Price & Milne (1965) with IC 5016 is rejected on positional grounds.

MRC B2031–359: Dumb-bell galaxy ESO 400–IG–40, the dominant member of the cluster A 3695 (ACO89). The radio source is identified with the northern, slightly fainter member of the pair (Bolton & Shimmins 1973).

MRC B2032–350: Galaxy, candidate 2 of di Serego Alighieri et al. (1994). The two faint candidates of Prestage & Peacock (1983) are rejected on positional grounds.

MRC B2041–604: The tentative ID of Westerlund & Smith (1966) is rejected on positional grounds.

MRC B2049–368: The ID of Savage et al. (1976a) is rejected on positional grounds.

MRC B2052–474: The tentative ID of Tritton & Whitworth (1973) is rejected on positional grounds.

MRC B2122–555: Unusual radio triple. The highly asymmetric structure is similar to that of the $z = 0.371$ quasar 3C 351 (see Miley & Hartsuijker 1978).

MRC B2140–434: The extended radio emission is poorly imaged but the ID is secure.

PKS B2148–555: In the cluster A 3816 (ACO89).

MRC B2153–699: Galaxy, object A of Schwarz et al. (1973), identified by Jones & McAdam (1992).

MRC B2201–555: The tentative ID of Bajaja (1970) is rejected on positional grounds.

MRC B2213–456: The IDs of Lasker & Smith (1974), Savage et al. (1976a), and Bajaja (1970) are rejected on positional grounds.

MRC B2223–528: Possible tidal interaction with neighbouring galaxy to south east.

MRC B2226–386: The $b_J = 16.4$ stellar object at 7'' W is a foreground star (Tritton 1971).

MRC B2250–412: Higher-resolution radio image in Morganti et al. (1993). There is an extended emission-line region adjacent to the western lobe (Tadhunter et al. 1994).

MRC B2319–550: The ID of Bolton & Savage (1977) is rejected on positional grounds.

MRC B2323–407: Faint clumpy galaxy, roughly aligned with the radio axis.

MRC B2332–668: A $b_J = 12.6$ foreground star obscures the optical field. The tentative ID of Bajaja (1970), a spiral galaxy, is rejected on positional grounds.

MRC B2354–350: Galaxy, ESO 349–G–10, brightest member of the cluster A 4059 (ACO89), which contains an extended X-ray source, peaked on the radio source (see Heinz et al. 2002).

5. SUMMARY OF SAMPLE CONTENT

We now summarise the global properties of the MS4 sample, and compare them with those of the 3CRR, the northern equivalent. For this purpose we also used the SMS4 sample, a subset of MS4 defined in Paper I to have the same flux-density cutoff, $S_{178\text{ MHz}} = 10.9\text{ Jy}$, so that we could test the uniqueness and completeness of the 3CRR sample. In the future, when more complete angular size and redshift information is available for SMS4, it may be advantageous to combine the 3CRR and SMS4 samples, to improve the statistical accuracy of the derived parameters.

Source numbers and median angular size, redshift (z), linear size (l), and radio power (P_{408}) for the MS4, SMS4, and 3CRR samples are summarised in Table 8. We used cosmological parameters of $H_0 = 71\text{ km s}^{-1}\text{ Mpc}^{-1}$, $\Omega_m = 0.3$, $\Omega_\Lambda = 0.7$ (Spergel et al. 2003) for these and subsequent calculations, unless otherwise stated. Errors of the median were esti-

mated using the method described by Condon & Jauncey (1974). Because fewer than half the MS4 sources have spectroscopic data, the median redshift, linear size, and radio power are uncertain, but even so the median radio power is very similar for SMS4 and 3CRR. The median redshifts for 3CRR and SMS4 are very similar, with the MS4 sample having a slightly higher median redshift, as expected from its lower flux-density limit. The slightly higher median linear size of SMS4 than of 3CRR may not be significant, because of the large errors.

The identification content of the three samples is summarised in Table 9. Taking into account unconfirmed candidates, the fraction of quasars in MS4 is $(18 \pm 3)\%$, compared with $(25 \pm 3)\%$ for 3CRR. The slightly lower proportion of quasars in MS4 is unexpected, given that the quasar fraction of flux-density-limited samples tends to increase with frequency, but the difference is barely significant.

Table 10 contains a brief summary of radio-structure information obtained from other observations besides those in this paper. Column 2 gives the Fanaroff-Riley (or other) structural classification: codes are explained in the footnote to the table. Columns 3 and 4 give the largest angular extent and position angle of extension (in degrees east of north) respectively, and column 5 the reference to the radio image from which these values were measured. The largest angular extent was measured by preference from high-resolution images for compact sources or sources with edge-brightened structure, and from lower-resolution images for sources with extended edge-darkened structures.

The Fanaroff-Riley structural classifications are summarised in Table 11. The radio structures were classified on the basis of the ATCA 5 GHz images or other radio images from the literature (references in Table 10). Fat doubles have been classed with FR1 sources (Owen & Laing 1989), as have sources of borderline FR1/FR2 category. D2 sources and triple sources with edge-brightened lobes have been classified as FR2. Of the unclassified MS4 sources, most do not have images which resolve their structure; five are well resolved but show structure which cannot be readily classified as FR1 or 2.

A detailed comparison of radio structures cannot be made until higher-resolution radio images are available for the unclassified MS4 sources, i.e. those which lie within specific ranges of angular size ($LAS \lesssim 5''$, $35'' < LAS < 75''$). The median angular size of the unclassified sources is around $2''$, much less than the median for the whole MS4 sample of $27''$. Given that FR2 sources in flux-density-limited samples have on average smaller angular size, an unclassified source is therefore much more likely to have FR2 structure. The smaller angular extent can be explained by the higher radio luminosity of FR2 sources, which because of Malmquist bias will ensure that FR2 sources lie on average at higher redshift than sources with FR1 structure. This expectation is supported by the fact that

the proportions of sources classified as FR 1 are similar in the SMS4 and 3CRR samples, suggesting that most of the SMS4 FR 1 sources are likely to have been classified as such already.

A colour-colour plot (α_{843}^{2700} versus α_{408}^{843} , defined in the sense $S_\nu \propto \nu^\alpha$) for the MS4 sample is shown in Figure 5. More sources tend to lie below the diagonal than above, indicating that on average spectra tend to steepen at high frequency. The median values of α_{408}^{843} and α_{843}^{2700} are -0.83 ± 0.02 and -0.91 ± 0.01 respectively.

The MS4 sample contains 41 CSS sources, here defined to have linear size < 25 kpc, and spectral index $\alpha_{408}^{2700} < -0.5$. Those CSS not listed in Table 3 are the ATCA calibrators MRC B1234–504 and MRC B2259–375. The two GPS sources in the MS4 sample are MRC B0008–421 and MRC B1934–638. The SMS4 sample contains no GPS sources; their absence is not surprising as these sources are intrinsically rare (O’Dea 1998), and with spectra that turn over at ~ 1 GHz, are likely to be weak at 178 MHz.

5.1. Apparent Magnitudes and Quasar Redshifts

Histograms of the b_J magnitudes for galaxies and quasars in the MS4 sample are shown in Figure 6. The distribution for quasars peaks at around $b_J = 18.5$, well above the plate limit. In contrast, the galaxy number counts increase up to the plate limit. Comparison with the 3CRR is not possible at present, as a complete set of b_J , B or V magnitudes is not yet available for the entire 3CRR sample.

We have, however, compared the magnitudes of MS4 quasars with those of another radio-selected quasar sample. The median b_J for MS4 quasars is $17.6_{-0.5}^{+0.4}$, compared with 18.8 ± 0.2 for the Molonglo Quasar Sample (MQS: Kapahi et al. 1998; Baker et al. 1999), which was selected to have $S_{408} > 0.95$ Jy. The difference in median magnitudes is consistent with a weak correlation between radio and optical luminosities which has been found for steep-spectrum quasars (Serjeant et al. 1998). The cause of the correlation is not clear, but it is not dominated by effects of redshift or jet orientation (Serjeant et al. 1998).

The median redshifts of quasars in the MS4, SMS4, and 3CRR samples are listed in Table 12. A Kolmogorov-Smirnov two-sample test of the redshift distributions for SMS4 and 3CRR quasars does not show a significant difference at the 10% level. A similar null result was obtained for a comparison between MS4 and 3CRR.

5.2. The V/V_m Test

The V/V_m test (Schmidt 1968; Rowan-Robinson 1968) is a method of studying the space distribution of a flux-density-limited sample. For each source, the volumes V and V_m of two spheres centred at the observer are calculated: the first sphere with the source on its surface, and the second extending to the distance at which the source's flux density would be equal to the sample's limit. The ratio V/V_m always lies between 0 and 1. For a sample uniformly distributed in space and with no luminosity evolution the mean value of V/V_m should be near 0.5. For samples of steep-spectrum quasars, such as those in 3CR, the mean value of V/V_m is around 0.67 ± 0.05 (Masson & Wall 1977; Schmidt 1978), suggesting an excess at high redshift. For samples of flat-spectrum quasars the mean V/V_m is smaller, around 0.57 (Schmidt 1978), suggesting less cosmological evolution. Laing et al. (1983) compared the distributions of V/V_m for the radio galaxies and quasars in the 3CRR sample, and found no significant differences between them at the 20% level. This is consistent with radio galaxies and radio quasars being different forms of the same kind of object.

In order to do a similar test, we calculated V/V_m for the radio galaxies and quasars in the MS4 sample. Because the samples were almost completely optically identified, only the radio flux-density limit of 4.0 Jy was considered, and no optical cutoff was used. For the 117 MS4 sources without spectroscopic redshifts, we used redshifts estimated from R or b_J magnitudes (§ 3.8). The value of V/V_m is not a strong function of estimated redshift. Table 13 shows that V/V_m is very similar for galaxies in each of the three samples. For quasars the SMS4 has a slightly larger mean V/V_m than the 3CRR, but the difference is not significant at the 2σ level.

5.3. Tests of Unified Models

The low selection frequencies of the MS4 and SMS4 samples make them ideal for testing unified schemes of powerful radio sources. In these models (see reviews by Antonucci 1993, Urry & Padovani 1995, Gopal-Krishna 1995, and Wills 1999), the observed properties of radio-loud active galaxies are assumed to be a strong function of the orientation of the radio jet with respect to the observer. At small viewing angles, core and jet flux densities will be enhanced by Doppler boosting (Blandford & Königl 1979). The only viable candidates for the corresponding unbeamed population at larger viewing angles are the powerful radio galaxies (Owen 1986; Scheuer 1987; Peacock 1987), with all radio quasars probably beamed versions of the same objects (Barthel 1989). The difference in their optical properties could be explained by a dusty torus obscuring the broad-line regions and quasar continuum (Barthel 1989).

Provided that the small- and large-scale radio structures are aligned, projected linear sizes of the unbeamed population should be larger on average than those of the beamed objects. As the steep-spectrum emission from the radio lobes is unlikely to be affected by beaming, samples selected at low radio frequency should be relatively free of orientation bias and therefore ideal for testing unified models. Barthel (1989) tested his model on a subset of the 3CRR sample with $0.5 < z < 1$, comparing the numbers and projected linear sizes of the 12 quasars and 30 powerful ($P_{178} \gtrsim 10^{28} \text{ W Hz}^{-1}$) radio galaxies in this redshift range. Barthel excluded the CSS sources from the comparison, but including them did not have a large effect on the results. From the number ratio he inferred that sources viewed at angles of $\psi < 44^\circ.4$ to their jet direction were quasars, and those at larger ψ were galaxies. This value was consistent with the ratio of median linear sizes of the quasars to that of the radio galaxies.

However, the study of Singal (1993) of 3CRR sources at other redshift ranges, and sources from the 1 Jy sample of Allington-Smith (1982), cast doubt on this unified model, because at other redshift ranges, the ratios of quasar to galaxy linear sizes were different. Furthermore, a study of a 408 MHz-selected 1 Jy sample of around 550 sources (Kapahi et al. 1995) found that for $z > 0.5$, the median linear size for quasars is actually larger than for galaxies. Because of the difficulty of interpreting these results in terms of a simple orientation picture, it was important to perform similar tests on another sample. Given the comparative rarity of powerful radio sources at any redshift range, a southern sample such as the MS4 is valuable in supplementing the 3CRR data, despite the fact that the MS4 sample does not yet have a uniform set of spectroscopic information, core flux densities, or high-resolution radio images. Although some of our redshifts are magnitude-based estimates (§ 3.8), in standard cosmological models the ratio of linear to angular size does not vary greatly over the expected range of redshift.

Of the galaxies with high-resolution radio images, only those with unambiguous FR 2 structure have been considered. Extended sources without high-resolution radio images have been classed as FR 2 unless there is evidence to the contrary. To avoid contamination from core-dominated sources, we considered only those sources with 408 MHz *extended* emission above the flux-density limit. We estimated the extended value of S_{408} by assuming the core had a flat radio spectrum ($\alpha = 0$), and subtracting the core flux density at 2300 or 5000 MHz from the total 408 MHz flux density. CSS sources were also excluded for consistency with previous work: it is not certain how the CSS sources may fit in to unified schemes.

In Table 14, linear sizes of MS4 galaxies and quasars in the range $0.5 < z < 1$ are compared with the 3CRR sample. The numbers are slightly different from those of Barthel (1989) because of revisions to 3CRR and because of the different cosmology used here. We

have excluded from the comparison galaxies known to have low-excitation optical spectra, as they may be lacking a quasar nucleus (Laing et al. 1994). The quasar fractions of MS4 and SMS4 are similar to those of 3CRR, but the ratios of quasar to galaxy linear sizes are larger in the southern samples. This may be due to the smaller number of quasars, but it certainly leads one to question the reliability of the earlier interpretation.

To increase the sample size, median linear sizes for the entire redshift range were then compared with two other samples for quasars and one other for galaxies (Table 15). Aside from the SMS4 sample, with only 14 quasars and therefore large uncertainty, the median quasar sizes are larger in the samples selected at lower flux density. On the other hand, the median galaxy sizes do not vary significantly with sample flux density limit.

The model of Gopal-Krishna et al. (1996) accounts for the discrepant linear-size ratios by invoking not only orientation, but temporal evolution of radio linear size and luminosity. Their model also assumes that the critical viewing angle ψ , within which the source's observed optical properties are those of a quasar, is larger for sources with greater initial radio power P_0 . Samples such as 3CRR, containing many sources of high radio luminosity, would be dominated by young sources of high P_0 . Given the similar ages and initial luminosities, orientation effects would dominate, with galaxies being larger than quasars. Samples of lower flux density would contain a greater mix of ages and P_0 values, with old sources of high P_0 likely to be quasars of large linear size, and young sources of low P_0 likely to be galaxies of small linear size. This could explain the comparatively large quasar sizes in the 1 Jy sample of Kapahi et al. (1995). Gopal-Krishna et al. (1996) found the relation between linear-size ratios and quasar fractions for several low-frequency samples to be consistent with their predictions. The MS4 is a useful addition to their data as it occupies a flux-density range between that of the 3CRR and those of weaker samples. For the 131 relevant sources from the MS4, the ratio of median galaxy to median quasar linear sizes is $1.83^{+0.45}_{-0.34}$ (using $H_0 = 50 \text{ km s}^{-1} \text{ Mpc}^{-1}$, $q_0 = 0.5$; the ratio is $1.77^{+0.39}_{-0.43}$ using the more up-to-date cosmological parameters of Spergel et al. 2003), and the quasar fraction is 0.20 ± 0.06 . This lies near the predicted relation for the standard unified scheme, but also near the curves corresponding to different sets of parameters of the model of Gopal-Krishna et al. (1996). It is therefore hard to draw a firm conclusion, but the fact that the MS4 point lies between the points for the stronger 3CRR sample and those for the weaker 1 Jy and B3 samples is consistent with the model of Gopal-Krishna et al. (1996).

6. CONCLUSION

Studies of powerful, steep-spectrum radio sources have for the last forty years drawn largely on the 3C sample and its revisions the 3CR and 3CRR. It is therefore important to know how representative this sample is, especially considering the comparative scarcity of radio sources of high flux density. An independent southern sample, the SMS4, has been constructed from the MS4 sample, and compared with 3CRR. The most important result is that, within the errors, most comparisons of similarly measured quantities show the properties of the 3CRR and its southern equivalent, the SMS4, to be very similar.

The MS4 and SMS4 samples have also been used to test some models of relativistic beaming. The results appear to be consistent with the model of Gopal-Krishna et al. (1996) which predicts that quasar-galaxy differences are affected by evolution as well as orientation.

Acknowledgements

We thank staff and students of the School of Physics, University of Sydney, of Australia Telescope National Facility, and of the Anglo-Australian Observatory for their generous help with observing and data reduction. Special thanks to T. Ye and M. H. Wieringa for their help with processing and calibrating ATCA data, and to J. C. Baker for obtaining redshifts for several objects. Many of the new optical identifications were made in a night of Director's Time on the Anglo-Australian Telescope in May 1994.

This research has used data from the COSMOS/UKST Southern Sky Catalogue provided by the Anglo-Australian Observatory, and the Digitized Sky Surveys, produced at the Space Telescope Science Institute. We have made use of NASA's Astrophysics Data System Abstract Service, and the NASA/IPAC Extragalactic Database (NED) which is operated by the Jet Propulsion Laboratory, Caltech, under contract with the US National Aeronautics and Space Administration. The Molonglo Observatory Synthesis telescope is funded by both the Australian Research Council and the Science Foundation for Physics within the University of Sydney. The Australia Telescope Compact Array (ATCA) is part of the Australia telescope, which is funded by the Commonwealth of Australia for operation as a National Facility managed by CSIRO. AMB acknowledges the receipt of an Australian Postgraduate Research Award over the period of this research.

REFERENCES

- Abell, G. O., Corwin, H. G., & Olowin, R. P. 1989, ApJS, 70, 1 (ACO89)
- Allington-Smith, J. R. 1982, MNRAS, 199, 611
- Alvarez, H., Aparici, J., May, J., & Navarrete, M. 1993, A&A, 271, 435
- Antonucci, R. 1993, ARA&A, 31, 473
- Baade, W. & Minkowski, R. 1954, ApJ, 119, 215
- Bahcall, J. N. & Soneira, R. M. 1980, ApJS, 44, 73
- Bajaja, E. 1970, AJ, 75, 667
- Baker, J. C. & Hunstead, R. W. 1995, ApJ, 452, L95
- Baker, J. C., Hunstead, R. W., Kapahi, V. K., & Subrahmanya, C. R. 1999, Ap. J. Suppl., 122, 29, arXiv:astro-ph/9902348
- Barthel, P. D. 1989, ApJ, 336, 606
- Basinski, J., Bok, B. J., & Gottlieb, K. 1959, in Paris Symposium on Radio Astronomy, ed. R. N. Bracewell, IAU Symp. 9 (Stanford, Calif.: Stanford University Press), 514
- Bergeron, J. & Kunth, D. 1984, MNRAS, 207, 263
- Blandford, R. D. & Königl, A. 1979, ApJ, 232, 34
- Bolton, J. G., Clarke, M. E., & Ekers, R. D. 1965, Aust. J. Phys., 18, 627
- Bolton, J. G., Gardner, F. F., & Mackey, M. B. 1964, Aust. J. Phys., 17, 340
- Bolton, J. G., Peterson, B. A., Wills, B. J., & Wills, D. 1976, ApJ, 210, L1
- Bolton, J. G. & Savage, A. 1977, Aust. J. Phys. Astrophys. Suppl., 41, 25
- Bolton, J. G. & Shimmins, A. J. 1973, Aust. J. Phys. Astrophys. Suppl., 30, 1
- Bolton, J. G., Shimmins, A. J., & Merkelijn, J. 1968, Aust. J. Phys., 21, 81
- Bolton, J. G., Stanley, G. J., & Slee, O. B. 1949, Nature, 164, 101
- Bridle, A. H. 1989, in ASP Conf. Ser., Vol. 6, Synthesis Imaging in Radio Astronomy, ed. R. A. Perley, F. R. Schwab, & A. H. Bridle (San Francisco: ASP), 443

- Bridle, A. H. & Fomalont, E. B. 1978, AJ, 83, 704
- Brinkmann, W., Siebert, J., & Boller, T. 1994, A&A, 281, 355
- Browne, I. W. & Savage, A. 1977, MNRAS, 179, 65P
- Bryant, J. J. & Hunstead, R. W. 2000, ApJ, 545, 216, arXiv:astro-ph/0008192
- Burbidge, E. M. & Burbidge, G. R. 1972, ApJ, 172, 37
- Burgess, A. M. & Hunstead, R. W. 1995, Publ. Astron. Soc. Aust., 12, 227
- . 2006, AJ, in press (Paper I)
- Burns, J. O. 1986, Can. J. Phys., 64, 373
- Campbell-Wilson, D. & Hunstead, R. W. 1994, Proc. Astron. Soc. Aust., 11, 33
- Carter, D. & Malin, D. F. 1983, MNRAS, 203, 49P
- Christiansen, W. N., Frater, R. H., Watkinson, A., O’Sullivan, J. D., Lockhart, I. A., & Goss, W. M. 1977, MNRAS, 181, 183
- Clark et al. 1997, MNRAS, 286, 558
- Collins, C. A., Guzzo, L., Nichol, R. C., & Lumsden, S. L. 1995, MNRAS, 274, 1071, arXiv:astro-ph/9502023
- Condon, J. J. & Jauncey, D. L. 1974, AJ, 79, 1220
- Cooper, B. F. C., Price, R. M., & Cole, D. J. 1965, Aust. J. Phys., 18, 589
- Cornwell, T. & Fomalont, E. B. 1989, in ASP Conf. Ser., Vol. 6, Synthesis Imaging in Radio Astronomy, ed. R. A. Perley, F. R. Schwab, & A. H. Bridle (San Francisco: ASP), 185
- Courbin, F., Hutsemékers, D., Meylan, G., Magain, P., & Djorgovski, S. G. 1997, A&A, 317, 656, arXiv:astro-ph/9606114
- Danziger, I. J., Fosbury, R. A., Goss, W. M., & Ekers, R. D. 1979, MNRAS, 188, 415
- Danziger, I. J., Fosbury, R. A., & Penston, M. V. 1977, MNRAS, 179, 41P
- Danziger, I. J. & Goss, W. M. 1979, MNRAS, 186, 93
- . 1983, MNRAS, 202, 703

- De Breuck, C., Hunstead, R. W., Sadler, E. M., Rocca-Volmerange, B., & Klamer, I. 2004, MNRAS, 347, 837, arXiv:astro-ph/0309814
- De Breuck, C., van Breugel, W., Röttgering, H. J. A., & Miley, G. 2000, A&AS, 143, 303, arXiv:astro-ph/0002297
- De Breuck, C., van Breugel, W., Stanford, S. A., Röttgering, H., Miley, G., & Stern, D. 2002, AJ, 123, 637, arXiv:astro-ph/0109540
- De Breuck et al. 2001, AJ, 121, 1241, arXiv:astro-ph/0012065
- de Vaucouleurs, G. 1964, ApJ, 139, 899
- de Vries, W. 2003, Publ. Astron. Soc. Aust., 20, 6
- de Vries, W. H., Barthel, P. D., & Hes, R. 1995, A&AS, 114, 259
- di Serego Alighieri, S., Danziger, I. J., Morganti, R., & Tadhunter, C. N. 1994, MNRAS, 269, 998
- Downes, A. J. B., Peacock, J. A., Savage, A., & Carrie, D. R. 1986, MNRAS, 218, 31
- Drinkwater, M. J., Barnes, D. G., & Ellison, S. L. 1995, Publ. Astron. Soc. Aust., 12, 248
- Drinkwater, M. J., Gregg, M. D., Holman, B. A., & Brown, M. J. I. 2001, MNRAS, 326, 1076, arXiv:astro-ph/0106376
- Duncan, R. A. & Sproats, L. N. 1992, Proc. Astron. Soc. Aust., 10, 16
- Eales, S. A. 1985, MNRAS, 213, 899
- Ebneter, K. & Balick, B. 1983, PASP, 95, 675
- Eggen, O. J. 1970, ApJ, 159, L95
- Ekers, R. D. 1970, Aust. J. Phys., 23, 217
- Ekers, R. D., Goss, W. M., Kotanyi, C. G., & Skellern, D. J. 1978, A&A, 69, L21
- Ekers et al. 1989, MNRAS, 236, 737
- Ellis, R. S., Gray, P. M., Carter, D., & Godwin, J. 1984, MNRAS, 206, 285
- Eracleous, M. & Halpern, J. P. 2004, ApJS, 150, 181, arXiv:astro-ph/0309498
- Evans, D. W. 1989, A&AS, 78, 249

- Fanaroff, B. L. & Riley, J. M. 1974, MNRAS, 167, 31P
- Fosbury, R. A. E., Morganti, R., Wilson, W., Ekers, R. D., di Serego Alighieri, S., & Tadhunter, C. N. 1998, MNRAS, 296, 701, arXiv:astro-ph/9801249
- Fosbury et al. 1982, MNRAS, 201, 991
- Frater, R. H., Brooks, J. W., & Whiteoak, J. B. 1992, Journal of Electrical and Electronics Engineering, Australia, 12, 103
- Fricke, K. J., Kollatschny, W., & Witzel, A. 1983, A&A, 117, 60
- Fugmann, W., Meisenheimer, K., & Röser, H.-J. 1988, A&AS, 75, 173
- Gearhart, M. R., Lund, J. M., Frantz, D. J., & Kraus, J. D. 1972, AJ, 77, 557
- Gopal-Krishna. 1995, Proc. Natl. Acad. Sci. USA, 92, 11399
- Gopal-Krishna, Kulkarni, V. K., & Wiita, P. J. 1996, ApJ, 463, L1, arXiv:astro-ph/9603096
- Graham, J. A. 1979, ApJ, 232, 60
- . 1982, PASP, 94, 244
- Grandi, S. A. 1983, MNRAS, 204, 691
- Gregorini, L., de Ruiter, H. R., Parma, P., Sadler, E. M., Vettolani, G., & Ekers, R. D. 1994, A&AS, 106, 1
- Gunn, J. E. & Stryker, L. L. 1983, ApJS, 52, 121
- Hambly et al. 2001, MNRAS, 326, 1279, arXiv:astro-ph/0108286
- Hardcastle, M. J., Worrall, D. M., & Birkinshaw, M. 1999, MNRAS, 305, 246, arXiv:astro-ph/9812148
- Heinz, S., Choi, Y., Reynolds, C. S., & Begelman, M. C. 2002, ApJ, 569, L79, arXiv:astro-ph/0201107
- Joint IRAS Science Working Group 1988, Infrared Astronomical Satellite Catalogs and Atlases, Vol. 1-6 (US Government Printing Office)
- Heydon-Dumbleton, N. H., Collins, C. A., & MacGillivray, H. T. 1988, in Large-scale structures in the universe – Observational and analytical methods, ed. W. C. Seitter, H. W. Dürbeck, & M. Tacke (Berlin: Springer-Verlag), 71

- Huang, Z. & Sarazin, C. L. 1998, ApJ, 496, 728, arXiv:astro-ph/9710213
- Humason, M. L., Mayall, N. U., & Sandage, A. R. 1956, AJ, 61, 97
- Hunstead, R. W. 1971, MNRAS, 152, 277
- . 1972, MNRAS, 157, 367
- . 1991, Aust. J. Phys., 44, 743
- . 1994, Aust. J. Phys., 47, 657
- Hunstead, R. W., Durdin, J. M., Little, A. G., Reynolds, J. E., & Kesteven, M. J. 1982, Proc. Astron. Soc. Aust., 4, 447
- Hunstead, R. W., Lasker, B. M., Mintz, B., & Smith, M. G. 1971, Aust. J. Phys., 24, 601
- Hunstead, R. W. & Murdoch, H. S. 1980, MNRAS, 192, 31P
- Hunstead, R. W., Murdoch, H. S., & Shobbrook, R. R. 1978, MNRAS, 185, 149
- Isobe, T., Feigelson, E. D., Akritas, M. G., & Babu, G. J. 1990, ApJ, 364, 104
- Israel, F. P. 1998, Astron. Astrophys. Rev., 8, 237, arXiv:astro-ph/9811051
- Jackson, C. A., Wall, J. V., Shaver, P. A., Kellermann, K. I., Hook, I. M., & Hawkins, M. R. S. 2002, A&A, 386, 97
- Jauncey, D. L., Batty, M. J., Gulkis, S., & Savage, A. 1982, AJ, 87, 763
- Jauncey, D. L., Batty, M. J., Wright, A. E., Peterson, B. A., & Savage, A. 1984, ApJ, 286, 498
- Jauncey, D. L., Savage, A., Morabito, D. D., Preston, R. A., Nicolson, D. G., & Tzioumis, A. K. 1989, AJ, 98, 54
- Jauncey, D. L., White, G. L., Batty, M. J., & Preston, R. A. 1986, AJ, 92, 1036
- Jauncey, D. L., Wright, A. E., Peterson, B. A., & Condon, J. J. 1978, ApJ, 219, L1
- Johnston, H. M., Hunstead, R. W., Cotter, G., & Sadler, E. M. 2005, MNRAS, 356, 515, arXiv:astro-ph/0410174
- Jones, L. R., Fong, R., Shanks, T., Ellis, R. S., & Peterson, B. A. 1991, MNRAS, 249, 481
- Jones, P. A. 1989, Proc. Astron. Soc. Aust., 8, 81

- . 1992, Aust. J. Phys., 45, 797
- Jones, P. A. & McAdam, W. B. 1992, ApJS, 80, 137
- Kapahi, V. K., Athreya, R. M., Subrahmanya, C. R., Baker, J. C., Hunstead, R. W., McCarthy, P. J., & van Breugel, W. 1998, Ap. J. Suppl., 118, 327
- Kapahi, V. K., Athreya, R. M., Subrahmanya, C. R., Hunstead, R. W., Baker, J. C., McCarthy, P. J., & van Breugel, W. 1995, J. Astrophys. Astr. (Suppl.), 16, 125
- Keel, W. C. 1986, ApJ, 302, 296
- Kemp, S. N. 1994, A&A, 282, 425
- Killeen, N. E. B. & Bicknell, G. V. 1988, ApJ, 325, 180
- Killeen, N. E. B., Bicknell, G. V., & Carter, D. 1986, ApJ, 309, 45
- Laing, R. A., Jenkins, C. R., Wall, J. V., & Unger, S. W. 1994, in ASP Conf. Ser., Vol. 54, The First Stromlo Symposium: The Physics of Active Galaxies, ed. G. V. Bicknell, M. A. Dopita, & P. J. Quinn (San Francisco: ASP), 201
- Laing, R. A., Riley, J. M., & Longair, M. S. 1983, MNRAS, 204, 151
- Lasker, B. M. & Smith, M. G. 1974, Aust. J. Phys., 27, 135
- Lasker, B. M., Sturch, C. R., McLean, B. J., Russell, J. L., Jenkner, H., & Shara, M. M. 1990, AJ, 99, 2019
- Lü, P. K. 1970a, AJ, 75, 1161
- . 1970b, AJ, 75, 1164
- Lü, P. K. 1974, AJ, 79, 453
- Ma et al. 1998, AJ, 116, 516
- Macdonald, G. H. & Miley, G. K. 1971, ApJ, 164, 237
- Marenbach, G. & Appenzeller, I. 1982, A&A, 108, 95
- Masson, C. R. & Wall, J. V. 1977, MNRAS, 180, 193
- McAdam, W. B. & Schilizzi, R. T. 1977, A&A, 55, 67
- McAdam, W. B., White, G. L., & Bunton, J. D. 1988, MNRAS, 235, 425

- Miley, G. K. & Hartsuijker, A. P. 1978, *A&AS*, 34, 129
- Mills, B. Y. 1954, *Observatory*, 74, 248
- Mills, B. Y., Slee, O. B., & Hill, E. R. 1960, *Aust. J. Phys.*, 13, 676
- Morganti, R., Killeen, N. E. B., & Tadhunter, C. N. 1993, *MNRAS*, 263, 1023
- Morganti, R., Oosterloo, T., Tadhunter, C. N., Aiudi, R., Jones, P., & Villar-Martin, M. 1999, *A&AS*, 140, 355, arXiv:astro-ph/9910150
- Morrison, J. E. 1995, in *ASP Conf. Ser.*, Vol. 77, *Astronomical Data Analysis Software and Systems IV*, ed. R. A. Shaw, H. E. Payne, & J. J. E. Haynes (San Francisco: ASP), 179
- Morton, D. C., Savage, A., & Bolton, J. G. 1978, *MNRAS*, 185, 735
- Mullan, D. J. 1970, *Irish Astr. J.*, 9, 246
- Murdoch, H. S., Hunstead, R. W., & White, G. L. 1984, *Proc. Astron. Soc. Aust.*, 5, 341
- Muriel, H., Nicotra, M. A., & Lambas, D. G. 1995, *AJ*, 110, 1032
- Norris et al. 1990, *Proc. Astron. Soc. Aust.*, 8, 252
- O'Dea, C. P. 1998, *PASP*, 110, 493
- Owen, F. N. 1986, in *Quasars*, ed. G. Swarup & V. K. Kapahi, IAU Symp. 119 (Dordrecht: Reidel), 173
- Owen, F. N. & Laing, R. A. 1989, *MNRAS*, 238, 357
- Parma, P., Cameron, R. A., & Deruitter, H. R. 1991, *AJ*, 102, 1960
- Peacock, J. A. 1987, in *Astrophysical jets and their engines*, ed. W. Kundt (Dordrecht: Reidel), 185
- Penston, M. V. & Fosbury, R. A. 1978, *MNRAS*, 183, 479
- Perryman, M. A. C. 1979, *MNRAS*, 187, 683
- Peterson, B. A. & Bolton, J. G. 1972, *Ap. Lett.*, 10, 105
- . 1973, *Ap. Lett.*, 13, 187
- Peterson, B. A., Bolton, J. G., & Shimmins, A. J. 1973, *Ap. Lett.*, 15, 109

- Peterson, B. A., Jauncey, D. L., Wright, A. E., & Condon, J. J. 1976, ApJ, 207, L5
- Peterson, C. J. 1980, PASP, 92, 397
- Prestage, R. M. & Peacock, J. A. 1983, MNRAS, 204, 355
- Price, R. M. & Milne, D. K. 1965, Aust. J. Phys., 18, 329
- Quintana, H. & Ramírez, A. 1995, ApJS, 96, 343
- Rayner, D. P., Norris, R. P., & Sault, R. J. 2000, MNRAS, 319, 484
- Reid, A. D. 1999, PhD thesis, University of Sydney
- Reynolds, J. 1994, Flux Scale for the AT Compact Array, Tech. Rep. 39.3/040, ATNF
- Reynolds et al. 1993, in Sub-arcsecond Radio Astronomy, ed. R. J. Davis & R. S. Booth (Cambridge: Cambridge University Press), 156
- Robertson, J. G. & Smith, R. M. 1981, Proc. Astron. Soc. Aust., 4, 187
- Röttgering, H. J. A., Miley, G. K., Chambers, K. C., & Macchetto, F. 1995, A&AS, 114, 51
- Röttgering, H. J. A., Wieringa, M. H., Hunstead, R. W., & Ekers, R. D. 1997, MNRAS, 290, 577
- Rowan-Robinson, M. 1968, MNRAS, 138, 445
- Safouris, V., Hunstead, R. W., & Prouton, O. R. 2003, Publ. Astron. Soc. Aust., 20, 1
- Sandage, A. 1972, ApJ, 178, 25
- Saripalli, L., Subrahmanyan, R., & Hunstead, R. W. 1994, MNRAS, 269, 37
- Savage, A. 1976, MNRAS, 174, 259
- Savage, A., Bolton, J. G., & Wright, A. E. 1976a, MNRAS, 175, 517
- . 1977, MNRAS, 179, 135
- Savage, A., Browne, I. W., & Bolton, J. G. 1976b, MNRAS, 177, 77P
- Savage, A. & Wright, A. E. 1981, MNRAS, 196, 927
- Scheuer, P. A. G. 1987, in Superluminal radio sources, ed. J. A. Zensus & T. J. Pearson (Cambridge: Cambridge University Press), 104

- Schilizzi, R. T. 1975, Mem. R. Astron. Soc., 79, 75
- Schilizzi, R. T. & McAdam, W. B. 1970, Proc. Astron. Soc. Aust., 1, 337
- Schmidt, M. 1968, ApJ, 151, 393
- . 1978, Physica Scripta, 17, 329
- Schneider et al. 1992, PASP, 104, 678
- Schwab, F. R. 1984, AJ, 89, 1076
- Schwarz, U. J., Cole, D. J., & Morris, D. 1973, Aust. J. Phys., 26, 661
- Schweizer, F. 1980, ApJ, 237, 303
- . 1981, ApJ, 246, 722
- Searle, L. & Bolton, J. G. 1968, ApJ, 154, L101
- Serjeant, S., Rawlings, S., Maddox, S. J., Baker, J. C., Clements, D., Lacy, M., & Lilje, P. B. 1998, MNRAS, 294, 494, arXiv:astro-ph/9710106
- Shectman, S. A., Landy, S. D., Oemler, A., Tucker, D. L., Lin, H., Kirshner, R. P., & Schechter, P. L. 1996, ApJ, 470, 172, arXiv:astro-ph/9604167
- Shen, B. S. P., Usher, P. D., & Barrett, J. W. 1972, ApJ, 171, 457
- Shimmins, A. J. & Bolton, J. G. 1974, Aust. J. Phys. Astrophys. Suppl., 32, 1
- Shimmins, A. J., Bolton, J. G., Peterson, B. A., & Wall, J. V. 1971, Ap. Lett., 8, 139
- Shobbrook, R. 1963, Observatory, 83, 36
- Shobbrook, R. & Hunstead, R. W. 1966, Observatory, 86, 204
- Shobbrook, R. R. & Shaver, P. A. 1967, Observatory, 87, 169
- Simpson, C., Clements, D. L., Rawlings, S., & Ward, M. 1993, MNRAS, 262, 889
- Singal, A. K. 1993, MNRAS, 262, L27
- Smith, R. M. 1983, PhD thesis, Australian National University
- Smith, R. M. & Bicknell, G. V. 1983, Proc. Astron. Soc. Aust., 5, 251
- . 1986, ApJ, 308, 36

- Sodré, L., Capelato, H. V., Steiner, J. E., Proust, D., & Mazure, A. 1992, MNRAS, 259, 233
- Spergel et al. 2003, ApJS, 148, 175, arXiv:astro-ph/0302209
- Spinrad, H., Kron, R. G., & Hunstead, R. W. 1979, ApJS, 41, 701
- Stein, W. A., Odell, S. L., & Strittmatter, P. A. 1976, ARA&A, 14, 173
- Stickel, M. & Kühr, H. 1996, A&AS, 115, 11
- Stickel, M., Meisenheimer, K., & Kühr, H. 1994, A&AS, 105, 211
- Subrahmanyan, R., Beasley, A. J., Goss, W. M., Golap, K., & Hunstead, R. W. 2003, AJ, 125, 1095, arXiv:astro-ph/0212154
- Subrahmanyan, R., Saripalli, L., & Hunstead, R. W. 1996, MNRAS, 279, 257
- Tadhunter, C., Shaw, M., N., C., & Morganti, R. 1994, A&A, 288, L21
- Tadhunter, C. N., Morganti, R., di Serego Alighieri, S., Fosbury, R. A., & Danziger, I. 1993, MNRAS, 263, 999
- Teague, P. F., Carter, D., & Gray, P. M. 1990, ApJS, 72, 715
- Thomson, D. J., Djorgovski, S., & de Carvalho, R. 1990, PASP, 102, 1235
- Torres, C. & Wroblewski, H. 1984, A&A, 141, 271
- Tritton, K. P. 1971, MNRAS, 155, 1P
- . 1972, MNRAS, 158, 277
- Tritton, K. P. & Schilizzi, R. T. 1973, MNRAS, 165, 245
- Tritton, K. P. & Whitworth, D. P. 1973, MNRAS, 165, 253
- Ulrich, M. H. 1981, A&A, 103, L1
- Unewisse, A. M. 1993, PhD thesis, University of Sydney
- Unewisse, A. M., Hunstead, R. W., & Piestrzynski, B. 1993, Proc. Astron. Soc. Aust., 10, 229
- Urry, C. M. & Padovani, P. 1995, PASP, 107, 803, arXiv:astro-ph/9506063
- Véron, M. P. 1977, AJ, 82, 937

- Véron, P., Véron, M. P., Djorgovski, S., Magain, P., Meylan, G., & Surdej, J. 1990, A&AS, 86, 543
- Vettolani, G., Cappi, A., Chincarini, G., Focardi, P., Garilli, B., Gregorini, L., & Maccagni, D. 1989, A&AS, 79, 147
- Villar-Martín, M., Tadhunter, C., Morganti, R., Clark, N., Killeen, N., & Axon, D. 1998, A&A, 332, 479, arXiv:astro-ph/9801039
- Wall, J. V. & Cannon, R. D. 1973, Aust. J. Phys. Astrophys. Suppl., 31, 1
- Westerlund, B. E. & Smith, L. F. 1966, Aust. J. Phys., 19, 181
- Westerlund, B. E. & Stokes, N. R. 1966, ApJ, 145, 354
- Westerlund, B. E. & Wall, J. V. 1969, AJ, 74, 335
- White, G. L., Batty, M. J., Bunton, J. D., Brown, D. R., & Corben, J. B. 1987, MNRAS, 227, 705
- White, G. L., Jauncey, D. L., Wright, A. E., Batty, M. J., Savage, A., Peterson, B. A., & Gulkis, S. 1988a, ApJ, 327, 561
- White, G. L., McAdam, W. B., & Jones, I. G. 1988b, MNRAS, 233, 189
- Whiteoak, J. B. 1972, Aust. J. Phys., 25, 233
- Willmer, C. N. A., Focardi, P., Chan, R., Pellegrini, P. S., & da Costa, L. N. 1991, AJ, 101, 57
- Wills, B. 1999, in ASP Conf. Ser., Vol. 162, Quasars and Cosmology, ed. G. Ferland & J. Baldwin (San Francisco: ASP), 101, arXiv:astro-ph/9905093
- Wright, A. E., Jauncey, D. L., Peterson, B. A., & Condon, J. J. 1977, ApJ, 211, L115
- Yentis, D. J., Cruddace, R. G., Gursky, H., Stuart, B. V., Wallin, J. F., MacGillivray, H. T., & Collins, C. A. 1992, in Digitised Optical Sky Surveys, ed. H. T. MacGillivray & E. B. Thomson (Dordrecht: Kluwer), 67

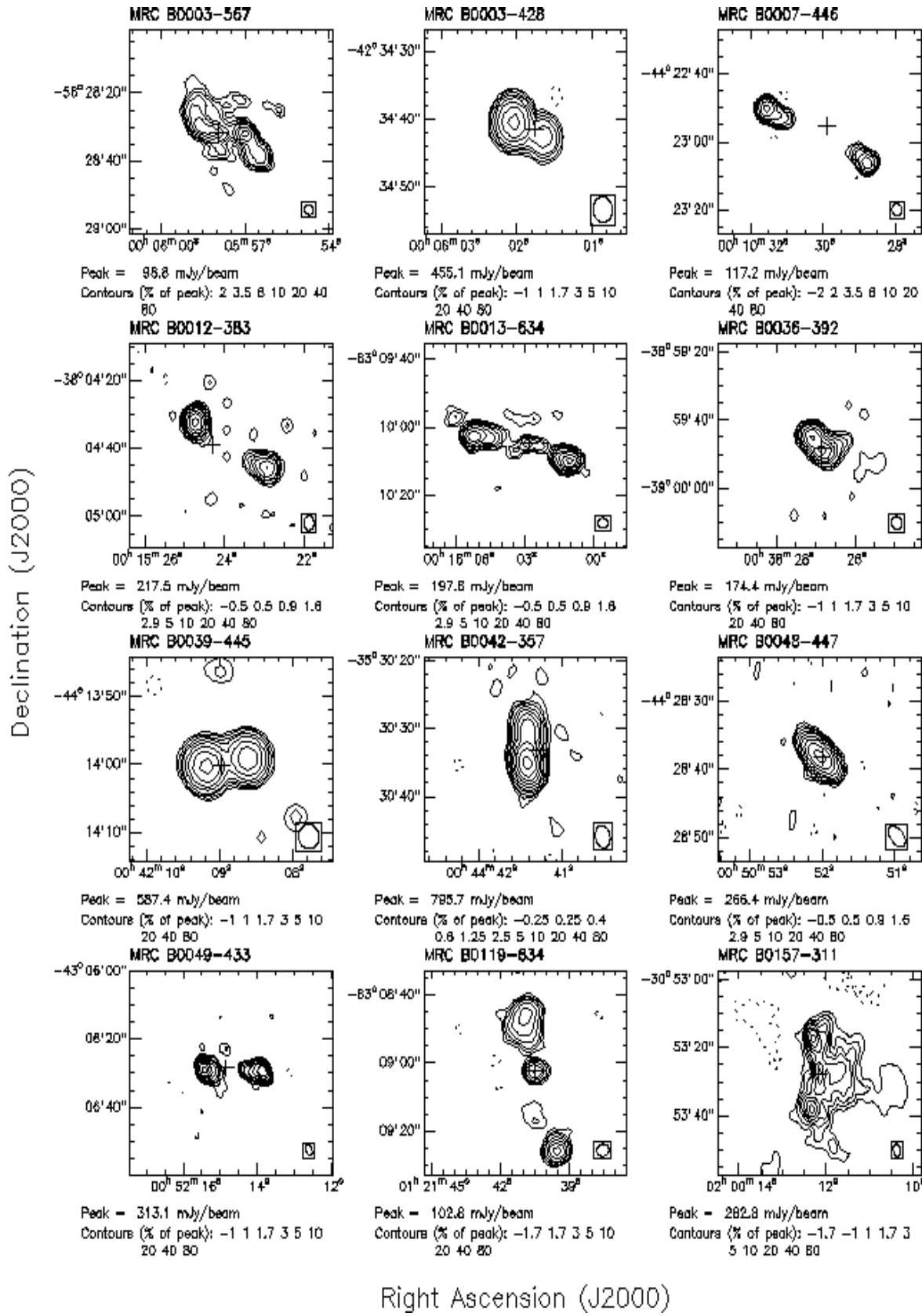


Fig. 1.— ATCA contour maps

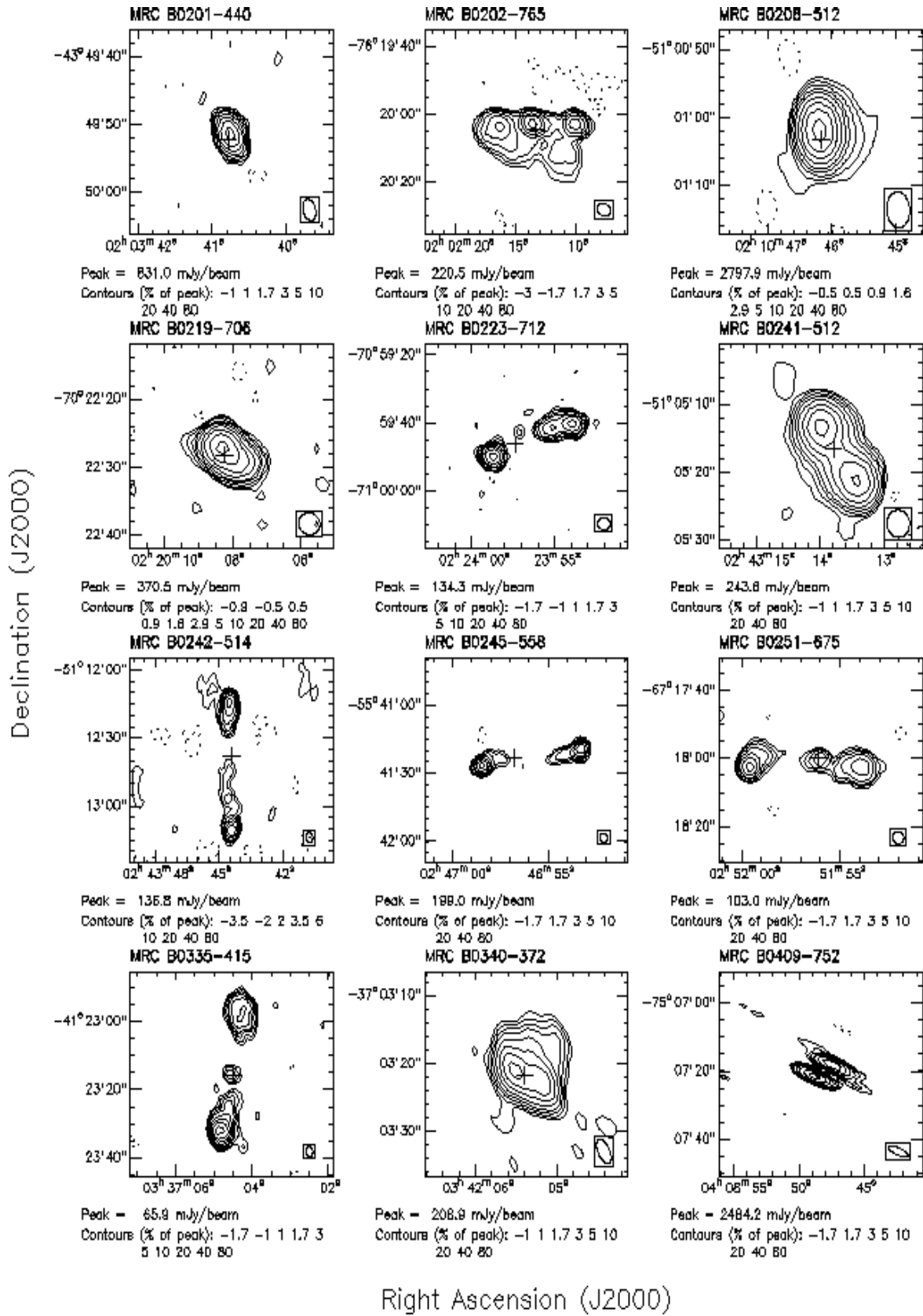


Fig. 1.— ATCA contour maps (continued).

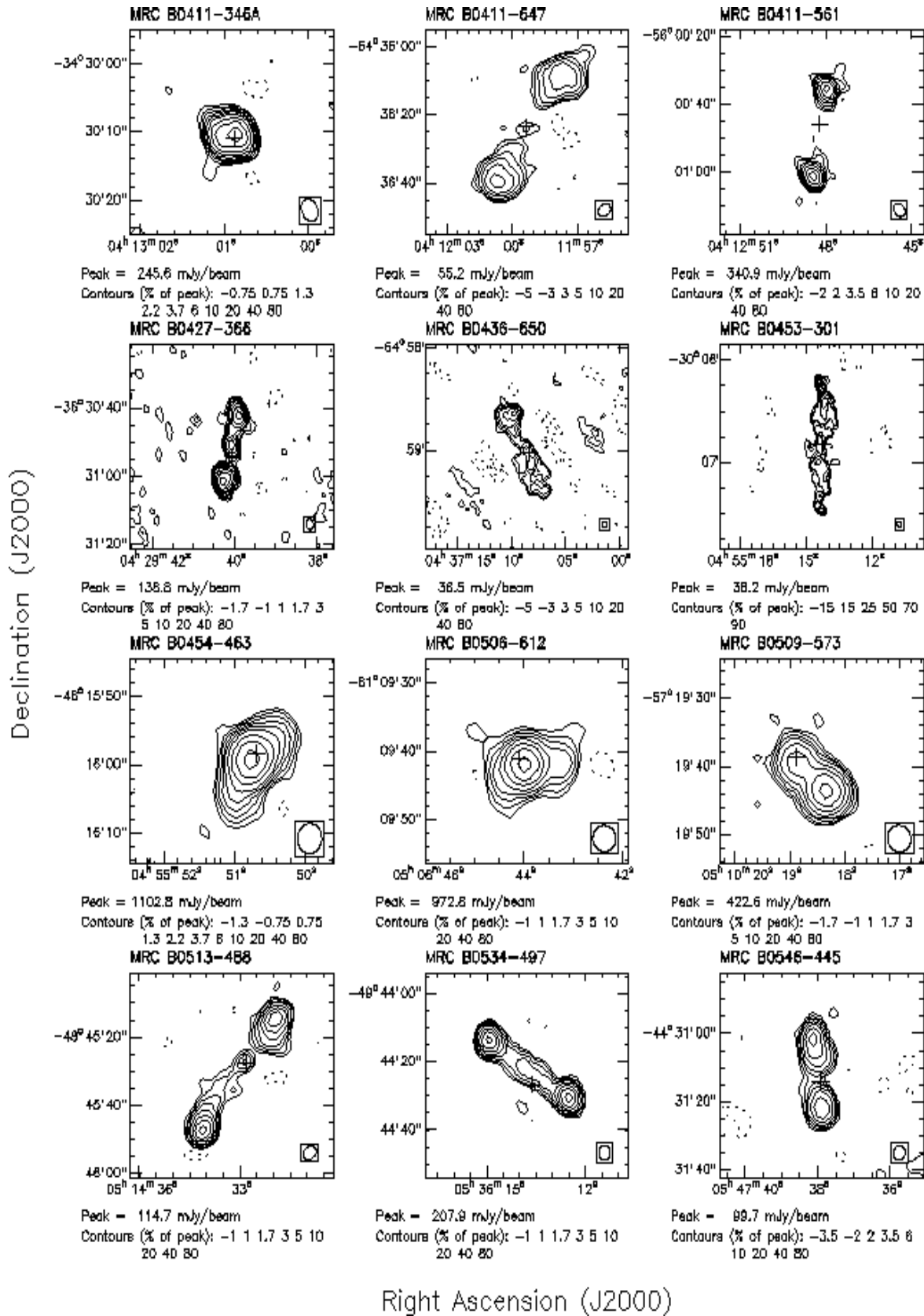


Fig. 1.— ATCA contour maps (continued).

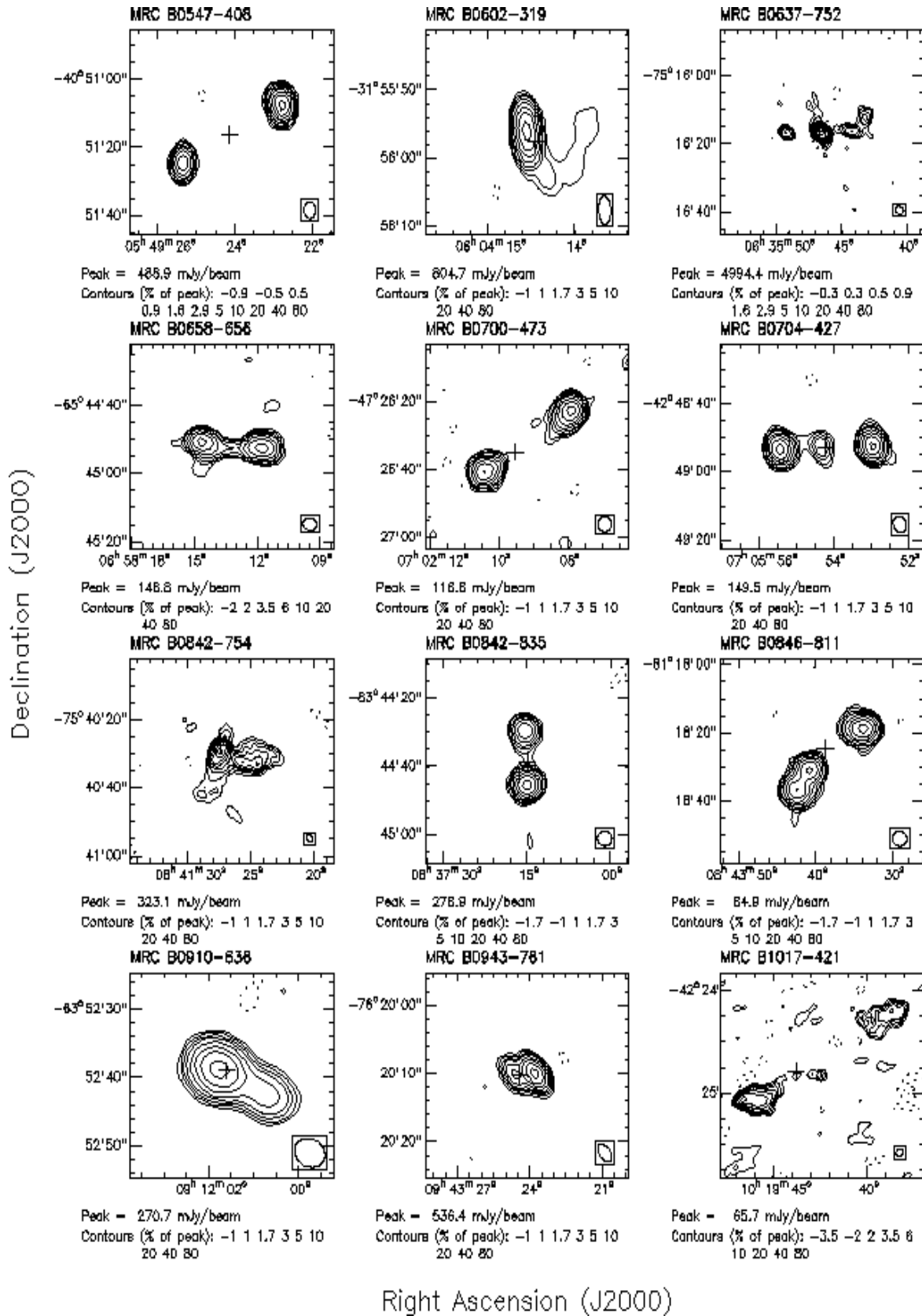


Fig. 1.— ATCA contour maps (continued).

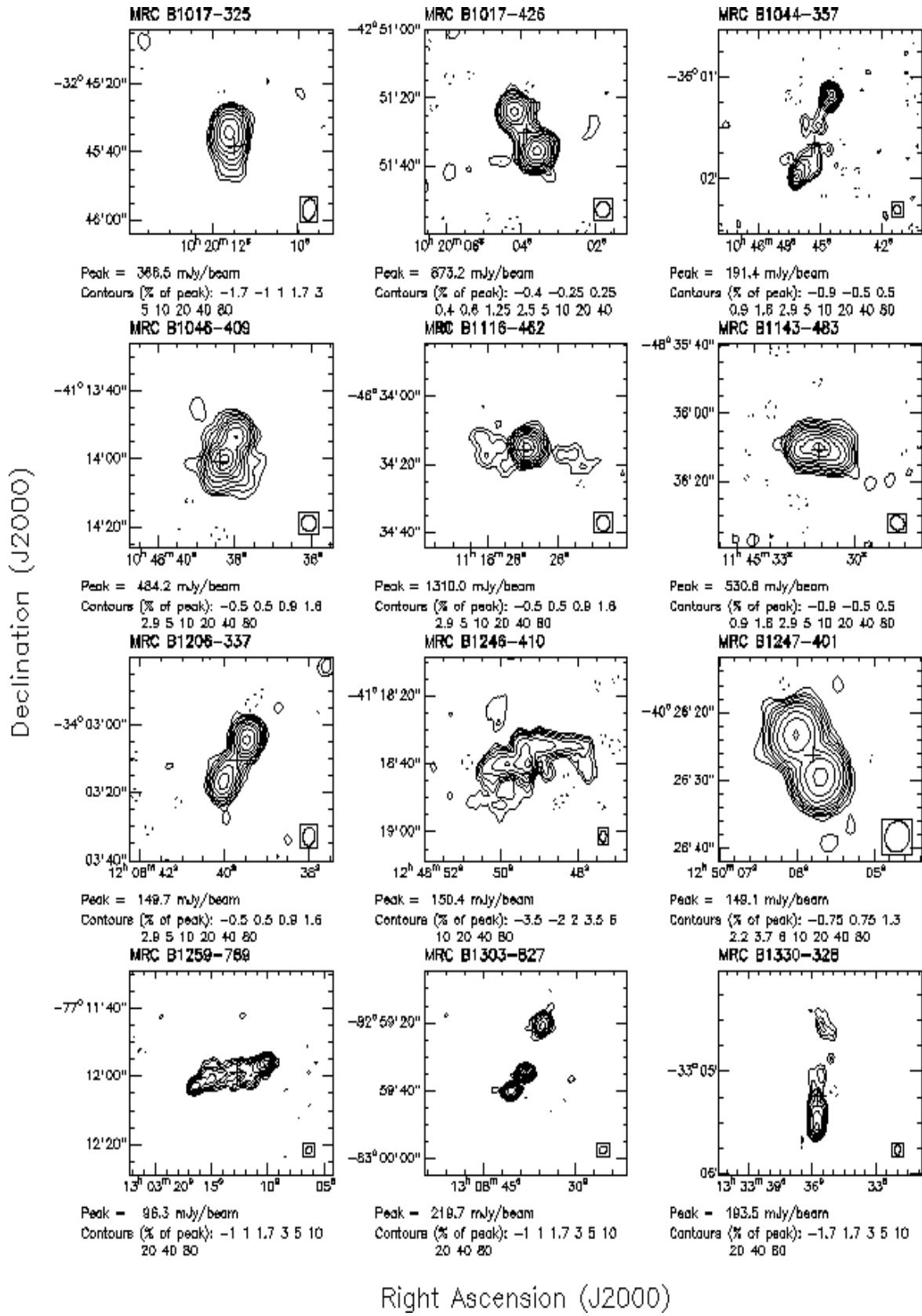


Fig. 1.— ATCA contour maps (continued).

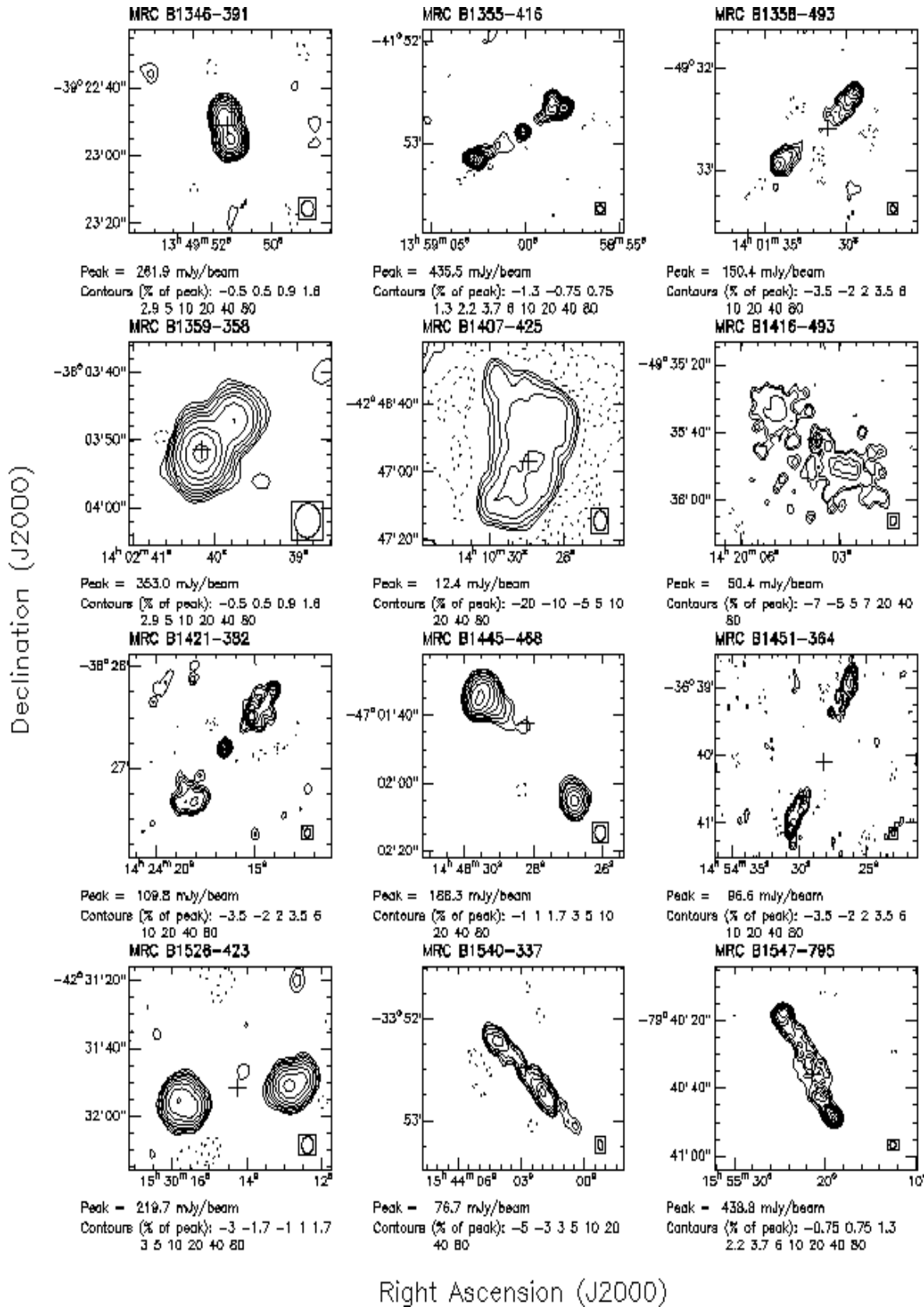


Fig. 1.— ATCA contour maps (continued).

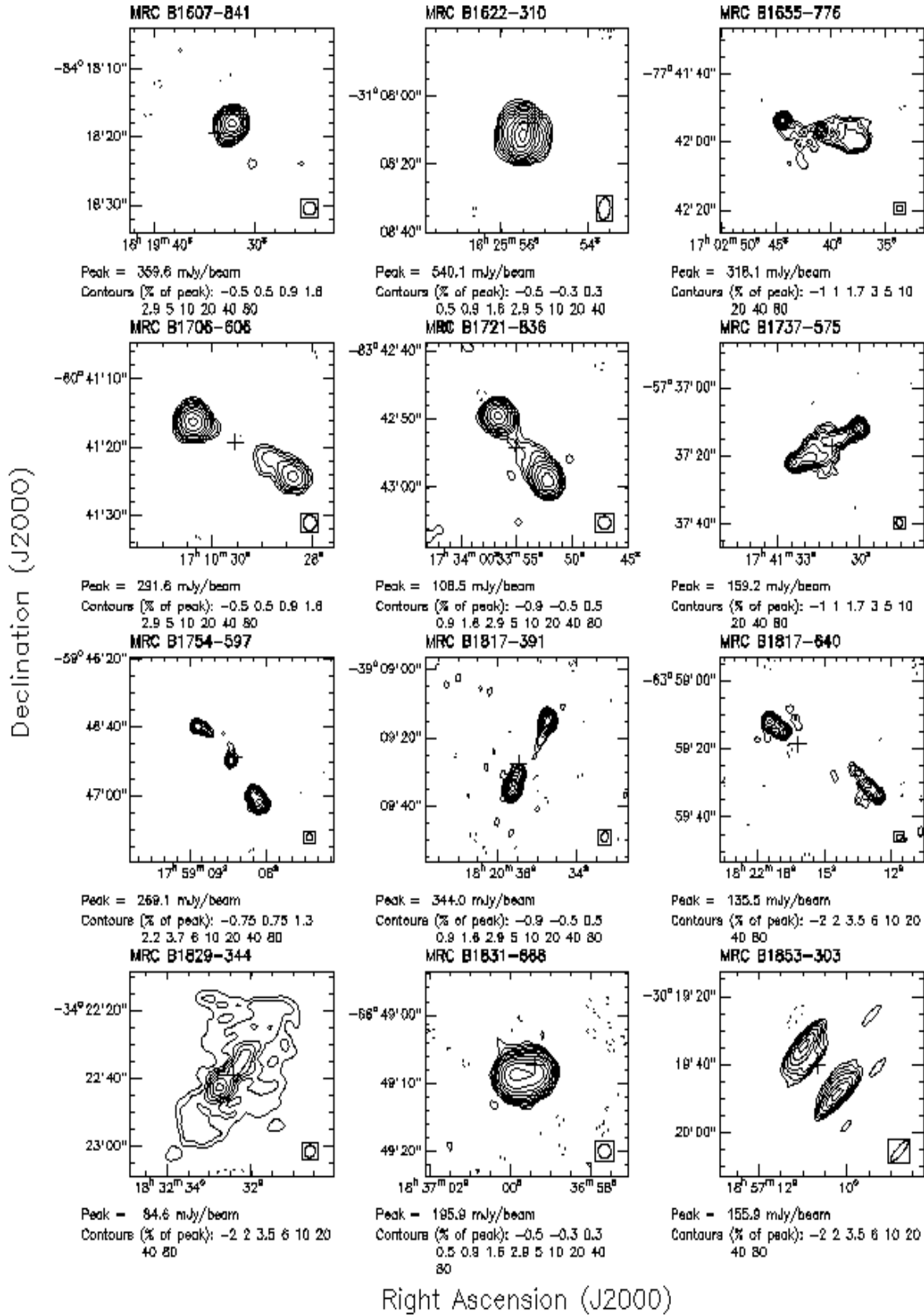


Fig. 1.— ATCA contour maps (continued).

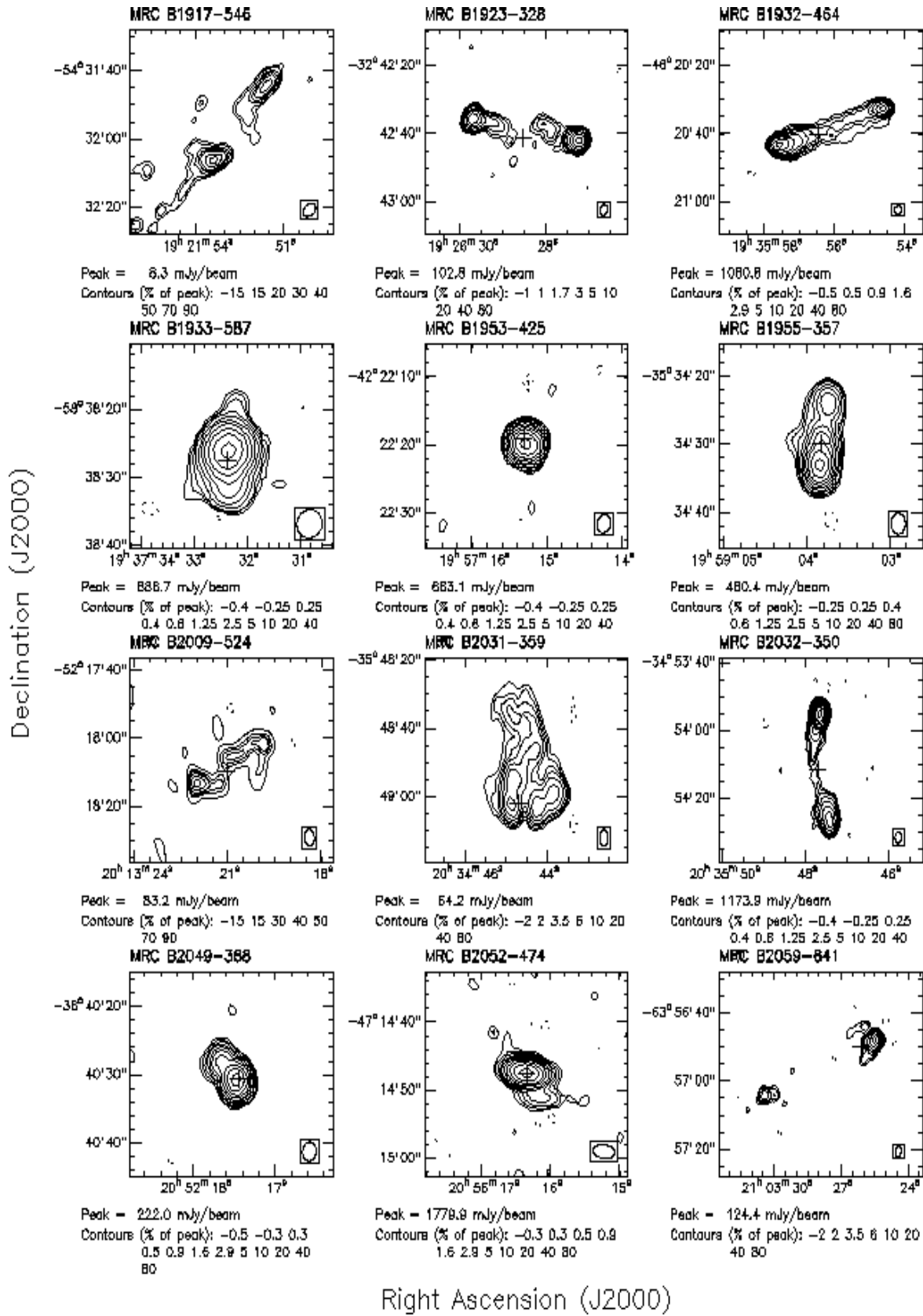


Fig. 1.— ATCA contour maps (continued).

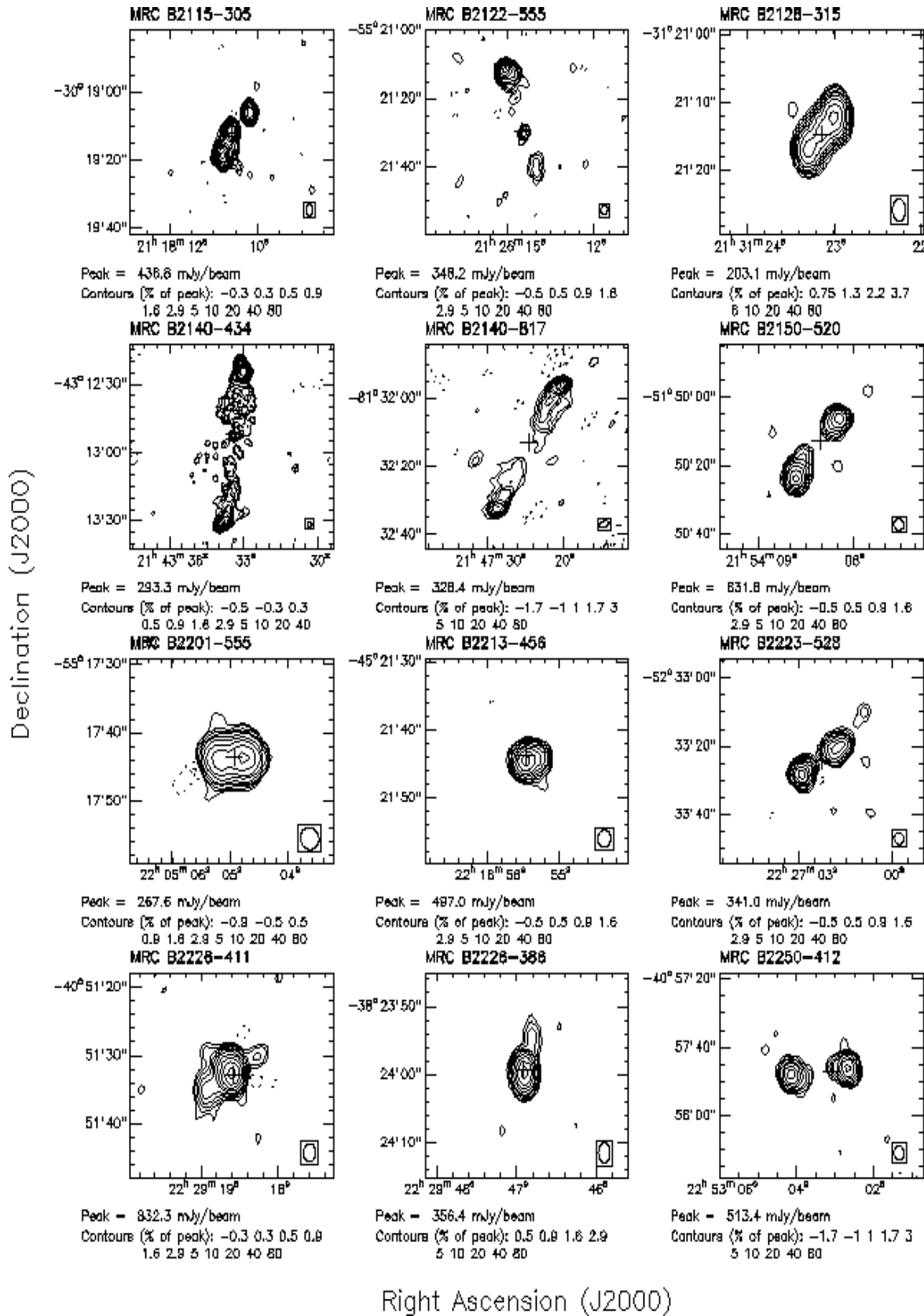


Fig. 1.— ATCA contour maps (continued).

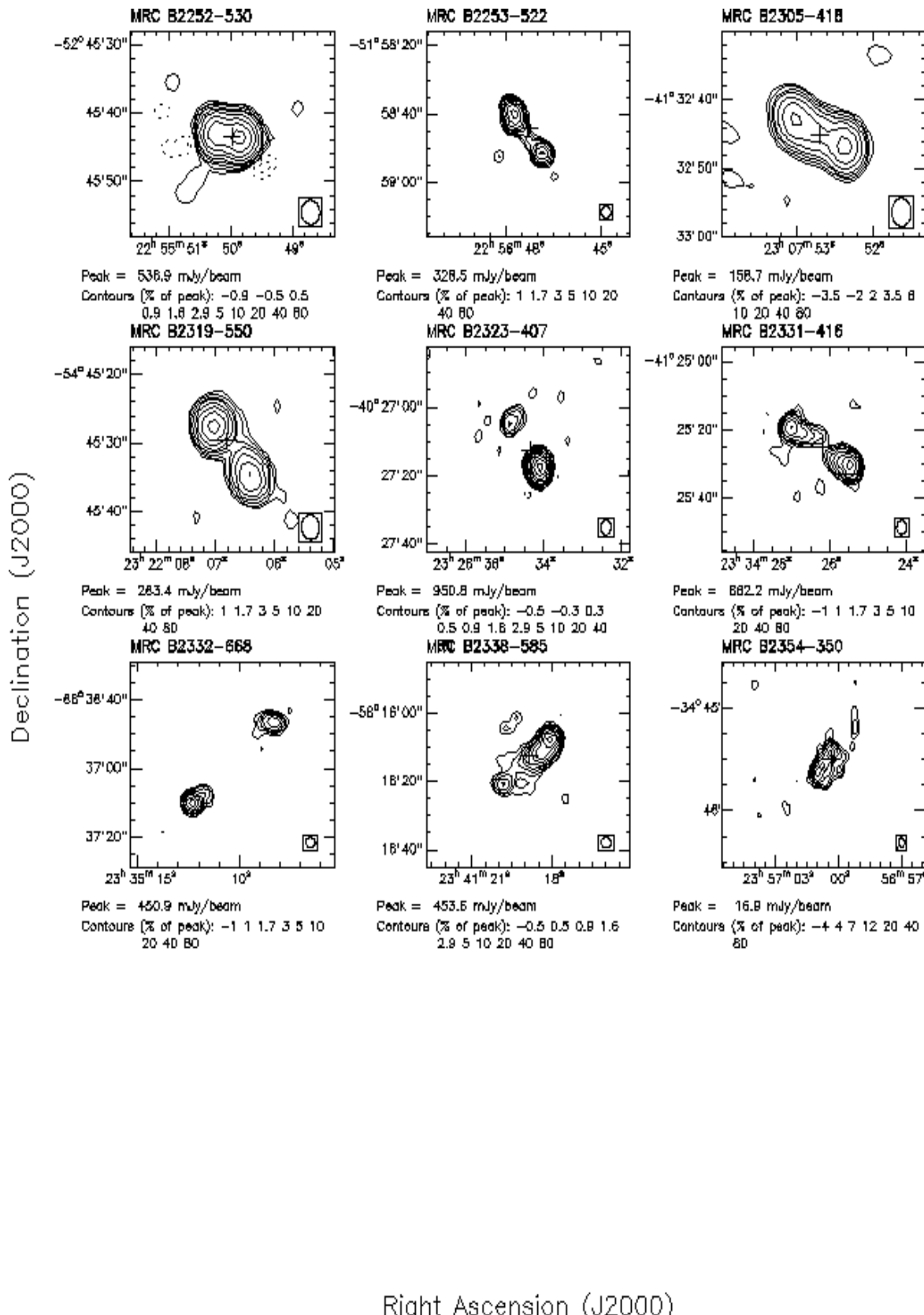


Fig. 1.— ATCA contour maps (continued).

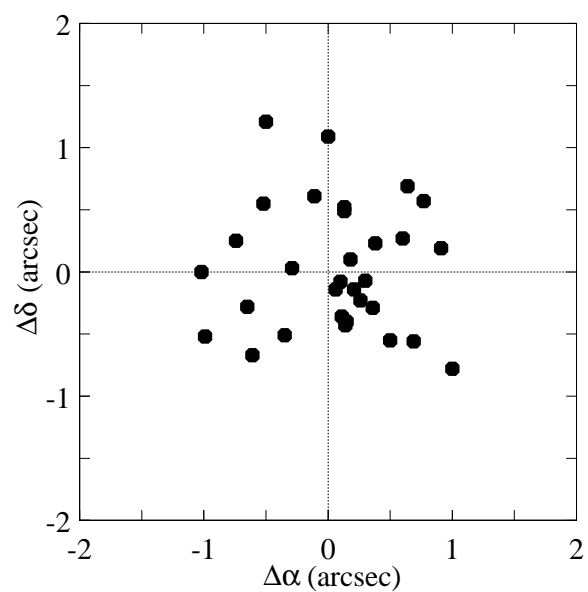


Fig. 2.— Comparison of BP and VLBI positions for 31 sources. Cross-plot of the difference in declination versus the difference in right ascension.

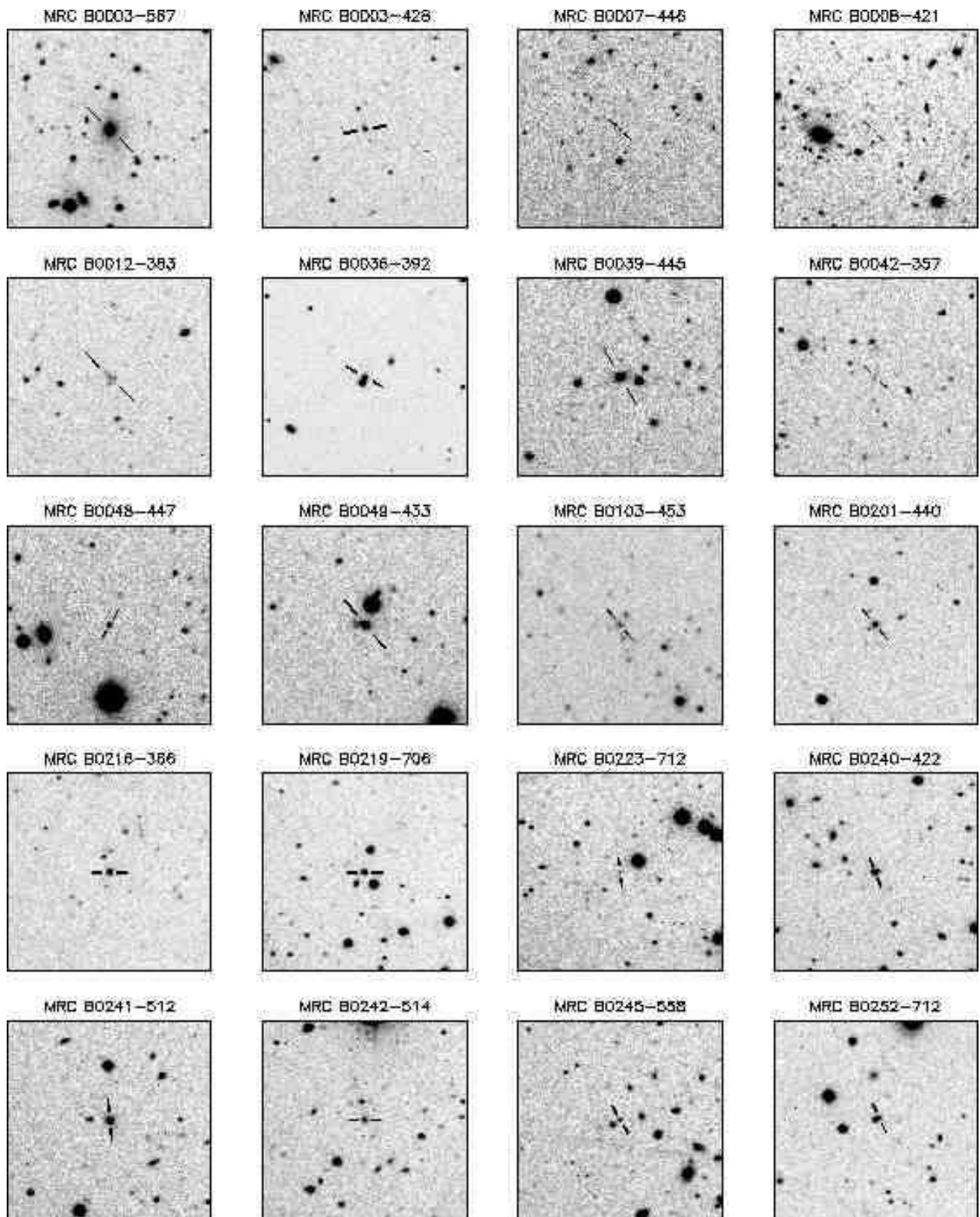


Fig. 3.— AAT CCD images. The side length of each plot is 1.97'.

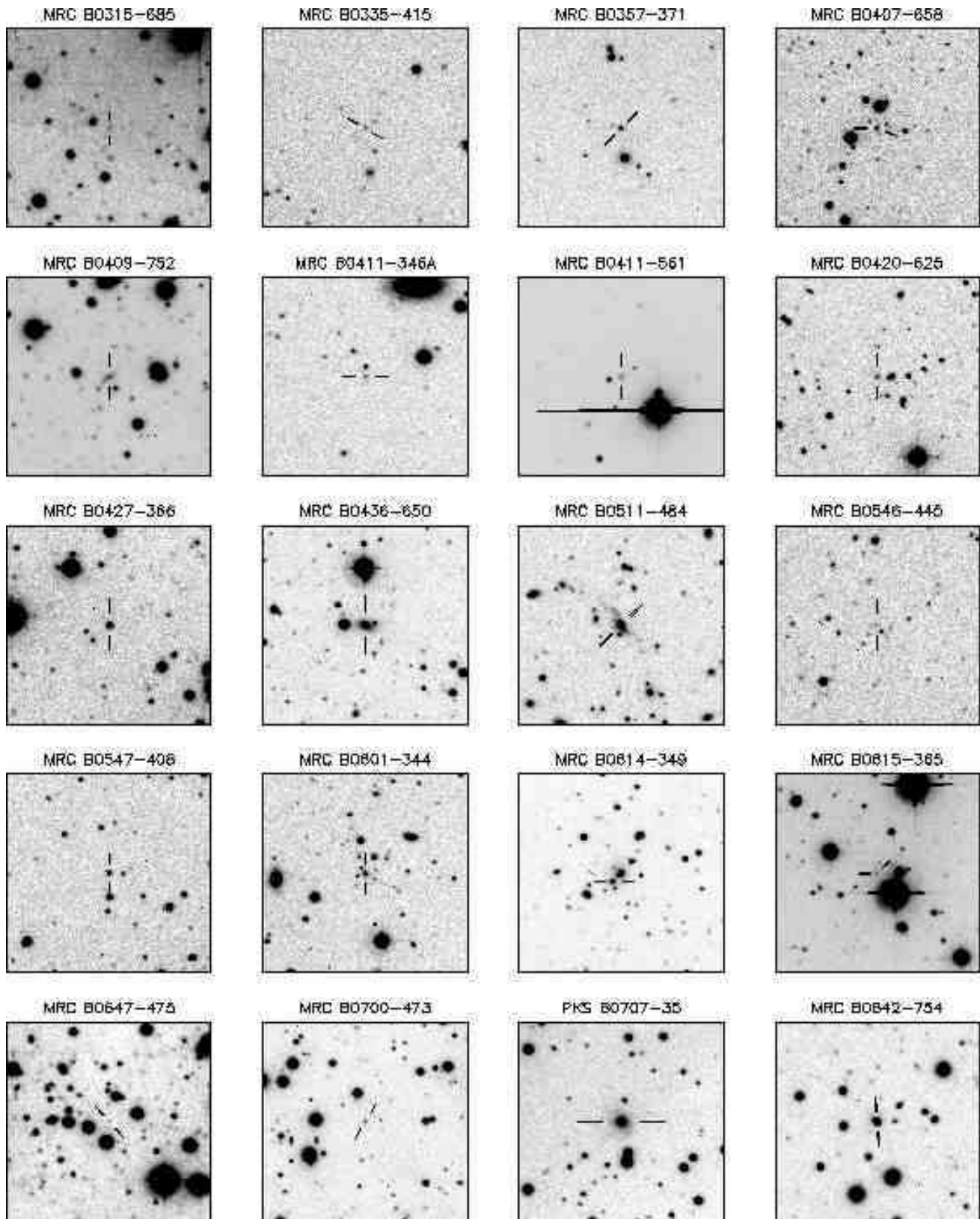


Fig. 3.— AAT CCD images (cont). The side length of each plot is $1.97'$.

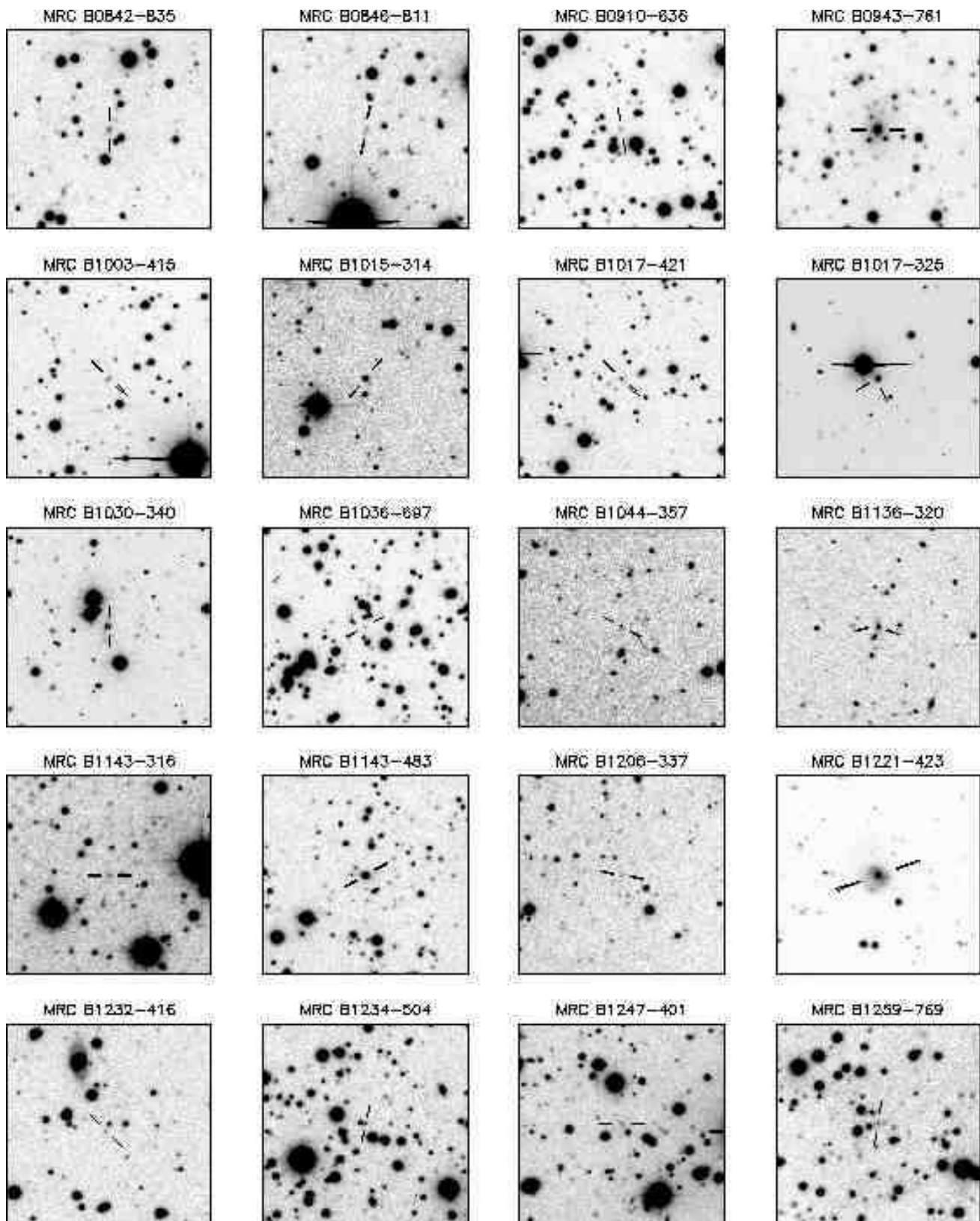


Fig. 3.— AAT CCD images (cont). The side length of each plot is 1.97'.

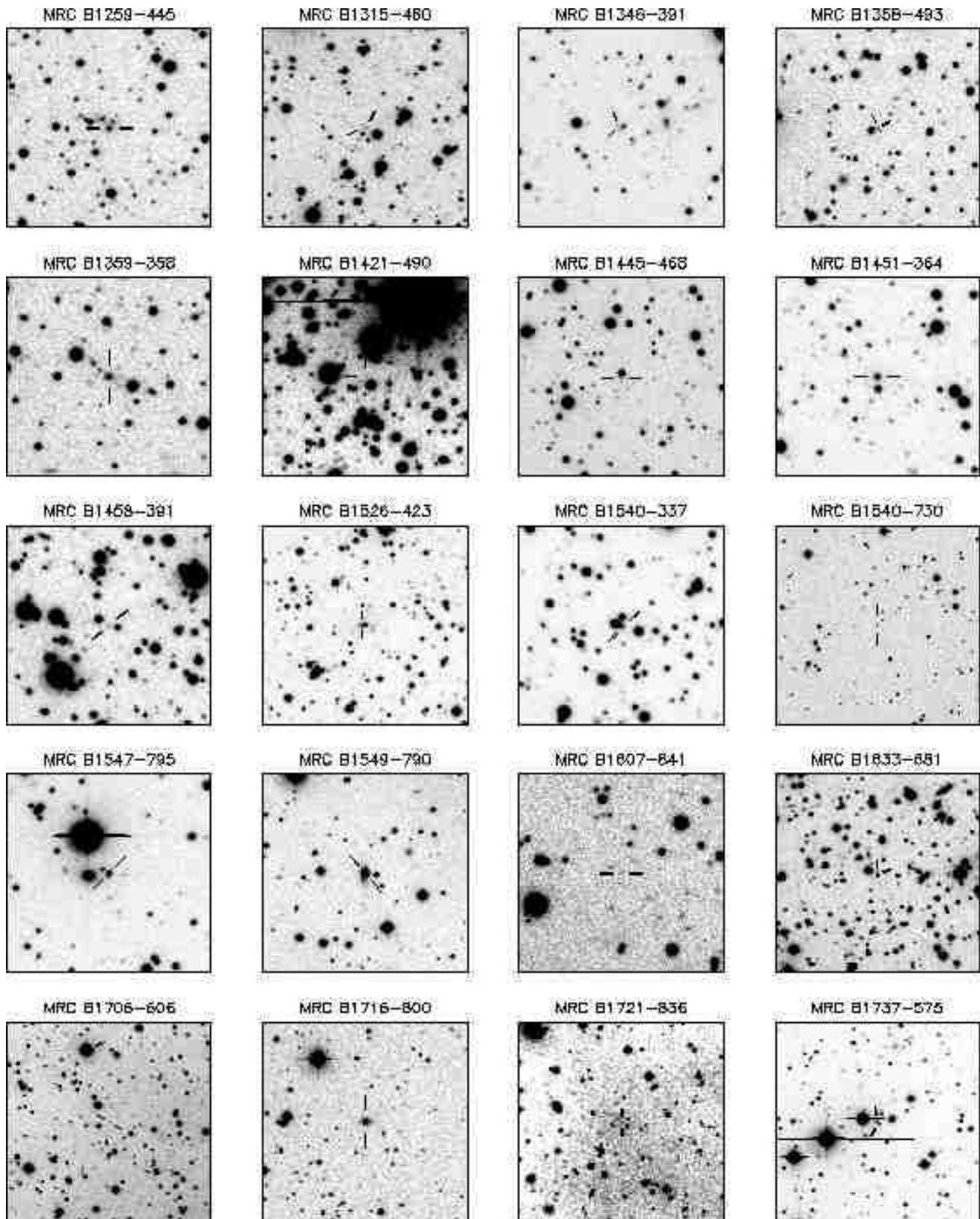


Fig. 3.— AAT CCD images (cont). The side length of each plot is 1.97'.

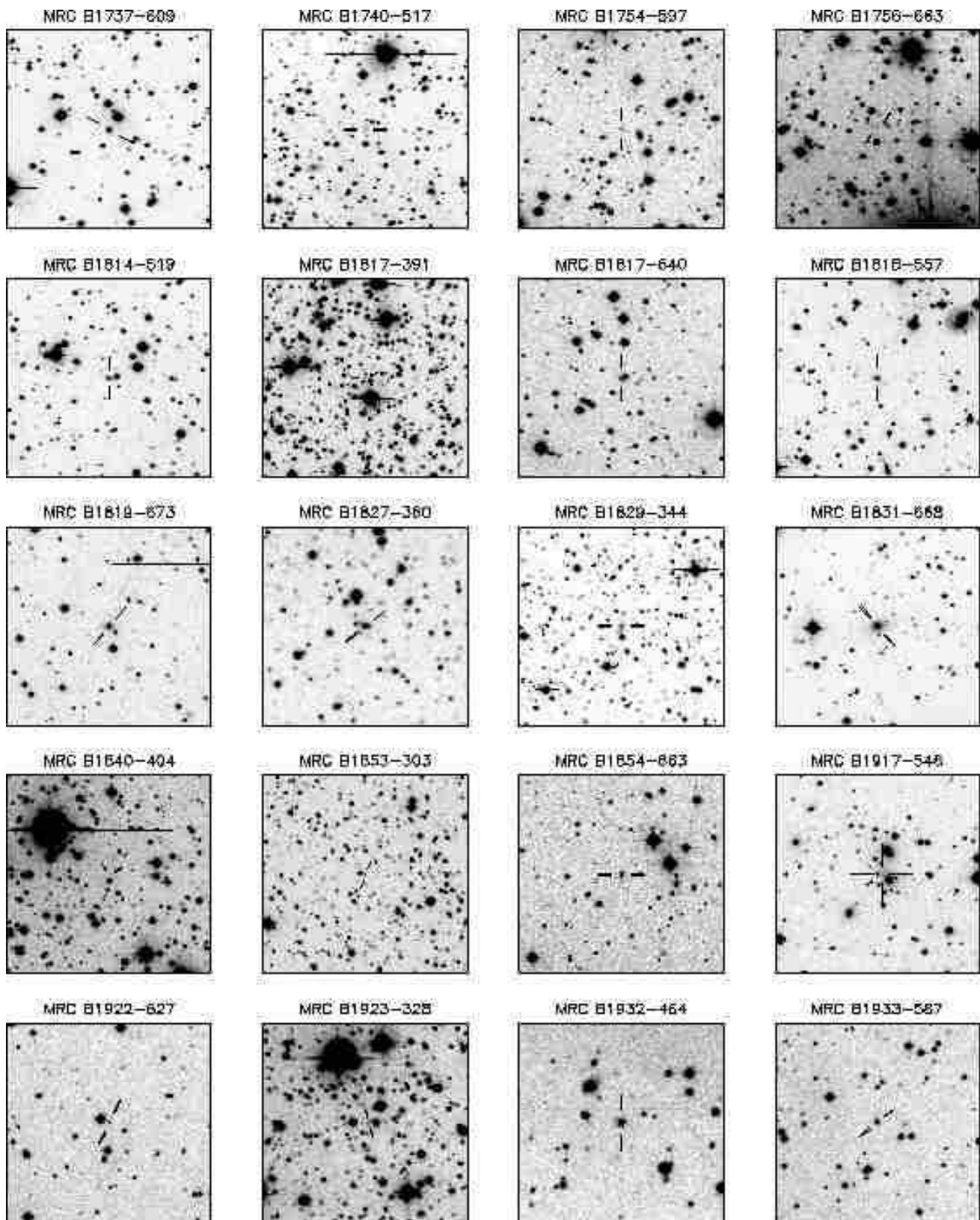


Fig. 3.— AAT CCD images (cont). The side length of each plot is 1.97'.

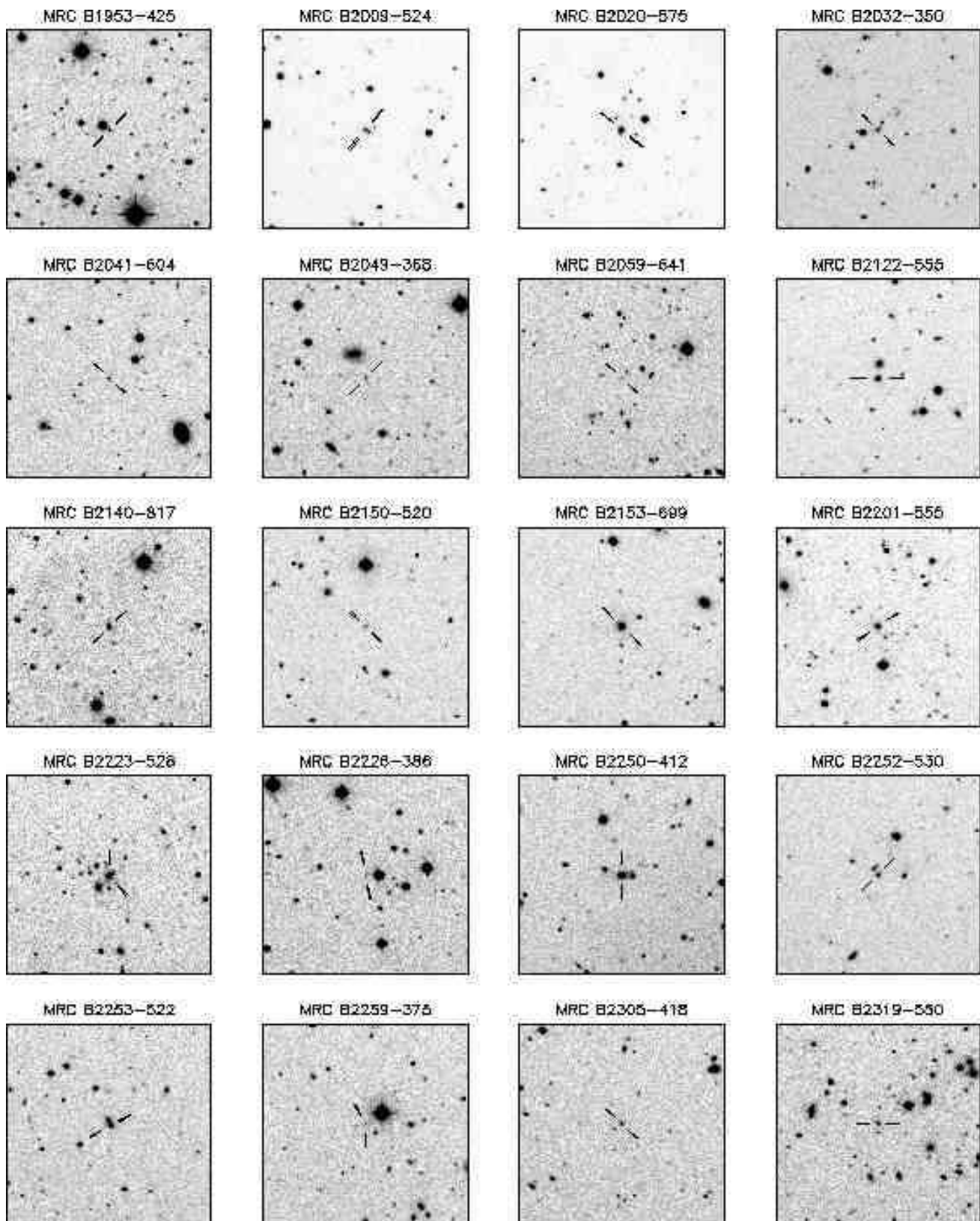


Fig. 3.— AAT CCD images (cont). The side length of each plot is $1.97'$.

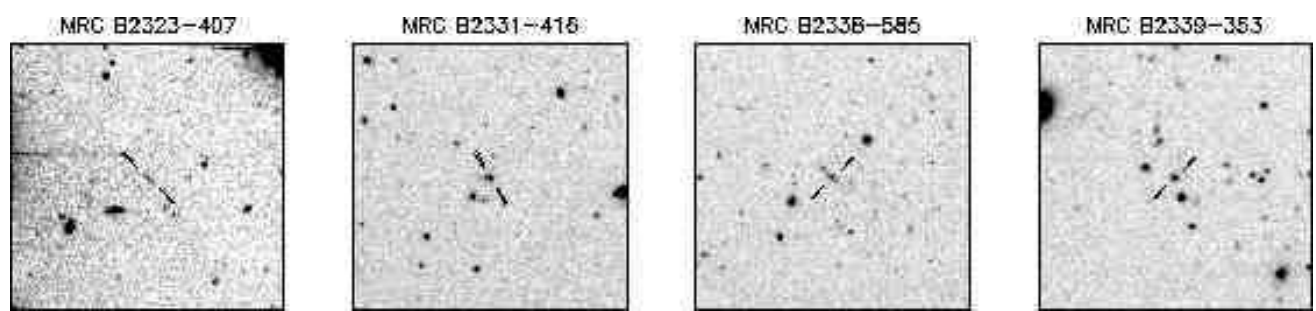


Fig. 3.— AAT CCD images (cont). The side length of each plot is $1.97'$.

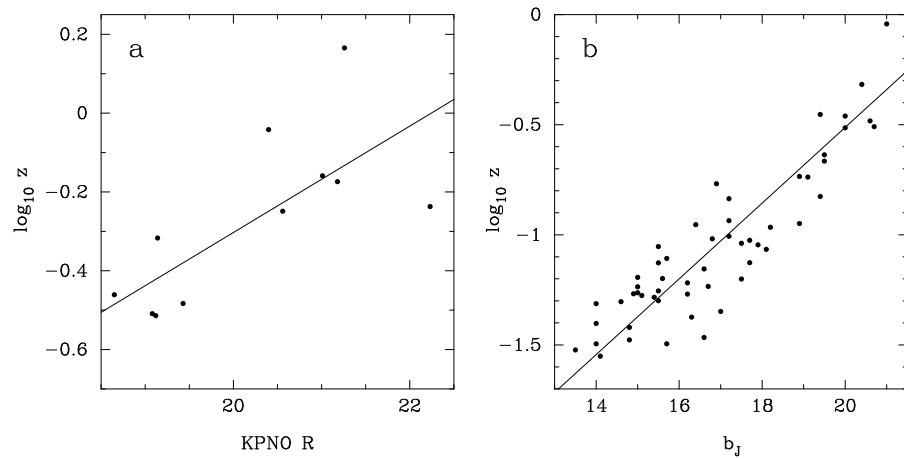


Fig. 4.— (a) Plot of logarithm of redshift versus R magnitude for MS4 galaxies. The line represents the fit to the data in Equation 2. (b) Plot of logarithm of redshift versus b_J magnitude for MS4 galaxies. The line represents the fit to the data in Equation 3.

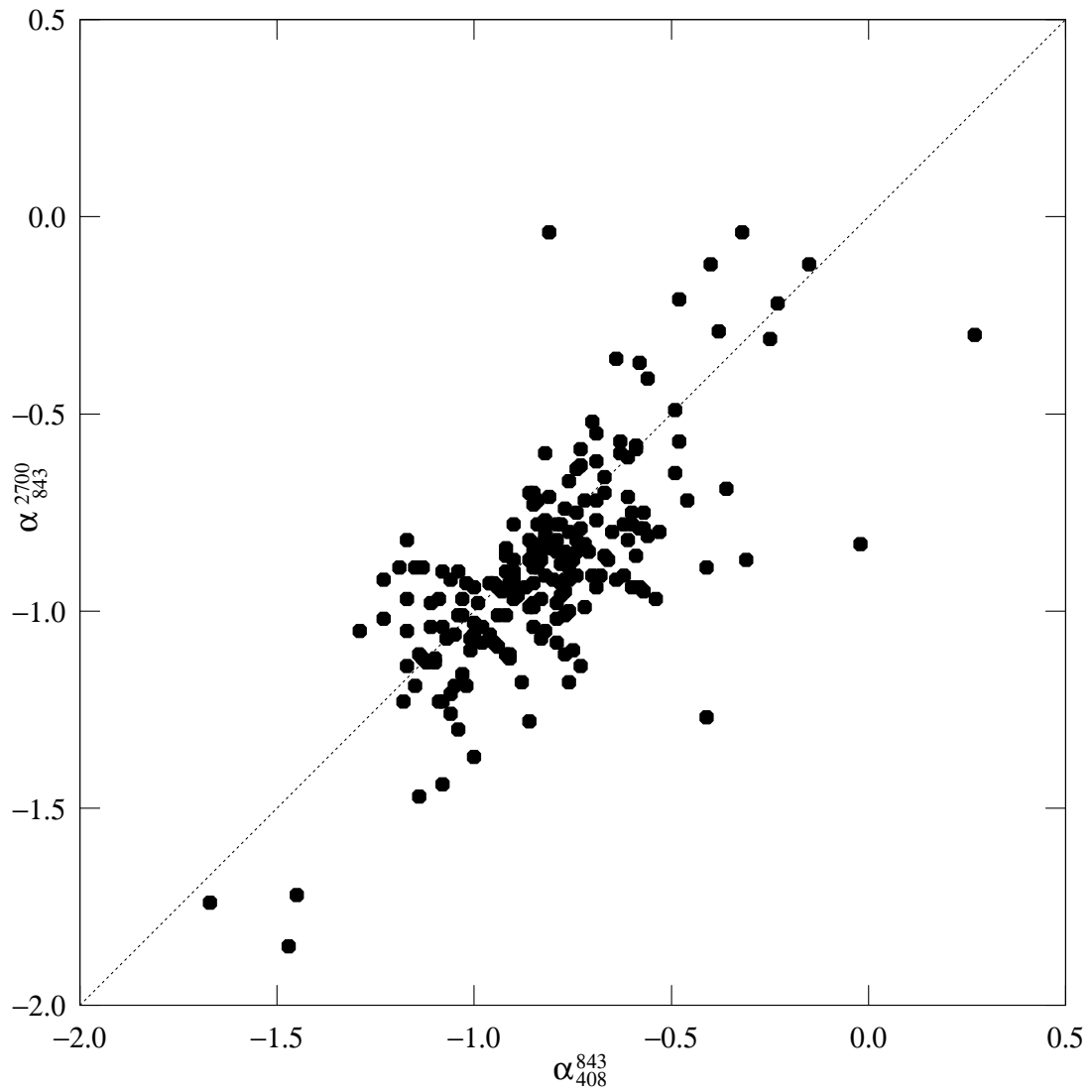


Fig. 5.— Plot of spectral index from 843–2700 MHz versus spectral index from 408–843 MHz for the MS4 sample. A source with a straight spectrum ($\alpha_{408}^{843} = \alpha_{843}^{2700}$) would lie somewhere on the dotted diagonal line. One source, MRC B1934–638, with $\alpha_{408}^{843} = 1.08$ and $\alpha_{843}^{2700} = -0.16$, lies off the right edge of the plot.

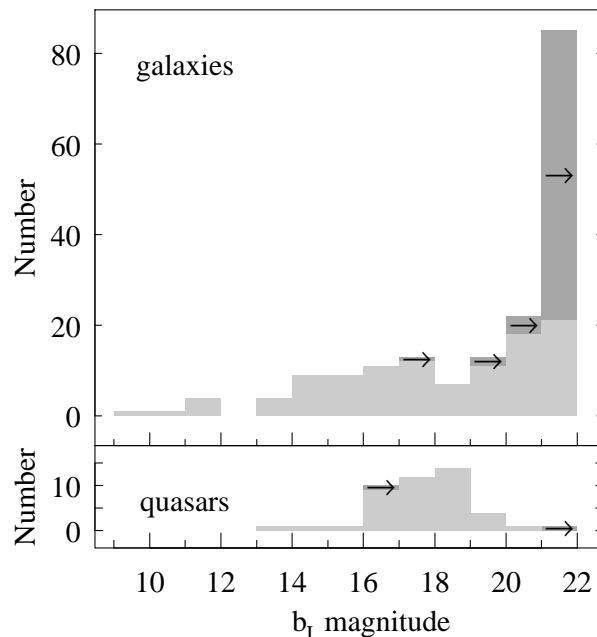


Fig. 6.— Histogram of apparent magnitudes of galaxies (top) and quasars and quasar candidates (bottom) from the MS4 sample. The darker grey bars with arrows represent lower limits to the magnitude for optical counterparts which are either fainter than the plate limit, or are confused with other objects. Most of the galaxies below the limit of the Schmidt plates were detected on *R*-band CCD images.

Table 1. Journal of ATCA Observations

(1) Run	(2) Date	(3) Frequency (MHz)	(4) Antenna Configuration	(5) Secondary Calibrators
1	1990 Aug 24	4790	3km #2 ^a	MRC B2326–477, MRC B2355–534
2	1990 Aug 25	4790	3km #2 ^a	MRC B2311–452, MRC B0008–421
3	1991 Jan 22	4790	3km #4 ^b	MRC B0647–475, MRC B0823–500
4	1991 Jan 23	4790	3km #4 ^b	MRC B1104–445, MRC B1151–348
5	1991 Apr 22	4740	3A	MRC B0208–512, MRC B0252–712
6	1991 Apr 23	4740	3A	MRC B1424–418 ^c , MRC B1458–391
7	1991 Apr 24	4740	3A	MRC B1215–457, MRC B1320–446
8	1991 Apr 24	4740	3A	MRC B0420–625, MRC B0537–441
9	1991 Aug 16	4740	6A	MRC B1549–790, MRC B1814–637 ^c
10	1991 Aug 17	4740	6A	MRC B1827–360, MRC B1954–388
11	1992 Jan 16	4800	6B	MRC B0022–423, MRC B0153–410, MRC B0208–512 MRC B0332–403, MRC B0438–436, MRC B1057–797 MRC B1234–504, MRC B1458–391, MRC B1610–771 PKS B1934–63, MRC B1954–388, MRC B2142–758
12	1992 Apr 17	4800	6C	MRC B2106–413, MRC B2149–306, MRC B2211–388
13	1993 Dec 19	4800	6A	PKS B0642–349 ^c , MRC B0646–306

^aThe full name is ‘3 km minimum redundancy # 2’.

^bThe full name is ‘3 km minimum redundancy # 4’.

^cObserved as a calibrator but not subsequently used.

Table 2. Summary of ATCA observing runs

(1) Source Name	(2) Run No.	(3) No. of cuts	(4) Int. time (min)	(5) Dynamic range	(6) Restoring beam ($\pi \times \pi$, °)
MRC B0003–567	1	7	50	330	$3.1 \times 2.6, +25$
MRC B0003–428	2	7	40	300	$3.8 \times 2.8, +3$
MRC B0007–446	2	8	51	200	$3.5 \times 2.9, +4$
MRC B0012–383	2	8	58	540	$4.3 \times 3.0, +1$
MRC B0013–634	1	8	57	660	$3.0 \times 3.0, -90$
MRC B0036–392	2	8	49	440	$3.9 \times 3.1, +5$
MRC B0039–445	2	8	48	530	$3.6 \times 3.1, +7$
MRC B0042–357	11	8	34	1000	$3.3 \times 2.1, +9$
MRC B0048–447	11	7	40	530	$3.4 \times 2.0, +34$
MRC B0049–433	11	7	29	450	$3.2 \times 1.8, +20$
MRC B0119–634	5	9	69	170	$3.6 \times 3.5, -62$
MRC B0157–311	11	8	37	180	$3.7 \times 2.0, +7$
MRC B0201–440	11	7	34	310	$3.2 \times 1.9, +14$
MRC B0202–765	5	8	47	160	$4.1 \times 3.6, +54$
MRC B0208–512	5	7	22	440	$5.3 \times 3.4, +4$
MRC B0219–706	5	8	60	410	$3.2 \times 3.1, +38$
MRC B0223–712	5	9	64	220	$3.7 \times 3.5, +57$
MRC B0241–512	5	8	60	220	$4.0 \times 3.3, +5$
MRC B0242–514	5	6	44	100	$4.4 \times 3.1, +2$
MRC B0245–558	5	8	54	250	$4.0 \times 3.4, +6$
MRC B0251–675	5	8	58	170	$3.6 \times 3.3, +9$
MRC B0252–712	5	10	33	300	$4.0 \times 3.4, +69$
MRC B0315–685	5	8	58	410	$3.3 \times 3.2, +37$
MRC B0335–415	11	7	35	220	$3.0 \times 2.0, +12$

Table 2—Continued

(1) Source Name	(2) Run No.	(3) No. of cuts	(4) Int. time (min)	(5) Dynamic range	(6) Restoring beam ($\prime\prime \times \prime\prime$, $^{\circ}$)
MRC B0340–372	11	5	24	810	$3.8 \times 1.7, +23$
MRC B0407–658	11	6	16	670	$2.3 \times 1.8, +28$
MRC B0409–752	11	4	18	190	$6.4 \times 2.1, +65$
MRC B0411–346A	11	6	28	410	$3.3 \times 2.4, +20$
MRC B0411–647	8	8	55	70	$4.0 \times 3.3, -45$
MRC B0411–561	8	6	43	180	$4.2 \times 3.1, +29$
MRC B0420–625	8	9	31	230	$4.4 \times 3.5, -68$
MRC B0427–366	11	7	30	200	$3.2 \times 2.1, +11$
MRC B0436–650	8	8	61	50	$3.7 \times 3.2, -3$
MRC B0453–301	11	6	25	20	$3.6 \times 2.5, +13$
MRC B0454–463	8	9	41	260	$4.5 \times 3.5, -3$
MRC B0506–612	8	8	42	360	$3.9 \times 3.4, +5$
MRC B0509–573	8	8	39	250	$3.9 \times 3.4, +9$
MRC B0513–488	8	8	58	230	$4.2 \times 3.5, -44$
MRC B0534–497	8	8	57	300	$4.3 \times 3.3, 0$
MRC B0546–445	8	7	50	80	$4.4 \times 3.4, -8$
MRC B0547–408	8	8	59	700	$5.0 \times 3.4, +1$
MRC B0602–319	13	14	88	260	$4.1 \times 1.8, +2$
MRC B0614–349	13	17	50	300	$3.9 \times 1.9, -4$
MRC B0615–365	13	12	74	550	$4.4 \times 1.5, +3$
MRC B0637–752	11	9	43	1090	$2.5 \times 2.1, +56$
MRC B0647–475	3	8	20	300	$4.2 \times 4.1, +40$
MRC B0658–656	3	9	72	210	$4.2 \times 3.5, +73$

Table 2—Continued

(1) Source Name	(2) Run No.	(3) No. of cuts	(4) Int. time (min)	(5) Dynamic range	(6) Restoring beam ($\pi \times \pi$, °)
MRC B0700–473	3	9	76	230	4.4×3.9 , 0
MRC B0704–427	3	7	59	380	4.9×3.6 , +16
MRC B0842–754	11	12	56	270	2.3×1.7 , +26
MRC B0842–835	3	8	68	250	4.3×4.3 , +45
MRC B0846–811	3	8	67	280	4.4×4.3 , +46
MRC B0906–682	3	8	60	260	6.0×3.6 , +67
MRC B0910–636	3	8	59	340	4.7×4.0 , +55
MRC B0943–761	11	8	40	490	2.9×1.6 , +33
MRC B1003–415	4	8	52	630	4.9×4.5 , -87
MRC B1015–314	4	5	40	580	6.8×3.7 , -11
MRC B1017–421	4	6	44	90	4.9×3.9 , -23
MRC B1017–325	4	5	36	230	6.4×3.8 , -10
MRC B1017–426	4	8	59	730	4.6×4.3 , -11
MRC B1030–340	4	6	49	200	6.2×3.9 , +3
MRC B1036–697	11	11	51	590	2.2×1.8 , +14
MRC B1044–357	4	7	54	480	5.7×4.0 , +5
MRC B1046–409	4	8	57	540	4.7×4.4 , +14
MRC B1116–462	4	7	52	470	4.6×3.8 , +6
MRC B1143–483	4	7	46	410	4.4×3.9 , +47
MRC B1151–348	4	7	20	150	6.2×4.3 , +7
MRC B1206–337	7	8	53	500	5.3×3.6 , -6
MRC B1215–457	7	10	35	340	4.1×3.7 , +31
MRC B1221–423	7	8	42	470	4.5×3.7 , -14

Table 2—Continued

(1) Source Name	(2) Run No.	(3) No. of cuts	(4) Int. time (min)	(5) Dynamic range	(6) Restoring beam ($\pi \times \pi$, °)
MRC B1232–416	7	8	42	560	$4.5 \times 3.7, -11$
MRC B1243–412	7	8	41	790	$4.5 \times 3.7, -4$
MRC B1246–410	11	13	61	100	$3.4 \times 1.8, -5$
MRC B1247–401	7	8	60	370	$4.6 \times 3.6, -9$
MRC B1259–769	11	10	44	320	$2.3 \times 1.7, -16$
MRC B1303–827	11	14	66	310	$2.5 \times 2.2, -53$
MRC B1315–460	11	12	64	2230	$3.0 \times 1.7, -2$
MRC B1320–446	7	8	27	580	$4.4 \times 3.9, -8$
MRC B1330–328	7	6	42	240	$5.7 \times 3.5, -3$
MRC B1346–391	7	8	58	440	$4.7 \times 3.7, -1$
MRC B1355–416	7	8	55	340	$4.4 \times 3.8, +4$
MRC B1358–493	6	8	56	140	$4.4 \times 3.3, +2$
MRC B1359–358	7	8	43	500	$5.0 \times 3.8, -3$
MRC B1407–425	6	8	58	20	$6.0 \times 3.7, 0$
MRC B1416–493	11	12	61	50	$2.8 \times 1.9, -10$
MRC B1421–382	6	9	59	120	$5.1 \times 3.5, -5$
MRC B1421–490	11	13	32	640	$3.2 \times 2.0, -8$
MRC B1424–418	6	8	24	1330	$5.0 \times 3.4, +3$
MRC B1445–468	6	8	55	470	$4.5 \times 3.4, 0$
MRC B1451–364	6	6	40	110	$5.7 \times 3.1, +11$
MRC B1458–391	6	8	58	400	$5.1 \times 3.4, -1$
MRC B1526–423	6	8	56	280	$4.9 \times 3.4, -2$
MRC B1540–337	6	6	39	100	$6.7 \times 3.0, +9$
MRC B1547–795	9	8	57	490	$1.9 \times 1.9, +67$

Table 2—Continued

(1) Source Name	(2) Run No.	(3) No. of cuts	(4) Int. time (min)	(5) Dynamic range	(6) Restoring beam ($\pi \times \pi$, °)
MRC B1549–790	9	8	23	530	$2.1 \times 2.0, +27$
MRC B1607–841	9	8	57	720	$1.9 \times 1.9, -1$
MRC B1622–310	6	8	47	900	$6.4 \times 3.4, -7$
MRC B1655–776	9	8	57	400	$1.9 \times 1.8, -1$
MRC B1706–606	9	8	50	970	$2.2 \times 1.9, 0$
MRC B1721–836	9	8	50	540	$1.9 \times 1.9, +2$
MRC B1737–575	9	8	55	400	$2.3 \times 1.9, -1$
MRC B1754–597	9	8	57	540	$2.2 \times 1.8, +6$
MRC B1756–663	9	8	57	810	$2.1 \times 1.9, +3$
MRC B1814–637	9	8	24	520	$2.4 \times 2.0, +7$
MRC B1817–391	10	9	60	570	$2.9 \times 2.1, -8$
MRC B1817–640	11	7	32	140	$1.7 \times 1.6, -41$
MRC B1827–360	10	10	30	470	$3.4 \times 2.5, -8$
MRC B1829–344	10	10	72	170	$3.6 \times 3.0, -16$
MRC B1831–668	9	8	61	650	$2.0 \times 1.9, +20$
MRC B1853–303	11	4	17	200	$7.6 \times 2.1, -40$
MRC B1854–663	9	8	57	740	$2.1 \times 1.9, +5$
MRC B1917–546	11	8	37	20	$4.4 \times 3.1, -40$
MRC B1923–328	10	9	60	520	$3.2 \times 2.3, -12$
MRC B1932–464	10	10	63	640	$2.3 \times 2.2, -11$
MRC B1933–587	...	18	71	990	$4.2 \times 3.7, -13$
MRC B1953–425	10	9	70	1660	$2.7 \times 2.0, -11$
MRC B1955–357	10	9	59	1200	$3.1 \times 2.1, +1$

Table 2—Continued

(1) Source Name	(2) Run No.	(3) No. of cuts	(4) Int. time (min)	(5) Dynamic range	(6) Restoring beam ($\pi \times \pi$, °)
MRC B2009–524	11	6	29	20	5.0×2.9 , +5
MRC B2031–359	10	7	44	130	4.9×2.4 , 0
MRC B2032–350	10	8	57	1300	3.3×1.9 , -2
MRC B2049–368	12	9	63	1110	2.8×2.0 , -4
MRC B2052–474	12	10	39	1370	3.2×2.0 , +80
MRC B2059–641	11	6	26	210	2.9×1.8 , -7
MRC B2115–305	12	9	63	1090	3.3×2.0 , +1
MRC B2122–555	11	7	34	580	2.5×1.9 , -8
MRC B2128–315	12	8	56	680	3.3×1.9 , +1
MRC B2140–434	12	9	69	980	2.4×1.9 , -3
MRC B2140–817	11	7	33	200	2.8×1.8 , -66
MRC B2150–520	1	7	41	700	3.4×2.9 , +12
MRC B2201–555	1	7	53	540	3.3×2.7 , +11
MRC B2213–456	12	8	55	830	2.5×1.9 , -3
MRC B2223–528	1	7	51	680	3.4×2.8 , +13
MRC B2226–411	12	8	56	1190	2.7×1.8 , -2
MRC B2226–386	12	7	49	890	3.0×1.7 , 0
MRC B2250–412	2	7	36	270	4.1×3.0 , +3
MRC B2252–530	1	7	51	490	3.5×2.7 , +2
MRC B2253–522	1	7	53	470	3.4×2.8 , +6
MRC B2305–418	2	6	39	100	4.1×2.8 , 0
MRC B2319–550	1	7	55	530	3.5×2.7 , +3
MRC B2323–407	2	7	22	680	4.3×2.9 , -1

Table 2—Continued

(1) Source Name	(2) Run No.	(3) No. of cuts	(4) Int. time (min)	(5) Dynamic range	(6) Restoring beam ($\pi \times \pi$, °)
MRC B2331–416	2	7	46	250	$4.1 \times 2.8, -1$
MRC B2332–668	1	8	56	560	$2.9 \times 2.8, +25$
MRC B2338–585	1	8	58	910	$3.1 \times 2.9, +23$
MRC B2339–353	2	7	41	300	$4.4 \times 2.8, +4$
MRC B2354–350	2	6	39	80	$5.8 \times 3.3, 0$

Table 3. Parameters measured from the ATCA images

(1) Source name	(2) Str. code ^a	(3) R.A. h m s	(4) dec ° ' "	(5) pos. code ^b	(6) S_{int} (mJy)	(7) S_{core} (mJy)	(8) R	(9) LAS (")	(10) PA (°)
MRC B0003–428	2	00 06 01.99	−42 34 40.8	ce	552	<143	<0.35	5.0	62
MRC B0003–567	1	00 05 57.70	−56 28 31.1	ce	635	26.2	83
MRC B0007–446	2	00 10 30.45	−44 22 56.5	ce	302	<2	<0.007	33.7	62
MRC B0012–383	2	00 15 24.37	−38 04 35.0	ce	307	<55	<0.22	25.3	58
MRC B0013–634	2	00 16 02.89	−63 10 04.8	co	417	8:	0.021:	29.4	76
MRC B0036–392	D2	00 38 26.84	−38 59 48.8	co	454	177:	0.64:	4.6	40
MRC B0039–445	2	00 42 08.96	−44 13 59.8	ce	1134	<204	<0.22	6.2	−79
MRC B0042–357	2	00 44 41.41	−35 30 34.3	ce	1007	<251	<0.33	4.8	−2
MRC B0048–447	c	00 50 52.03	−44 28 38.1	f	317	...	css	1.8	55
MRC B0049–433	2	00 52 14.70	−43 06 29.3	ce	900	<7	<0.009	17.3	88
MRC B0119–634	2	01 21 40.48	−63 09 02.4	co	388	43	0.13	41.3	13
MRC B0157–311	2	02 00 12.16	−30 53 27.0	co	1470	130:	0.097:	20.7	−1
MRC B0201–440	c	02 03 40.76	−43 49 51.4	f	1014	...	css	1.5	64
MRC B0202–765	2	02 02 13.62	−76 20 02.7	co	922	214	0.30	22.1	−88
MRC B0208–512	T	02 10 46.20	−51 01 01.9	co	2950	2779:	16:	6.0	79
MRC B0219–706	2?	02 20 08.20	−70 22 27.8	ce	539	<373	css	3.3	48
MRC B0223–712	2	02 23 56.72	−70 59 45.7	ce	271	<6	<0.03	25.2	−67
MRC B0241–512	2	02 43 13.74	−51 05 17.1	ce	645	<40	<0.07	9.3	33
MRC B0242–514	2	02 43 44.52	−51 12 34.5	ce	580	<3	<0.006	56.3	1
MRC B0245–558	2	02 46 56.16	−55 41 23.4	ce	556	<4	<0.008	44.6	−80
MRC B0251–675	2	02 51 56.00	−67 18 00.2	co	308	18	0.063	33.1	−89
MRC B0252–712	c	02 52 46.16	−71 04 35.3	ce	1708	...	css	<1.8	...
MRC B0315–685	c	03 16 10.44	−68 21 05.4	f	380	...	css	<1.5	...
MRC B0335–415	2	03 37 04.56	−41 23 15.6	co	307	3	0.011	35.8	−11
MRC B0340–372	2	03 42 05.36	−37 03 21.2	ce	766	<63	css	4.4	67
MRC B0407–658	c	04 08 20.37	−65 45 09.7	f	3371	...	css	<1.0	...
MRC B0409–752	2	04 08 48.16	−75 07 20.1	ce	4429	<757	<0.21	6.0	−57
MRC B0411–346A	2?	04 13 00.92	−34 30 10.5	ce	397	...	css	1.7	−77
MRC B0411–561	2	04 12 48.22	−56 00 48.5	ce	800	<3	<0.005	25.6	−9
MRC B0411–647	1	04 11 59.19	−64 36 24.3	ce	417	37.5	−31
MRC B0420–625	c	04 20 56.09	−62 23 39.6	f ^c	945	...	css	<2.0	...
MRC B0427–366	2	04 29 40.13	−36 30 54.5	ce	471	19.9	−14
MRC B0436–650	1/2	04 37 09.28	−64 58 53.4	ce	320	48.6	22
MRC B0453–301	2	04 55 14.29	−30 06 44.7	ce	1329	<10	<0.008	74.9	1
MRC B0454–463	T	04 55 50.75	−46 15 59.2	ce	1436	14.2	−31
MRC B0506–612	T	05 06 43.99	−61 09 41.9	p	1300	5.3	−88
MRC B0509–573	D2	05 10 18.48	−57 19 42.5	ce	614	5.8	46

Table 3—Continued

(1) Source name	(2) Str. code ^a	(3) R.A. h m s	(4) (J2000) ° ' "	(5) pos. code ^b	(6) S_{int} (mJy)	(7) S_{core} (mJy)	(8) R	(9) LAS (")	(10) PA (°)
MRC B0513–488	2	05 14 32.87	−48 45 27.4	co	340	6:	0.019:	38.9	−33
MRC B0534–497	2	05 36 13.67	−49 44 22.6	ce	604	<14	<0.03	29.0	54
MRC B0546–445	2	05 47 38.01	−44 31 10.7	ce	383	<12	<0.04	20.5	7
MRC B0547–408	2	05 49 23.39	−40 51 11.6	ce	740	<1	<0.002	33.6	−60
MRC B0602–319	T	06 04 14.56	−31 55 56.0	co	1120	815	2.7	7.9	...
MRC B0614–349	c	06 16 35.99	−34 56 16.8	f	1368	...	css	<1.8	...
MRC B0615–365	c	06 17 32.32	−36 34 15.0	f	726	...	css	<2.0	...
MRC B0637–752	T	06 35 46.58	−75 16 16.8	co	5790	4993	6.3	18.7	−89
MRC B0647–475	c	06 48 48.40	−47 34 27.0	f	661	...	css	<2.0	...
MRC B0658–656	2	06 58 12.97	−65 44 51.8	ce	530	<86	<0.20	18.0	84
MRC B0700–473	2	07 02 08.99	−47 26 30.7	ce	279	<1	<0.005	31.0	−55
MRC B0704–427	2	07 05 54.30	−42 48 52.4	co	353	13	0.041	27.3	−88
MRC B0842–754	T	08 41 27.47	−75 40 29.2	co	1586	329:	0.26:	11.8	71
MRC B0842–835	2	08 37 14.79	−83 44 41.4	ce	443	<37	<0.10	16.0	2
MRC B0846–811	2	08 43 38.69	−81 18 28.0	ce	277	<8	<0.04	26.4	−47
MRC B0906–682	c	09 06 52.53	−68 29 40.2	f	487	...	css	<2.8	...
MRC B0910–636	2	09 12 01.54	−63 52 39.6	ce	349	<88	<0.34	7.4	62
MRC B0943–761	2	09 43 23.97	−76 20 10.0	ce	757	<177	css	2.8	−87
MRC B1003–415	c	10 05 57.33	−41 48 52.1	f	592	...	css	<2.2	...
MRC B1015–314	c	10 18 09.23	−31 44 13.9	f	1361	...	css	<3.1	...
MRC B1017–325	c	10 20 11.60	−32 45 34.8	ce	589	...	css	6.5	0
MRC B1017–421	2	10 19 44.34	−42 24 52.3	ce	418	<1	<0.004	101.5	−59
MRC B1017–426	2	10 20 03.68	−42 51 33.2	ce	1203	<288	<0.32	13.4	30
MRC B1030–340	c	10 33 13.03	−34 18 45.4	f	289	...	css	<2.8	...
MRC B1036–697	c	10 38 28.58	−70 03 08.7	f	692	...	css	<1.0	...
MRC B1044–357	2	10 46 44.83	−36 01 22.5	ce	360	<4	<0.02	52.2	−23
MRC B1046–409	D2	10 48 38.28	−41 14 00.2	co	934	491:	1.1:	7.7	−29
MRC B1116–462	T	11 18 26.89	−46 34 15.1	co	1524	1336	7.1	31.3	74
MRC B1143–483	1	11 45 31.07	−48 36 10.0	p	1258	10.7	65
MRC B1151–348	c	11 54 21.79	−35 05 29.0	f	2621	<2.9	...
MRC B1206–337	2	12 08 39.60	−34 03 07.6	ce	238	<33	<0.16	14.2	−29
MRC B1215–457	c	12 18 06.25	−46 00 29.0	f	2213	...	css	<1.9	...
MRC B1221–423	2	12 23 43.40	−42 35 32.1	f	1048	...	css	<2.1	...
MRC B1232–416	c	12 35 41.96	−41 53 18.8	f	483	...	css	<2.1	...
MRC B1243–412	c	12 45 57.63	−41 28 45.8	f	655	...	css	<2.1	...
MRC B1246–410	1	12 48 49.33	−41 18 38.1	ce	1400	...	css	32.3	−77
MRC B1247–401	2	12 50 05.84	−40 26 26.6	ce	298	<49	<0.20	7.2	29

Table 3—Continued

(1) Source name	(2) Str. code ^a	(3) R.A. h m s	(4) (J2000) ° ' "	(5) pos. code ^b	(6) S_{int} (mJy)	(7) S_{core} (mJy)	(8) R	(9) LAS ('')	(10) PA (°)
MRC B1259–769	2	13 03 12.36	−77 11 58.4	ce	384	<4	<0.02	21.9	−72
MRC B1303–827	2	13 08 38.24	−82 59 34.8	co	494	219	0.80	20.9	−26
MRC B1315–460	c	13 18 30.08	−46 20 35.1	f	670	...	css	<1.4	...
MRC B1320–446	c	13 23 04.25	−44 52 33.9	f	1152	...	css	<2.0	...
MRC B1330–328	2?	13 33 35.75	−33 05 24.1	ce	691	29.1	−2
MRC B1346–391	2	13 49 51.39	−39 22 52.2	ce	555	<111	<0.25	6.8	14
MRC B1355–416	2	13 59 00.18	−41 52 53.3	co	1408	85	0.065	59.4	−59
MRC B1358–493	2	14 01 31.37	−49 32 31.9	ce	778	<1	<0.003	62.9	−47
MRC B1359–358	2	14 02 40.11	−36 03 51.2	ce	440	<122	<0.39	6.7	−45
MRC B1407–425	x	14 10 29.02	−42 46 54.3	ce	232:	<2	<0.02	49.0	−18
MRC B1416–493	1	14 20 03.71	−49 35 42.4	co	1059	48	0.048	30.8	50
MRC B1421–382	2	14 24 16.54	−38 26 47.9	co	620	109	0.21	83.7	−38
MRC B1421–490	c	14 24 32.25	−49 13 50.0	f	5305	<1.5	...
MRC B1424–418	c	14 27 56.33	−42 06 19.1	f	2471	<2.3	...
MRC B1445–468	2	14 48 28.26	−47 01 43.1	co	540	<3	<0.006	41.4	44
MRC B1451–364	2	14 54 28.53	−36 40 01.1	ce	692	<1	<0.002	152.5	−22
MRC B1458–391	c	15 01 34.79	−39 18 40.0	f ^c	1171	...	css	<2.4	...
MRC B1526–423	2	15 30 14.31	−42 31 53.5	ce	1212	<2	<0.002	32.9	−82
MRC B1540–337	1/2?	15 44 02.94	−33 52 29.5	co	565	<24	<0.05	46.6	42
MRC B1547–795	2	15 55 21.23	−79 40 36.7	ce:	1573	<6	<0.005	34.5	25
MRC B1549–790	c	15 56 58.87	−79 14 04.3	f	4660	<1.0	...
MRC B1607–841	c	16 19 32.30	−84 18 18.0	ce:	420	...	css	1.3	−28
MRC B1622–310	T	16 25 55.52	−31 08 11.2	ce:	717	6.8	84
MRC B1655–776	2	17 02 40.84	−77 41 56.7	co:	1120	<86:	<0.09:	24.2	74
MRC B1706–606	2	17 10 30.12	−60 41 17.1	ce:	451	<3	<0.007	16.7	62
MRC B1721–836	2	17 33 54.72	−83 42 53.5	ce:	226	<1	<0.008	12.1	38
MRC B1737–575	2	17 41 31.14	−57 37 16.7	ce:	769	<19	<0.03	21.7	−62
MRC B1754–597	2	17 59 07.37	−59 46 49.5	co:	737	24	0.035	28.8	39
MRC B1756–663	c	18 01 18.34	−66 23 02.0	f:	601	...	css	<1.0	...
MRC B1814–519	2	18 18 06.99	−51 58 09.5	ce	775	...	css	2.7	−78
MRC B1814–637	c	18 19 35.29	−63 45 48.5	f:	4380	...	css	<1.1	...
MRC B1817–391	2	18 20 35.30	−39 09 27.6	ce	662	<6	<0.01	24.9	−25
MRC B1817–640	2	18 22 15.82	−63 59 19.3	ce	756	<1	<0.003	38.8	56
MRC B1827–360	c	18 30 58.90	−36 02 30.3	f ^c	1327	...	css	<1.5	...
MRC B1829–344	1	18 32 32.41	−34 22 37.6	co	488	26:	0.057:	11.4	−39
MRC B1831–668	2	18 36 59.68	−66 49 08.7	ce:	725	<117	css	2.7	−88

Table 3—Continued

(1) Source name	(2) Str. code ^a	(3) R.A. h m s	(4) (J2000) ° ' "	(5) pos. code ^b	(6) S_{int} (mJy)	(7) S_{core} (mJy)	(8) R	(9) LAS (")	(10) PA (°)
MRC B1853–303	2	18 57 10.62	−30 19 41.4	ce	507	<20	<0.05	17.3	36
MRC B1854–663	c	18 59 58.26	−66 15 02.9	f:	448	...	css	<1.0	...
MRC B1917–546	2	19 21 52.89	−54 31 56.4	ce	78	<1	<0.008	26.9	−35
MRC B1923–328	2	19 26 28.33	−32 42 39.1	ce	321	<1	<0.002	32.1	78
MRC B1932–464	2	19 35 56.99	−46 20 41.5	ce	3860	<24	<0.007	32.4	−71
MRC B1933–587	T	19 37 32.36	−58 38 26.1	p	988	<893	<9.5	14.0	−3
MRC B1953–425	c	19 57 15.28	−42 22 19.9	ce	930	...	css	2.0	64
MRC B1954–552	1	19 58 16.50	−55 09 37.4	co	1900	<68	<0.04	17.0	26
MRC B1955–357	2	19 59 03.83	−35 34 31.9	ce	683	<210	<0.44	9.2	−8
MRC B2009–524	2	20 13 20.96	−52 18 07.8	ce	690	<17	<0.03	22.8	−60
MRC B2020–575	2	20 24 20.54	−57 23 43.9	co	1095	172	0.19	53.8	19
MRC B2028–732	2	20 33 52.77	−73 03 58.7	co	420	13	0.032	92.8	60
MRC B2031–359	1	20 34 44.56	−35 49 02.7	m	591	3.2	70
MRC B2032–350	2	20 35 47.62	−34 54 01.9	ce	1960	<2	<0.002	32.0	5
MRC B2049–368	2	20 52 17.50	−36 40 30.4	ce	283	<73	<0.35	3.4	39
MRC B2052–474	T	20 56 16.36	−47 14 47.4	co	1925	1806	15	3.9	26
MRC B2059–641	2	21 03 26.19	−63 56 50.4	ce	290	<15	<0.06	36.1	−63
MRC B2115–305	2	21 18 10.59	−30 19 11.6	co	847	174	0.26	15.0	−32
MRC B2122–555	2	21 26 14.42	−55 21 30.0	co	568	15	0.029	31.0	17
MRC B2128–315	2	21 31 23.15	−31 21 14.3	co	480	106	0.28	6.0	−39
MRC B2140–434	2	21 43 33.39	−43 12 52.5	co	790	6	0.0086	71.2	−7
MRC B2140–817	2	21 47 23.25	−81 32 08.2	ce	1095	<2	<0.003	39.8	−27
MRC B2150–520	2	21 54 07.51	−51 50 19.5	ce	1159	<12	<0.02	21.5	−36
MRC B2201–555	2	22 05 04.93	−55 17 43.8	ce	484	<88	css	3.6	−85
MRC B2213–456	c	22 16 55.45	−45 21 44.5	ce	628	...	css	1.5	−86
MRC B2223–528	2	22 27 02.58	−52 33 25.9	ce	690	<51	<0.09	14.1	−53
MRC B2226–386	2	22 29 46.90	−38 23 59.7	ce	378	<110	<0.41	5.4	−11
MRC B2226–411	T	22 29 18.61	−40 51 32.6	co	1086	836	3.4	8.9	−56
MRC B2250–412	2	22 53 03.45	−40 57 47.1	ce	1248	<234	<0.23	16.8	−83
MRC B2252–530	2	22 55 50.01	−52 45 43.3	ce	996	<187	css	3.5	80
MRC B2253–522	2	22 56 47.55	−51 58 42.9	ce	758	<168	<0.29	14.4	36
MRC B2305–418	2	23 07 52.70	−41 32 44.9	ce	473	<72	<0.18	8.2	62
MRC B2319–550	2	23 22 06.84	−54 45 29.8	ce	459	<93	<0.26	8.9	34
MRC B2323–407	2	23 26 34.12	−40 27 17.3	ce	1076	<1	<0.002	15.6	34
MRC B2331–416	2	23 34 25.97	−41 25 26.9	ce	1471	<33	<0.03	20.6	57
MRC B2332–668	2	23 35 11.59	−66 37 05.7	ce	690	<6	<0.009	33.6	−45
MRC B2338–585	2	23 41 18.28	−58 16 09.7	ce	898	<258	<0.40	19.1	−46

Table 3—Continued

(1) Source name	(2) Str. code ^a	(3) R.A. h m s	(4) (J2000) ° ' "	(5) pos. code ^b	(6) S_{int} (mJy)	(7) S_{core} (mJy)	(8) R ()	(9) LAS ()	(10) PA (°)
MRC B2339–353	c	23 41 45.88	–35 06 22.7	f	486	...	css	<2.0	...
MRC B2354–350	1	23 57 00.64	–34 45 32.7	ce	99	<17	<0.21	13.1	–33

^aCode for source structure. “1” = FR 1 double, “2” = FR 2 double, “1/2” = structure borderline between FR 1 and FR 2, “D2” = double with one component coincident with the optical counterpart (Macdonald & Miley 1971), “T” = core-dominated triple, “c” = structure not resolved well enough to classify, “x” = extended source which does not fall into any of the usual categories.

^bCode for the type of position given in columns 2 and 3. “p” stands for peak, “ce” for centroid, “co” for core, “f” for the peak of a Gaussian fit to a compact source, and “m” for the midpoint of the two inner peaks of a tailed radio source. A colon “:” after the position code denotes that the position is suspect, usually because the source was observed in Run 9: see Section 2.3.

^cPosition is from the MOST calibrator list. The source was a secondary calibrator observed before a good ATCA position was available.

Table 4. Mean and median separations from candidate to position of confirmed optical counterpart for 43 FR 2 sources. Separations are in units of largest angular extent. Here “midway point” stands for the point midway between the midpoint and the centroid, and σ is the standard deviation of the mean.

Radio search position	Radio-optical Separation		
	Median	Mean	σ
Centroid	0.081	0.101	0.077
Midpoint	0.078	0.093	0.069
Midway point	0.057	0.074	0.057

Table 5. Journal of AAT imaging observations

Run No.	Date	Observers	Seeing (arcsec)	Remarks
1	1993 Feb 26	Burgess, Hunstead	1.6	Mostly clear
2	1993 Feb 27	"	1.6	Clear
3	1993 Aug 15	Burgess, Sadler	1.4	Mostly cloudy
4	1993 Aug 16	"	2.1	Partly cloudy
5	1994 Feb 14	Da Costa, Heisler	1.6	Service run
6	1994 May 14	Baker, Hunstead, Burgess	1.2	Clear

Table 6. Photometric solutions for AAT CCD imaging.

Runs	Photometric solution ^a
1, 2	$R = 31.03 - 2.5 \log_{10}(ADUs^{-1}) - 0.205 \chi$
6	$R = 30.97 - 2.5 \log_{10}(ADUs^{-1}) - 0.109 \chi$

^a $ADUs^{-1}$ stands for the number of counts in Analogue to Digital Units per second, and χ stands for air-mass.

Table 7. Positions, magnitudes, and redshifts for the optical counterparts.

(1) Source Name	(2) ID ^a	(3) Optical position		(4)	(5)	(6)	(7)	(8)	(9) References			
		R. A. (J2000)	dec	b_J	R	Seeing ('')	z	ID	FC	pos	b_J	z
MRC B0003–567	g	00 05 57.94	−56 28 31.5	19.6	18.7	1.4	(0.26)	1	1	2	3	4
MRC B0003–428	g	00 06 01.76	−42 34 41.4	21.2	20.2	1.5	(0.53)	5	5	2	3	6
MRC B0003–833	g	00 06 16.64	−83 06 07.8	20.1	(0.32)	7	5	7	3	4
MRC B0007–446	g	00 10 29.89	−44 22 55.4	>21.5 ^b	22.2	1.3	(1.00)	8	8	9	...	6
MRC B0008–421	g	00 10 52.54	−41 53 10.6	>21.5 ^b	22.6	1.3	(1.12)	10	11	12	...	6
MRC B0012–383	g	00 15 24.31	−38 04 38.8	>21.5 ^b	20.4	1.4	(0.57)	5	5	9	...	6
MRC B0013–634	g	00 16 02.82	−63 10 04.8	>21.5	(>0.56)	5	...	2	...	4
MRC B0023–333	g	00 25 31.37	−33 02 46.7	14.6 ^c	0.0497	13	14	15	16	17
MRC B0036–392	Q	00 38 26.84	−38 59 48.1	>16.2 ^c	0.592	18	19	20	3	21
MRC B0039–445	g	00 42 08.98	−44 14 00.1	20.0	18.7	1.9	0.346	22	11	2	3	23
MRC B0042–357	g	00 44 41.30	−35 30 33.1	23.2	22.2	1.5	(0.98)	5	5	20	3	6
MRC B0043–424	g	00 46 17.64	−42 07 51.1	17.2	0.116	24	14	7	3	23
MRC B0048–447	g	00 50 52.00	−44 28 38.1	21.5	20.9	2.0	(0.67)	5	25	2	3	6
MRC B0049–433	g	00 52 14.85	−43 06 28.5	20.6	19.1	1.9	(0.39)	5	5	26	3	4
MRC B0103–453	g ^d	01 05 22.12	−45 05 17.1	>21.5 ^b	21.1	2.2	(0.71)	5	5	9	...	6
MRC B0110–692	BF	>21.5 ^b	(>0.56)	4
PKS B0114–47	g	01 16 25.05	−47 22 41.6	17.2	0.146	13	24	7	3	27
MRC B0119–634	Q	01 21 40.48	−63 09 02.2	17.1	0.837	28	28	2	3	29
MRC B0131–449	g	01 33 33.14	−44 44 17.8	17.9	0.0897	30	30	15	3	31
PKS B0131–36	g	01 33 57.78	−36 29 35.2	13.5 ^c	0.0300	13	32	7	7	24
MRC B0157–311	Q	02 00 12.18	−30 53 27.9	19.0	0.677	14	33	2	3	34

Table 7—Continued

(1) Source Name	(2) ID ^a	(3) Optical position		(5) b_J mag	(6) R mag	(7) Seeing ($''$)	(8) z	(9) References				
		R. A. (J2000)	dec					ID	FC	pos	b_J	z
MRC B0201–440	g	02 03 40.78	−43 49 52.3	21.2	19.7	1.6	(0.45)	35	35	2	3	6
MRC B0202–765	Q	02 02 13.41	−76 20 04.7	14.5	0.38925	36	36	2	3	37
MRC B0208–512	Q	02 10 46.17	−51 01 03.2	16.9	1.003	38	38	2	3	21
MRC B0214–480	g	02 16 45.09	−47 49 09.4	15.0	0.0641	39	40	7	3	41
MRC B0216–366	Q? ^d	02 19 02.88	−36 26 07.3	18.9	19.1	1.7	...	5	5	15	3	...
MRC B0219–706	g	02 20 08.24	−70 22 28.2	21.1	19.3	1.6	(0.40)	5	5	20	3	6
MRC B0223–712	g ^d	02 23 57.38	−70 59 46.3	>21.5 ^b	23.0	1.5	(1.27)	5	5	20	...	6
MRC B0240–422	g ^d	02 42 34.64	−42 01 52.8	20.7	19.4	1.4	(0.42)	5	5	20	3	6
MRC B0241–512	g	02 43 13.79	−51 05 16.6	20.6	19.1	1.5	(0.39)	5	5	2	3	4
MRC B0242–514	g ^d	02 43 44.40	−51 12 37.9	>21.5 ^b	21.2	1.6	(0.72)	5	5	9	...	6
MRC B0245–558	g ^d	02 46 56.80	−55 41 23.0	>21.5 ^b	21.6	1.4	(0.82)	5	5	20	...	6
MRC B0251–675	Q	02 51 56.08	−67 18 00.0	17.1	1.002	42	43	2	3	43
MRC B0252–712	g	02 52 46.28	−71 04 34.6	>21.1 ^c	20.6:	1.4	0.563	44	11	20	3	11
MRC B0315–685	g ^e	03 16 10.60	−68 21 04.3	>21.5 ^b	23.1	1.9	(1.30)	5	5	20	...	6
PKS B0319–45	g	03 20 57.42	−45 15 10.5	15.6	0.0633	45	45	7	3	45
MRC B0320–373	g	03 22 41.72	−37 12 29.6	10.6	0.0058	46	47	48	3	49
PKS B0332–39	g	03 34 03.30	−39 00 36.6	15.7 ^c	0.0623	14	14	7	3	50
MRC B0335–415	g	03 37 04.48	−41 23 15.8	21.5	21.7	1.8	(0.86)	5	5	2	3	6
MRC B0336–355	g	03 38 45.97	−35 22 53.0	18.9	0.1126	51	52	7	3	52
MRC B0340–372	Q	03 42 05.39	−37 03 21.8	18.4	0.28513	53	53	2	3	37
MRC B0344–345	g	03 46 30.52	−34 22 45.8	16.2	0.0538	14	54	7	3	55
MRC B0357–371	g ^d	03 59 46.90	−37 00 27.0	20.9	19.5	1.4	(0.43)	5	25	2	3	6

Table 7—Continued

(1) Source Name	(2) ID ^a	(3) Optical position		(5)	(6)	(7)	(8)	(9) References				
		R. A. (J2000)	dec	b_J mag	R mag	Seeing ('')	z	ID	FC	pos	b_J	z
MRC B0407–658	g	04 08 20.34	−65 45 08.8	>21.5 ^b	21.4	1.4	(0.77)	56	56	9	...	6
MRC B0409–752	g	04 08 48.63	−75 07 19.5	>21.5:	21.0	1.8	0.694	57	11	9	...	57
MRC B0411–346A	g	04 13 00.88	−34 30 11.0	23.1	21.6	1.7	(0.83)	5	5	20	3	6
MRC B0411–647	g	04 11 59.38	−64 36 23.5	17.3:	(0.11)	58	58	2	59	4
MRC B0411–561	g ^d	04 12 48.22	−56 00 45.8	20.4	19.4	1.6	(0.42)	5	5	20	3	6
MRC B0420–625	g	04 20 56.09	−62 23 39.1	>21.5 ^b	21.6	1.2	(0.81)	5	28	20	...	6
MRC B0424–728	g	04 23 57.61	−72 46 01.6	19.0	(0.21)	7	5	7	7	4
MRC B0427–366	Q?	04 29 40.05	−36 30 54.3	19.1	19.5	1.8	...	5	5	2	3	...
PKS B0427–53	g	04 29 07.90	−53 49 39.4	14.0	0.0396	60	61	2	3	61
MRC B0429–616	g	04 30 22.12	−61 32 01.3	15.5	0.0556	62	63	7	3	64
MRC B0436–650	g ^d	04 37 08.38	−64 59 01.6	20.4:	18.8	1.5	(0.36)	5	58	9	59	4
MRC B0438–436	Q	04 40 17.17	−43 33 09.1	19.1	2.852	65	65	2	3	65
MRC B0453–301	g	04 55 14.29	−30 06 49.0	19.1	(0.22)	66	66	15	3	4
MRC B0454–463	Q	04 55 50.69	−46 15 58.4	17.3	0.8580	22	1	2	3	67
MRC B0456–301	g	04 58 25.55	−30 07 06.9	17.5	0.0630	66	66	7	3	68
MRC B0506–612	Q	05 06 44.09	−61 09 41.2	17.0	1.093	69	70	2	3	71
MRC B0509–573	Q	05 10 18.88	−57 19 38.6	18.7	1.194	1	1	2	3	72
MRC B0511–484	g	05 12 47.23	−48 24 16.4	20.0	19.1	1.4	0.30638	73	73	7	3	37
PKS B0511–30	g	05 13 31.90	−30 28 48.7	16.7	0.0583	14	14	7	3	74
MRC B0513–488	Q	05 14 32.83	−48 45 27.8	18.8	0.90	5	...	2	3	75
PKS B0518–45	g	05 19 49.72	−45 46 44.5	16.6	0.03498	13	76	2	3	37
MRC B0521–365	1	05 22 57.96	−36 27 30.8	16.7	0.0554	14	77	2	3	78

Table 7—Continued

(1) Source Name	(2) ID ^a	(3) Optical position		(4)	(5)	(6)	(7)	(8)	(9) References			
		R. A. (J2000)	dec	b _J mag	R mag	Seeing (")	z	ID	FC	pos	b _J	z
MRC B0534–497	g	05 36 13.61	−49 44 26.7	18.9	0.184	79	79	2	3	68
MRC B0546–445	g	05 47 37.92	−44 31 14.0	>21.5 ^b	22.7	1.5	(1.15)	5	5	9	...	6
MRC B0547–408	g	05 49 24.13	−40 51 16.4	21.5	20.8	1.4	(0.64)	5	5	2	3	6
MRC B0601–344	g	06 03 12.13	−34 26 33.7	21.5	20.5	1.3	(0.58)	5	5	2	3	6
MRC B0602–319	Q	06 04 14.45	−31 55 57.5	17.1	0.452	69	69	2	3	80
MRC B0602–647	g	06 02 39.27	−64 43 18.3	17.0	0.0449	38	38	2	38	68
MRC B0614–349	g	06 16 35.90	−34 56 15.8	20.6	19.4	1.3	0.329	18	81	2	3	82
MRC B0615–365	g	06 17 32.27	−36 34 15.5	>21.5 ^b	22.8	1.3	(1.18)	5	5	20	...	6
MRC B0618–371	g	06 20 00.93	−37 11 42.4	14.8 ^c	0.0326	14	14	2	3	83
MRC B0620–526	g	06 21 43.22	−52 41 36.0	15.5 ^c	0.0502	84	84	7	7	84
MRC B0625–536	g	06 26 20.47	−53 41 33.9	14.9	0.054	39	30	2	3	27
MRC B0625–354	g	06 27 06.69	−35 29 15.3	15.0 ^c	0.0546	14	33	2	33	64
MRC B0625–545	g	06 26 49.51	−54 32 34.1	15.4	0.052	38	38	2	3	7
MRC B0637–752	Q	06 35 46.77	−75 16 16.3	15.9	0.651	85	38	2	3	86
MRC B0646–398	Q?	06 48 11.09	−39 57 10.3	17.8	87	...	2	3	...
MRC B0647–475	g	06 48 48.44	−47 34 26.8	>21.5 ^b	24.4	1.7	(1.94)	5	5	20	...	6
MRC B0658–656	O	>18.0	(>0.14)	4
MRC B0700–473	g	07 02 09.55	−47 26 34.8	>21.5 ^b	21.7	1.3	(0.86)	5	5	20	...	6
MRC B0704–427	Q	07 05 54.22	−42 48 52.8	18.9	1.33	87	...	2	3	75
PKS B0707–35	g	07 09 13.97	−36 01 22.8	20.5	17.8	1.6	0.1108	7	5	7	3	137
MRC B0715–362	g	07 17 08.12	−36 22 00.6	15.7	0.032	14	14	7	3	7

Table 7—Continued

(1) Source Name	(2) ID ^a	(3) Optical position		(4)	(5)	(6)	(7)	(8)	(9) References				
		R. A.	(J2000)	dec	b_J mag	R mag	Seeing ($''$)	z	ID	FC	pos	b_J	z
MRC B0719–553	g	07 20 15.05	–55 25 20.0	19.5	0.216	79	79	2	3	82	
MRC B0743–673	Q	07 43 31.73	–67 26 25.3	16.2	1.512	79	70	2	3	88	
MRC B0842–754	Q	08 41 27.42	–75 40 27.6	18.1	0.524	85	89	2	3	89	
MRC B0842–835	g	08 37 14.90	–83 44 38.8	>21.5 ^b	21.6	1.8	(0.82)	5	5	20	...	6	
MRC B0846–811	g	08 43 38.79	–81 18 24.7	>21.5 ^b	22.3	1.8	(1.01)	5	5	20	...	6	
MRC B0906–682	g	09 06 52.64	–68 29 40.3	>21.5	(>0.56)	5	...	2	...	4	
MRC B0910–636	g	09 12 01.60	–63 52 39.0	>21.5 ^b	21.0	1.7	(0.68)	5	5	20	...	6	
MRC B0943–761	g	09 43 24.42	–76 20 10.3	19.7	(0.27)	85	5	2	3	4	
MRC B1003–415	g	10 05 57.28	–41 48 52.7	>21.5 ^b	21.6:	1.4	(0.81)	5	5	20	...	6	
MRC B1015–314	Q	10 18 09.29	–31 44 13.1	20.4	19.6	1.4	1.346	33	33	2	3	11	
MRC B1017–421	g ^d	10 19 43.78	–42 24 47.3	>21.5 ^b	21.1	1.2	(0.70)	5	5	20	...	6	
MRC B1017–325	g	10 20 11.48	–32 45 38.3	18.5	18.4:	1.4	(0.17)	5	5	2	3	4	
MRC B1017–426	Q	10 20 03.85	–42 51 30.2	18.1	1.280	33	43	2	3	43	
MRC B1030–340	g	10 33 13.03	–34 18 46.2	>20.7 ^c	20.0	1.3	(0.50)	5	5	9	3	6	
MRC B1036–697	g ^e	10 38 28.82	–70 03 07.6	>21.5 ^b	21.8	1.5	(0.87)	5	79	20	...	6	
MRC B1044–357	g	10 46 45.22	–36 01 39.8	>21.5 ^b	22.0	1.4	(0.94)	5	5	9	...	6	
MRC B1046–409	Q	10 48 38.38	–41 14 00.8	16.9	0.620	90	90	2	3	91	
MRC B1056–360	g	10 58 54.78	–36 19 22.9	16.6	0.070	25	25	7	3	7	
MRC B1116–462	Q	11 18 26.97	–46 34 15.6	16.6	0.713	85	79	2	3	91	
MRC B1123–351	g	11 25 52.90	–35 23 41.3	14.0	0.0320	14	14	7	3	84	
MRC B1136–320	g ^d	11 39 16.90	–32 22 22.0	>21.5 ^b	20.9	1.3	(0.67)	5	5	9	...	6	
MRC B1143–483	g	11 45 31.05	–48 36 10.9	20.2	19.1	1.5	(0.33)	85	5	2	3	4	

Table 7—Continued

(1) Source Name	(2) ID ^a	(3) Optical position		(5) b_J mag	(6) R mag	(7) Seeing ('')	(8) z	(9) References				
		R. A. (J2000)	dec					ID	FC	pos	b_J	z
MRC B1143–316	g ^d	11 46 20.67	−31 57 13.4	>21.5 ^b	23.2	1.7	(1.35)	5	5	20	...	6
MRC B1151–348	Q	11 54 21.77	−35 05 30.4	14.0	0.25799	92	93	2	3	37
MRC B1206–337	g	12 08 39.68	−34 03 10.6	>21.5 ^b	22.9	1.5	(1.24)	5	5	20	...	6
MRC B1215–457	Q	12 18 06.24	−46 00 29.3	19.0	0.529	85	43	2	3	43
MRC B1221–423	g	12 23 43.30	−42 35 32.8	16.9	0.1706	14	14	2	3	94
MRC B1232–416	g ^e	12 35 42.09	−41 53 19.8	22.6	21.6	1.5	(0.82)	5	38	12	3	6
MRC B1234–504	Q? ^e	12 37 15.55	−50 46 23.5	>21.5 ^b	21.1:	1.7	(>0.56)	5	5	20	...	4
MRC B1243–412	Q	12 45 57.58	−41 28 45.8	18.6	1.58	95	95	2	3	75
MRC B1246–410	g	12 48 49.20	−41 18 42.9	11.5	0.00930	96	96	2	3	83
MRC B1247–401	g	12 50 05.80	−40 26 26.2	>21.5 ^b	22.8	1.4	(1.20)	5	5	20	...	6
MRC B1259–769	g	13 03 12.70	−77 11 58.8	>21.5 ^b	22.2	1.9	0.58	5	5	20	...	138
MRC B1259–445	g ^d	13 02 31.97	−44 46 38.7	>21.5 ^b	20.6	1.6	(0.60)	5	5	20	...	6
PKS B1302–325	{ g g }	13 04 58.46 13 04 58.58	−32 49 12.9 −32 49 17.5	18.0	0.153	7	...	7	3	94
MRC B1302–491	g	13 05 26.20	−49 28 15.7	9.4	0.00184	97	98	7	3	83
MRC B1303–827	Q	13 08 38.01	−82 59 35.2	17.0	18.2	2.1	0.87	5	5	2	3	139
MRC B1315–460	g	13 18 30.02	−46 20 35.2	>21.5 ^b	22.6	1.5	(1.12)	5	5	20	...	6
PKS B1318–434	g	13 21 12.80	−43 42 16.4	12.0 ^c	0.0106	99	100	7	7	101
MRC B1320–446	Q	13 23 04.19	−44 52 34.1	17.6	1.95	102	102	2	3	75
MRC B1322–427	g	13 25 29.01	−43 00 59.9	11.7	0.00183	103	104	7	3	105
MRC B1330–328	g	13 33 35.74	−33 05 14.2	18.1	0.0859	94	...	2	3	94
PKS B1333–33	g	13 36 39.37	−33 57 59.5	11.7	0.0124	97	106	7	3	107

Table 7—Continued

(1) Source Name	(2) ID ^a	(3) Optical position		(4)	(5)	(6)	(7)	(8)	(9) References			
		R. A. (J2000)	dec	b _J mag	R mag	Seeing (")	z	ID	FC	pos	b _J	z
MRC B1346–391	g ^f	13 49 51.12	−39 22 51.2	>21.5 ^b	22.4:	1.6	(1.06)	5	5	108	...	6
MRC B1355–416	Q	13 59 00.23	−41 52 53.8	16.1	0.3145	87	95	2	3	37
MRC B1358–493	g ^d	14 01 31.15	−49 32 35.3	>21.5 ^b	(>0.56)	5	5	20	...	4
MRC B1359–358	g	14 02 40.16	−36 03 51.3	22.4	20.2	1.8	(0.53)	5	5	20	3	6
PKS B1400–33	R	0.0139 ^g	109
MRC B1407–425	g	14 10 28.96	−42 46 56.7	15.1	0.053	25	110	2	3	111
MRC B1413–364	g	14 16 33.11	−36 40 56.1	17.7	0.0747	14	14	2	3	94
MRC B1416–493	g	14 20 03.72	−49 35 42.1	17.5	0.0915	36	...	2	112	94
MRC B1421–382	Q	14 24 16.50	−38 26 48.3	16.2	0.4068	87	...	2	3	37
MRC B1421–490	g	14 24 32.26	−49 13 50.4	>21.5 ^b	24.2	1.7	(1.84)	5	5	20	...	6
MRC B1424–418	Q	14 27 56.31	−42 06 20.5	17.6	1.522	87	113	2	3	53
MRC B1425–479	g	14 28 57.08	−48 12 07.7	17.5	(0.11)	7	...	7	7	4
MRC B1445–468	g	14 48 28.20	−47 01 42.5	>21.5 ^b	(>0.56)	5	5	9	...	4
MRC B1451–364	g ^d	14 54 28.17	−36 40 06.3	21.7	19.5	1.8	(0.43)	5	5	2	3	6
MRC B1458–391	g	15 01 34.81	−39 18 39.7	>21.5 ^b	22.9	1.9	(1.24)	5	5	20	...	6
MRC B1526–423	g ^d	15 30 14.25	−42 31 51.5	>20.0 ^c	20.0:	2.1	(0.50)	5	5	20	3	6
MRC B1540–730	g? ^d	15 46 08.76	−73 10 46.2	>21.5	21.0	2.1	(0.68)	5	5	20	...	6
MRC B1540–337	g	15 44 02.84	−33 52 29.0	20.5: ^c	19.5:	1.9	(0.43)	5	5	20	59	6
MRC B1545–321	g	15 48 58.02	−32 16 56.2	18.2	0.1082	7	5	7	3	94
MRC B1547–795	g	15 55 21.37	−79 40 35.7	20.4	19.1	1.6	0.482	85	5	2	3	11
MRC B1549–790	g	15 56 58.83	−79 14 03.9	19.4	18.2	1.2	0.1494	90	90	2	3	114

|
∞
|

Table 7—Continued

(1) Source Name	(2) ID ^a	(3) Optical position		(5) b_J mag	(6) R mag	(7) Seeing (")	(8) z	(9) References				
		R. A. (J2000)	dec					ID	FC	pos	b_J	z
MRC B1607–841	g ^e	16 19 33.78	−84 18 19.5	>21.5 ^b	22.6	2.2	(1.11)	5	5	9	...	6
MRC B1610–771	Q	16 17 49.42	−77 17 18.3	19.3 ^c	1.710	79	79	2	115	116
MRC B1622–310	Q	16 25 55.40	−31 08 07.8	18.3	1.124	117	118	2	3	91
MRC B1633–681	g ^d	16 38 11.02	−68 14 17.8	>21.5 ^b	23.0:	1.0	(1.27)	5	5	20	...	6
MRC B1637–771	g	16 44 16.26	−77 15 48.4	16.3	0.0423	36	119	2	3	17
MRC B1655–776	g	17 02 41.17	−77 41 56.9	17.7	0.0944	120	119	2	3	94
MRC B1706–606	g	17 10 29.54	−60 41 19.2	>21.5	22.5	1.0	(1.09)	5	5	20	...	6
MRC B1716–800	g	17 25 26.85	−80 04 46.8	22.4	19.6	1.0	(0.45)	79	79	2	3	6
MRC B1721–836	g	17 33 55.00	−83 42 54.1	>21.5 ^b	>23.4	1.0	(1.42)	5	5	9	...	6
PKS B1733–56	g	17 37 35.85	−56 34 03.7	17.2	0.0985	121	121	7	3	121
MRC B1737–575	g	17 41 31.01	−57 37 17.3	>20.2 ^c	20.1:	1.0	(0.51)	5	5	20	3	6
MRC B1737–609	g	17 42 02.25	−60 55 19.9	21.0	19.4	1.1	(0.41)	7	5	7	3	6
MRC B1740–517	g	17 44 25.49	−51 44 43.3	>21.5 ^b	20.8	1.1	(0.63)	11	11	9	...	6
MRC B1754–597	g	17 59 07.25	−59 46 48.9	>21.5	21.5	1.0	(0.80)	5	79	20	...	6
MRC B1756–663	g	18 01 18.05	−66 23 01.7	>21.5 ^b	>22.0	1.0	(0.93)	5	38	20	...	6
MRC B1814–519	g	18 18 06.96	−51 58 09.7	21.0: ^c	19.9	1.1	(0.48)	5	79	20	59	6
MRC B1814–637	g	18 19 35.16	−63 45 48.2	>17.1 ^c	0.0627	79	122	2	3	122
MRC B1817–391	g ^d	18 20 35.48	−39 09 27.7	>21.5 ^b	21.9:	1.0	(0.91)	5	5	20	...	6
MRC B1817–640	g	18 22 16.21	−63 59 18.7	21.5: ^c	21.2:	1.1	0.67	5	5	20	59	140
MRC B1818–557	g ^d	18 22 19.17	−55 41 36.5	>21.5	19.8	1.0	(0.47)	5	5	20	...	6
MRC B1819–673	g	18 24 34.44	−67 17 30.2	22.5	19.7	1.0	(0.45)	5	5	2	3	6
MRC B1827–360	g	18 30 58.83	−36 02 31.3	17.7: ^c	(0.12)	5	5	2	59	4

Table 7—Continued

(1) Source Name	(2) ID ^a	(3) Optical position		(5) b_J mag	(6) R mag	(7) Seeing ('')	(8) z	(9) References				
		R. A. (J2000)	dec					ID	FC	pos	b_J	z
MRC B1829–344	g	18 32 32.42	−34 22 38.8	>20 ^c	17.9	1.0	(>0.31)	5	5	123	...	4
MRC B1831–668	g	18 36 59.40	−66 49 07.4	19.6	18.6	1.1	(0.26)	5	5	20	3	4
MRC B1839–487	g	18 43 14.59	−48 36 23.4	16.4	0.1112	39	30	2	3	94
MRC B1840–404	g ^d	18 44 28.77	−40 21 57.5	>21.5 ^b	24.1	1.0	(1.77)	5	5	20	...	6
MRC B1853–303	g? ^d	18 57 10.67	−30 19 40.1	>21.5 ^b	20.1:	1.0	(0.53)	5	5	20	...	6
MRC B1854–663	g	18 59 58.09	−66 15 02.4	22.3	20.5	0.8	(0.58)	5	5	20	3	6
MRC B1917–546	BF	>21.5 ^b	>22.0	1.0	(>0.56)	4
MRC B1922–627	g ^d	19 27 27.29	−62 39 35.4	>21.5 ^b	21.8	1.0	(0.88)	5	5	20	...	6
MRC B1923–328	g ^d	19 26 28.53	−32 42 41.2	>21.5 ^b	23.2	1.1	(1.36)	5	5	20	...	6
MRC B1929–397	g	19 33 24.97	−39 40 22.4	15.5 ^c	0.0746	25	25	2	7	94
MRC B1932–464	g	19 35 56.45	−46 20 40.2	19.5	0.231	92	11	2	3	23
MRC B1933–587	Q	19 37 32.38	−58 38 27.5	17.9	19.1	1.0	1.92	5	5	20	3	140
MRC B1934–638	g	19 39 24.95	−63 42 45.9	19.1	0.183	124	36	2	3	125
MRC B1940–406	g	19 43 51.69	−40 30 12.0	18.7	(0.18)	7	...	2	3	4
MRC B1953–425	g	19 57 15.31	−42 22 19.1	>21.5 ^b	21.6:	1.0	(0.82)	5	5	9	...	6
MRC B1954–552	g	19 58 16.26	−55 09 38.9	15.0 ^c	0.0581	36	...	2	7	94
MRC B1955–357	Q	19 59 03.83	−35 34 29.9	18.6	0.36	87	...	2	3	140
MRC B2006–566	R	0.055 ^h	126
MRC B2009–524	g	20 13 21.04	−52 18 09.7	>20.5 ^c	19.5:	1.1	(0.43)	5	5	9	3	6
MRC B2013–557	g	20 18 01.31	−55 39 30.8	16.2	0.0605	24	24	7	3	17
MRC B2020–575	g	20 24 20.61	−57 23 43.5	19.4	17.2	1.1	0.352	127	5	2	3	7
MRC B2028–732	Q	20 33 53.02	−73 03 58.1	17.9	0.455	7	...	2	3	7

Table 7—Continued

(1) Source Name	(2) ID ^a	(3) Optical position		(4)	(5)	(6)	(7)	(8)	(9) References			
		R. A. (J2000)	dec	b _J mag	R mag	Seeing (")	z	ID	FC	pos	b _J	z
MRC B2031–359	g	20 34 44.70	–35 49 01.8	15.5 ^c	0.0884	25	25	2	16	128
MRC B2032–350	g ^d	20 35 47.71	–34 54 11.5	21.4	20.4	1.1	(0.56)	11	11	2	3	6
MRC B2041–604	g	20 45 21.28	–60 18 54.9	>21.5	21.3	1.1	1.464	129	129	20	...	130
MRC B2049–368	g	20 52 17.45	–36 40 30.7	>21.5 ^b	21.9	1.2	(0.89)	5	58	9	...	6
MRC B2052–474	Q	20 56 16.35	–47 14 47.7	17.9	1.489	43	43	2	3	91
MRC B2059–641	g ^d	21 03 26.11	–63 56 49.7	>21.5 ^b	22.6	1.0	(1.11)	5	5	20	...	6
MRC B2115–305	Q	21 18 10.59	–30 19 12.1	16.4	0.98	14	14	2	3	131
MRC B2122–555	Q? ^d	21 26 14.49	–55 21 29.6	19.4	17.9	1.1	...	5	5	15	3	...
MRC B2128–315	Q	21 31 23.15	–31 21 14.6	17.6	0.99	19	19	2	3	118
MRC B2140–434	Q	21 43 33.36	–43 12 52.2	18.0	0.650	22	...	2	3	5
MRC B2140–817	g	21 47 24.52	–81 32 12.9	22.8	20.8	1.2	(0.64)	5	5	9	3	6
PKS B2148–555	g	21 51 29.99	–55 20 13.2	14.8	0.0388	58	58	7	3	132
MRC B2150–520	g	21 54 07.04	–51 50 12.7	>21.5	21.4	1.0	(0.79)	5	33	20	...	6
MRC B2152–699	g	21 57 06.26	–69 41 23.6	14.1	0.0281	120	133	2	3	133
MRC B2153–699	g	21 57 48.46	–69 41 52.6	20.2	(0.33)	7	5	7	3	4
MRC B2158–380	g	22 01 17.11	–37 46 25.4	14.8	0.03333	25	134	2	3	134
MRC B2201–555	g	22 05 04.94	–55 17 43.7	21.4	20.0	1.2	(0.51)	5	5	2	3	6
MRC B2213–456	Q?	22 16 55.46	–45 21 43.8	18.4	5	28	2	3	...
MRC B2223–528	g	22 27 02.27	–52 33 24.4	20.3	19.4	1.0	(0.41)	5	5	20	3	6
MRC B2226–411	Q	22 29 18.58	–40 51 32.9	18.8	0.4462	92	53	2	3	53
MRC B2226–386	g	22 29 46.91	–38 23 59.3	>21.5 ^b	23.1	1.1	(1.30)	5	5	9	...	6

Table 7—Continued

(1) Source Name	(2) ID ^a	(3) Optical position		(4)	(5)	(6)	(7)	(8)	(9) References			
		R. A. (J2000)	dec	b _J mag	R mag	Seeing (")	z	ID	FC	pos	b _J	z
MRC B2250–412	g	22 53 03.08	–40 57 46.9	20.7	19.1	1.2	0.310	85	11	20	3	23
MRC B2252–530	g	22 55 49.98	–52 45 43.5	21.8	20.3	1.2	(0.55)	5	28	9	3	6
MRC B2253–522	g ^d	22 56 47.28	–51 58 44.1	>20.5 ^c	19.5	1.1	(0.43)	5	5	9	3	6
MRC B2259–375	g	23 02 23.89	–37 18 06.9	>21.5 ^b	22.6	1.1	(1.14)	5	5	12	...	6
MRC B2305–418	g	23 07 52.70	–41 32 45.2	>21.5 ^b	20.7	1.2	(0.63)	5	5	9	...	6
MRC B2319–550	g	23 22 06.81	–54 45 29.7	>21.5	21.2	1.1	(0.73)	5	1	9	...	6
MRC B2323–407	g	23 26 34.36	–40 27 12.6	>21.5 ^b	21.5	1.1	(0.81)	5	5	20	...	6
MRC B2331–416	g	23 34 26.19	–41 25 25.0	21.0	20.4	1.4	0.907	92	11	2	3	11
MRC B2332–668	O	>16.5	(>0.08)	4
MRC B2338–585	g ^d	23 41 18.87	–58 16 12.6	>21.5 ^b	20.8	1.1	(0.64)	5	5	9	...	6
MRC B2339–353	g	23 41 45.82	–35 06 23.0	22.4	20.4	1.5	(0.56)	135	135	2	3	6
MRC B2354–350	g	23 57 00.37	–34 45 30.0	14.0	0.0487	14	136	62	3	17
PKS B2356–61	g	23 59 04.38	–60 54 59.3	16.8	0.0959	120	24	7	3	17

^aType of optical ID: g = galaxy, g? = possible galaxy, l = BL Lac object, Q = quasar, Q? = quasar candidate, BF = blank field, O = field obscured by star, R = unidentified relic radio source in cluster

^bBlank field on the Schmidt plates

^cCrowded field not well analysed by COSMOS

^dExtended radio source with more than one candidate

^eCompact radio source with large radio-optical offset

^fPosition quoted is that of the VLA core

^gThe redshift quoted is that of the galaxy NGC 5419

^hThe redshift quoted is that of the cluster Abell 3667

Table 7. Positions, magnitudes, and redshifts for the optical counterparts.

Source	(1) ID ^a	(2) Optical position Name	(3) R. A. (J2000)		(4) Seeing		(5) b_J		(6) R		(7) mag		(8) mag		(9) References	
			dec	(")	ID	FC	pos	b_J	z							

References. — (1) Bolton & Savage (1977); (2) BP position, measured from Schmidt plates; (3) UKST/COSMOS database; (4) estimated from b_J magnitude; (5) this paper; (6) estimated from R magnitude; (7) Jones & McAdam (1992); (8) Hunstead (1994); (9) CCD position, referenced to DSS position; (10) de Vries (2003); (11) di Serego Alighieri et al. (1994); (12) CCD position, referenced to SuperCOSMOS position (Hambly et al. 2001); (13) Bolton et al. (1964); (14) Bolton et al. (1965); (15) DSS position; (16) Ekers et al. (1989); (17) Whiteoak (1972); (18) Hunstead (1972); (19) Peterson & Bolton (1973); (20) CCD position, referenced to BP position; (21) Peterson et al. (1976); (22) Lü (1974); (23) Tadhunter et al. (1993); (24) Westerlund & Smith (1966); (25) Bolton & Shimmmins (1973); (26) COSMOS position, referenced to BP position; (27) Danziger & Goss (1983); (28) Lasker & Smith (1974); (29) Hunstead et al. (1978); (30) Tritton & Whitworth (1973); (31) Shectman et al. (1996); (32) Ekers et al. (1978); (33) Prestage & Peacock (1983); (34) Stickel et al. (1994); (35) Fugmann et al. (1988); (36) Ekers (1970); (37) Eracleous & Halpern (2004); (38) Savage (1976); (39) Bajaja (1970); (40) Tritton & Schilizzi (1973); (41) White et al. (1988b); (42) Savage & Wright (1981); (43) Murdoch et al. (1984); (44) Savage et al. (1977); (45) Jones (1989); (46) Mills (1954); (47) Schweizer (1980); (48) Schweizer (1981); (49) Humason et al. (1956); (50) Collins et al. (1995); (51) Schilizzi & McAdam (1970); (52) Carter & Malin (1983); (53) White et al. (1988a); (54) Wall & Cannon (1973); (55) Drinkwater et al. (2001); (56) Stickel & Kühr (1996); (57) Alvarez et al. (1993); (58) Savage et al. (1976a); (59) estimated from COSMOS magnitudes of other objects; (60) Basinski et al. (1959); (61) Ellis et al. (1984); (62) Unewisse (1993); (63) Teague et al. (1990); (64) Quintana & Ramírez (1995); (65) Morton et al. (1978); (66) Shobbrook & Hunstead (1966); (67) Fricke et al. (1983); (68) J. Peacock (1992), priv. comm.; (69) Peterson et al. (1973); (70) Schneider et al. (1992); (71) Wright et al. (1977); (72) R. Hunstead (1984), unpublished; (73) Robertson & Smith (1981); (74) P. Shaver (1995), priv. comm.; (75) J. Baker (1991), priv. comm.; (76) Danziger et al. (1977); (77) Westerlund & Stokes (1966); (78) Danziger et al. (1979); (79) Hunstead et al. (1971); (80) Bolton et al. (1976); (81) Shimmmins & Bolton (1974); (82) Spinrad et al. (1979); (83) Burbidge & Burbidge (1972); (84) Tritton (1972); (85) Hunstead (1971); (86) Savage et al. (1976b); (87) Lü (1970a); (88) Bergeron & Kunth (1984); (89) Browne & Savage (1977); (90) Jauncey et al. (1989); (91) Jauncey et al. (1984); (92) Lü (1970b); (93) Shimmmins et al. (1971); (94) Simpson et al. (1993); (95) Peterson & Bolton (1972); (96) Shobbrook (1963); (97) Mills et al. (1960); (98) Shobbrook & Shaver (1967); (99) Cooper et al. (1965); (100) Smith & Bicknell (1983); (101) Smith & Bicknell (1986); (102) Torres & Wroblewski (1984); (103) Bolton et al. (1949); (104) Baade & Minkowski (1954); (105) Graham (1979); (106) Kemp (1994); (107) Killeen et al. (1986); (108) VLA radio position (P. Barthel 2003, priv. comm.); (109) Willmer et al. (1991); (110) Véron (1977); (111) Grandi (1983); (112) Westerlund & Wall (1969); (113) Jackson et al. (2002); (114) Véron et al. (1990); (115) estimated from SuperCOSMOS magnitudes of other objects (Hambly et al. 2001); (116) Hunstead & Murdoch (1980); (117) Bolton et al. (1968); (118) Jauncey et al. (1982); (119) White et al. (1987); (120) Price & Milne (1965); (121) Hunstead et al. (1982); (122) Danziger & Goss (1979); (123) CCD position, referenced to COSMOS position; (124) Jauncey et al. (1986); (125) Penston & Fosbury (1978); (126) Sodré et al. (1992); (127) Mullan (1970); (128) Vettolani et al. (1989); (129) De Breuck et al. (2002); (130) De Breuck et al. (2001); (131) Searle & Bolton (1968); (132) Muriel et al. (1995); (133) Marenbach & Appenzeller (1982); (134) Fosbury et al. (1982); (135) De Breuck et al. (2004); (136) Huang & Sarazin (1998); (137) J. Baker (1992), priv. comm.; (138) R. Hunstead (1995), unpublished; (139) R. Hunstead (1994), unpublished; (140) R. Hunstead (1989), unpublished.

Table 8. Sample size and median values of various quantities for sources in the MS4, SMS4, and 3CRR samples.

	(1)	(2)	(3)	(4)	(5)	(6)
Sample	N	LAS (")	z	l (kpc)	P_{408} (W Hz $^{-1}$)	Median values
MS4	228	27^{+5}_{-2}	$0.53^{+0.05}_{-0.05}$	126^{+22}_{-9}	$5.9^{+2.2}_{-0.9} \times 10^{27}$	
SMS4	137	34^{+6}_{-2}	$0.50^{+0.06}_{-0.07}$	159^{+45}_{-11}	$6.6^{+5.7}_{-1.8} \times 10^{27}$	
3CRR	172	32^{+11}_{-6}	$0.50^{+0.07}_{-0.08}$	137^{+33}_{-33}	$8.4^{+4.0}_{-3.2} \times 10^{27}$	

Table 9. Numbers and percentages of galaxies and quasars in the MS4, SMS4, and 3CRR samples.

Sample	Galaxies		Quasars		Unclassified	
	N	%	N	%	N	%
MS4	174	76.3	39	17.1	15	6.6
SMS4	109	79.6	19	13.9	9	6.6
3CRR	129	75.0	43	25.0	0	0.0

Table 10. Radio-structure data from the literature.

(1) Source name	(2) Struc. code ^a	(3) LAS ()	(4) PA (deg)	(5) Map ref.
MRC B0003–833	2	69	–26	1
MRC B0023–333	1	68	17	2
MRC B0039–445	2	6.5	–79	3
MRC B0043–424	2	144	–45	3
MRC B0103–453	2	140	54	2
MRC B0110–692	2	77	–13	1
PKS B0114–47	2	690	–18	4
MRC B0131–449	c	36	–80	2
PKS B0131–36	2	546	–77	5
MRC B0157–311	2	21.3	–1	5
MRC B0214–480	1	426	–5	6
MRC B0216–366	c	61.6	–9	2
MRC B0240–422	c	70.4	40	2
PKS B0319–45	2	1540	49	6
MRC B0320–373	1	2880	–81	6
PKS B0332–39	1	420	...	6
MRC B0336–355	2	116	37	7
MRC B0344–345	1/2	271	78	8
MRC B0357–371	2	62	–32	9
MRC B0409–752	2	6.4	–57	10
MRC B0424–728	2	254	–14	4
PKS B0427–53	1	276	82	6
MRC B0429–616	1	114	14	6
MRC B0456–301	x	348	2	6
MRC B0511–484	2	123	73	11
PKS B0511–30	2	666	26	4
PKS B0518–45	2	435	–78	12
MRC B0521–365	T	53.3	–48	13
MRC B0601–344	2?	64.3	30	2

Table 10—Continued

(1) Source name	(2) Struc. code ^a	(3) LAS ('')	(4) PA (deg)	(5) Map ref.
MRC B0602–647	1?	70	8	2
MRC B0618–371	2	98	90	14
MRC B0620–526	1	318	...	6
MRC B0625–536	1	118	1	2
MRC B0625–354	1	118	...	2
MRC B0625–545	1	330	-4	6
MRC B0646–398	2?	81.6	-5	2
PKS B0707–35	2	489	-56	4
MRC B0715–362	1	450	74	6
MRC B0719–553	2	43.8	-30	1
MRC B0743–673	2	21.3	-86	15
MRC B1056–360	1	480	-21	6
MRC B1123–351	1	60	87	6
MRC B1136–320	2	71	-11	16
MRC B1143–316	c	46	82	2
MRC B1221–423	2	1.5	2	17
MRC B1259–445	2	132	37	6
PKS B1302–325	2	328	33	18
MRC B1302–491	x	510	40	6
PKS B1318–434	1	1020	37	6
MRC B1322–427	1/2	18000	49	6
PKS B1333–33	1/2	1920	-47	6
PKS B1400–33	x	960	35	19
MRC B1413–364	2	190	29	20
MRC B1416–493	1	40	54	2
MRC B1425–479	1	270	52	6
MRC B1540–730	c	42	86	2
MRC B1545–321	2	490	-33	4
MRC B1633–681	2?	60.2	-24	2

Table 10—Continued

(1) Source name	(2) Struc. code ^a	(3) LAS ('')	(4) PA (deg)	(5) Map ref.
MRC B1637–771	2	262	–25	5
MRC B1716–800	2?	43.2	–54	2
PKS B1733–56	2	241	37	5
MRC B1737–609	c	78	–33	6
MRC B1814–519	2	2.7	–78	21
MRC B1818–557	2?	94	–44	2
MRC B1819–673	2	47.7	–22	16
MRC B1829–344	1	25	...	2
MRC B1839–487	1	62	...	2
MRC B1840–404	2	49.5	–60	16
MRC B1922–627	2?	65.6	57	2
MRC B1929–397	2?	113	–45	20
MRC B1932–464	2	34.7	–71	22
MRC B1940–406	1/2	126	–11	2
MRC B1954–552	1	360	35	6
MRC B2006–566	x	1680	–30	6
MRC B2013–557	1	1200	–23	6
MRC B2020–575	2	53.8	19	23
MRC B2028–732	2	92.8	60	23
MRC B2031–359	1	22	0	2
MRC B2041–604	c	32.2	47	2
PKS B2148–555	1	780	26	6
MRC B2152–699	2	79.2	19	24
MRC B2153–699	2	26.7	24	24
MRC B2158–380	2	115	40	20
MRC B2250–412	2	16.7	–83	25
MRC B2354–350	1	68	–39	2
PKS B2356–61	2	396	–46	4

Table 10—Continued

(1) Source name	(2) Struc. code ^a	(3) LAS ()	(4) PA (deg)	(5) Map ref.

^aCode for source structure. “1” = FR 1 double, “2” = FR 2 double, “1/2” = structure borderline between FR 1 and FR 2, “D2” = double with one component coincident with the optical counterpart (Macdonald & Miley 1971), “T” = core-dominated triple, “c” = structure not resolved well enough to classify, “x” = extended source which does not fall into any of the usual categories.

References. — (1) P. A. Jones, unpublished ATCA image (1992); (2) MOST image, Paper I; (3) Morganti et al. (1999); (4) Subrahmanyam et al. (1996); (5) Morganti et al. (1993); (6) MOST image, Jones & McAdam (1992); (7) Killeen & Bicknell (1988); (8) Smith (1983); (9) R. Subrahmanyam, unpublished ATCA image (1992); (10) Reynolds et al. (1993); (11) Robertson & Smith (1981); (12) Christiansen et al. (1977); (13) Hardcastle et al. (1999); (14) Parma et al. (1991); (15) Rayner et al. (2000); (16) Duncan & Sproats (1992); (17) Safroris et al. (2003); (18) Jones (1992); (19) McAdam & Schilizzi (1977); (20) Ekers et al. (1989); (21) M. Wieringa, unpublished ATCA image; (22) Villar-Martín et al. (1998); (23) R. Hunstead, unpublished ATCA image; (24) Fosbury et al. (1998); (25) Clark et al. (1997).

Table 11. Numbers and percentages of Fanaroff-Riley class 1 and 2 sources in the MS4, SMS4, and 3CRR samples. Since not all MS4 sources have been imaged at high enough resolution, the structures of 47 sources are uncertain. The structures of 5 MS4 sources do not fit into either FR 1 or FR 2 categories. The 3CRR classifications are from the compilation of Laing (1998, priv. comm.).

Sample	FR 1		FR 2		Unclassified	
	N	%	N	%	N	%
MS4	34	14.9	142	62.3	52	22.8
SMS4	22	16.1	91	66.4	24	17.5
3CRR	28	16.3	141	82.0	3	1.7

Table 12. Median redshifts for confirmed quasars in the MS4, SMS4, and 3CRR samples.

Sample	<i>n</i>	Median quasar <i>z</i>
MS4	39	$0.87^{+0.13}_{-0.19}$
SMS4	19	$0.65^{+0.22}_{-0.12}$
3CRR	43	$0.90^{+0.14}_{-0.06}$

Table 13. V/V_m for galaxies and quasars in the MS4, SMS4, and 3CRR samples.

ID	MS4			SMS4			3CRR		
	Mean	S.E.	<i>n</i>	Mean	S.E.	<i>n</i>	Mean	S.E.	<i>n</i>
g	0.60	0.02	176	0.61	0.03	109	0.63	0.02	129
Q	0.70	0.03	45	0.76	0.04	21	0.70	0.03	43

Table 14. Comparison of quasar fractions and median linear sizes l_{med} of radio galaxies and quasars in the redshift range $0.5 < z < 1$ from the MS4, SMS4, and 3CRR samples. f_Q stands for the fraction of quasars, and “ratio of l_{med} ” for the median linear size of quasars divided by the median linear size of galaxies.

Sample	Galaxies		Quasars		ratio	
	n	l_{med} (kpc)	n	l_{med} (kpc)	f_Q	of l_{med}
MS4	39	199^{+30}_{-40}	11	119^{+41}_{-46}	0.22 ± 0.10	$0.60^{+0.38}_{-0.44}$
SMS4	25	206^{+23}_{-46}	7	149^{+163}_{-76}	0.22 ± 0.12	$0.72^{+1.10}_{-0.56}$
3CRR	28	192^{+94}_{-90}	16	66^{+30}_{-24}	0.36 ± 0.15	$0.34^{+0.67}_{-0.59}$

Table 15. Median linear sizes for quasars and radio galaxies for four different samples selected at low frequency. The data for the Molonglo Quasar Sample (MQS) are from Kapahi et al. (1998).

Sample			<i>n</i>	l_{med} (kpc)
MQS	$S_{408} > 0.95 \text{ Jy}$	Q	69	162^{+48}_{-28}
MS4	$S_{408} > 4 \text{ Jy}$	Q	26	116^{+44}_{-43}
SMS4	$S_{178} > 10.9 \text{ Jy}$	Q	14	154^{+109}_{-37}
3CRR	$S_{178} > 10.9 \text{ Jy}$	Q	37	89^{+19}_{-17}
MS4	$S_{408} > 4 \text{ Jy}$	g	103	209^{+25}_{-46}
SMS4	$S_{178} > 10.9 \text{ Jy}$	g	69	214^{+31}_{-22}
3CRR	$S_{178} > 10.9 \text{ Jy}$	g	79	234^{+58}_{-32}